Integrated Renewable Energy Polygeneration Networks: A Multi-Objective Optimisation and Game Theoretic Approach

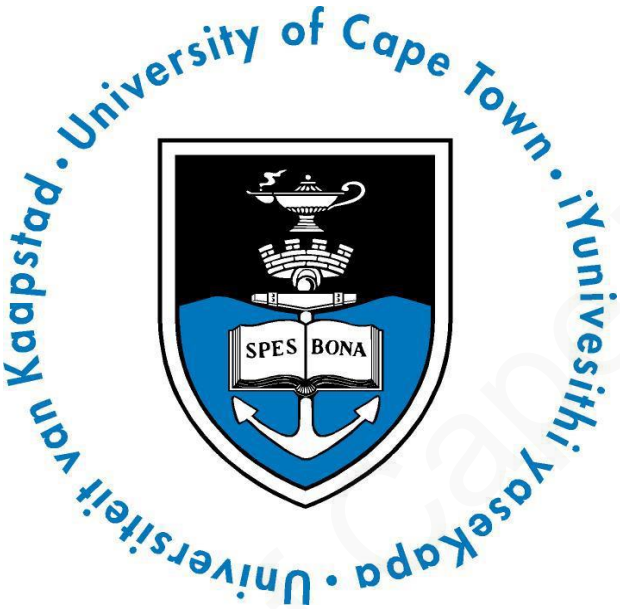

Dissertation submitted to the University of Cape Town in fulfilment of the requirements for

Master of Science Degree in Chemical Engineering

by

Takudzwa Brian Chitsiga

Supervised by: Prof. Adeniyi Isafiade

Department of Chemical Engineering

December 2024

University of Cape Town

The copyright of this thesis vests in the author. No quotation from it or information derived from it is to be published without full acknowledgement of the source. The thesis is to be used for private study or non-commercial research purposes only.

Published by the University of Cape Town (UCT) in terms of the non-exclusive license granted to UCT by the author.

University of Cape Town

Plagiarism Declaration

I know the meaning of plagiarism and declare that all the work in the document, save for that which is properly acknowledged, is my own. This dissertation has been submitted to the Turnitin module and I confirm that my supervisor has seen my report and any concerns revealed by such have been resolved with my supervisor.

Signature: Signed by candidate Date: 03/12/2024

Publication Disclosure

The work in this dissertation has been published in the papers listed below. Although efforts have been made to paraphrase the material, a high similarity index remains due to its alignment with the published work.

1. Chitsiga, T.B. & Isafiade, A.J. 2023. Integrated Renewable Energy and Polygeneration Hub Design for Industrial Heat and Power Utilisation. Chemical Engineering Transactions. 103:529–534. DOI: 10.3303/CET23103089.

2. Chitsiga, T.B. & Isafiade, A.J. 2024. Game theoretic approach for the synthesis and optimization of economically optimal coalitions in integrated renewable energy and polygeneration networks. Journal of Cleaner Production. 470. DOI: 10.1016/j.jclepro.2024.143308.

Acknowledgements

I would like to express my heartfelt thanks to my supervisor Prof. A. J. Isafiade for his guidance and encouragement throughout this work. His patient and compassionate approach was instrumental to the successful completion of this dissertation. I would also like to thank the Mastercard Foundation Scholarship Program for providing the necessary funding for my degree.

Many thanks to my friends and family, whose unwavering love, support, and encouragement have been my guiding light along this journey. I want to express my gratitude to my family for supporting me through difficult times and for always having faith in me. Your confidence in my skills has always given me strength. I am grateful to my friends for their understanding, companionship, and the innumerable moments of laughter and joy that have helped me stay grounded. Having all of you by my side has been a true blessing, and your support has been priceless.

The following abstract was written in the Shona language of the Bantu people native to the southern African country of Zimbabwe to encourage STEM education in native African languages. This is essential for enhancing comprehension and engagement among local communities. The use of familiar languages encourages participation from diverse backgrounds and empowers individuals to contribute to local innovations and solutions, as STEM concepts become more accessible.

Chidimbu

Kubatanidzwa kwe*renewable energy* uye kuvandudzwa kwemaitiro zvave kushandiswa kugadzirisa dambuidziko guru rekuwanikwa nechengetedzo ye*energy*, uye kusvibiswa kwemweya mumhepo pasi rose. Kushandiswa kwesvomhu kuumba mienzaniso nekombiyuta pamwewe ne*game theory* zvinogona kushandiswa kurerutsa mibatanidzwa pakati pemapoka akasiyana kuitira kugovana kwema*resources* uye kuronga mubhizimusi. Zvekare, kukosha kwe*industrial symbiosis* kunoburitswa zvikuru sezvo ichipembedza kutsivana kwema*resources* pakati pema*processes* akasiyana-siyana uye kuderedza kutambiswa kwezvinokosha. Kushandiswa kwesvomhu kuumba mienzaniso kunogona kubatsira kuita ongororo yakadzama panhau yekugadzirwa nekushandiswa kwe*energy* pasina mutengo uye njodzi dzekugadzira zviedzo zvinoshanda muupenyu chaihwo.

Mudhisatesheni ino munotaridzwa *network* yemhando dze*energy* dzakabatanidzwa inosanganisira *bioenergy supply chain*, uye *polygeneration hub*. Nzira yakashandiswa kugadzira *network* iyi inosanganisira chimiro chakatemwa chezvikamu zvitatu. Chikamu chekutanga chinosanganisira *supply chain network* yekuunganidza *renewable energy* inowanikwa zvinoenderana nemwaka, uye *non-renewable energy*. Chikamu chekutanga ichi chonobatanidzwa nechechipiri nenzira yema*system* ekutakura anosanganisira njanji, migwagwa, uye mapaipi. Chikamu chechipiri, chinoti polygeneration hub, chinosanganisira bhaira rekugadzira mvura inopisa yakanyanya, ma*turbine* emhepo inopisa yekugadzira magetsi, *system* ye*multi-effect evaporation* yekubvisa munyu mumvura yegungwa, uye *absorption refrigeration system* yekugadzira mvura inotonhora. Chikamu ichi chinosanganisirawo mukana wekubatanidza bhaira kune *subnetwork* ye*solar-thermal energy* uye *heat storage* yekudziisa mvura isati yapinda mubhaira. Chikamu chepiri chnobatanidzwa nechetatu nemapaipi uye tambo dzemagetsi. Chikamu chechitatu, chine *heat exchanger network* inoda chando nekudziya, maererano nekusshanda kweindasitiri, uyezve magetsi. Muenzaniso wakagadzirwa mubasa rino, uyo unova *mixed-integer non-linear program*, wakashandiswa kuenzanisa pazviitiko zviviri. Muchiitiko chekutanga makashandiswa kuvandudza kwe*multi-objective* kune kukosha kwakaenzana pakati pemutengo we*energy network* uye kuburitswa kweCO_2 pagore. Pakawanikwa mutengo wemadhora 40.2×10^6 uye kuburitswa kwematani 73.7×10^6 eCO_2 pagore. Uyewo, kuongororwa kwe*sensitivity* kwakaitwa kuti kuonekwe mashandukiro emhinduro maererano nekushanduka kwekuwanikwa

kwe*energy* inobva mubiofuel uye mashandukurio ekukosheswa pakati pemutengo nekuburitswa kweCO_2. Izvi zvakaburitsa kuti muenzaniso unoda kutanga kushandisa *fuel* inemutengo wepasi uye iinehushoma hwe*carbon*, usati washandisa *fuel* inotevera. Pakupedzisira, muenzaniso unotanga kushandisa *fossil fuel* kuitira kuburitsa *energy* inodiwa. Shanduko yekukosheswa kwemutengo nekubuda kweCO_2 zvichitsigira mutengo, inounza mutengo wepasi, zvichikonzerwa nekuwedzera *fuel* uye nzira dzekutakura zvine mutengo wepasi, uyezve kuderedza nhamba yema*units* mu*heat exchanger network* nemu*multi-effect evaporation system*. Kana kukosheswa kukashandurwa kuti kutsigire kuderedzwa kwekuburitswa kweCO_2, kuburitswa kweCO_2 kunowanikwa kuchiderera zvichikonzerwa nekubatanidzwa kwe*solar thermal energy* uye kuwedzera nhamba yema*units* mu*heat exchanger network* nemu*multi-effect evaporation system*

Muchiitiko chechipiri, zvikamu zvarehwa pakutanga zvinobatwa semaindasitiri akazvimiririra anokwanisa kuita mutambo wekushandira pamwe. *Objective function* yechiitiko ichi ine chinangwa chekuderedza mutengo weindasitiri imwe neimwe, nekupa kuenzana kune wese, mukusanganiswa kwemutengo wegore rose wemubatanidzwa. Zvakawanikwa zvinoratidza kufarira kugadzira musangano pakati pe*combined heat and power*, *multi-effect evaporation*, uye *heat exchanger network*. Izvi zvakapa kuderedzwa mutengo kwakanyanya kwemadhora 465.5×10^5 pagore. *Cooperative game theory* yakashindswa kuoongorora kuenzana kwemitengo yakabatanidzwa.

Abstract

Renewable energy integration and process optimisation have been employed to address the ever-increasing concerns regarding energy security and pollutant emissions worldwide. Mathematical modelling, paired with game theory principles, can optimize decision-making among stakeholders, enhancing resource allocation and strategic planning. Furthermore, the necessity of industrial symbiosis becomes evident, as it promotes the efficient exchange of resources between different processes, reducing waste and enhancing sustainability. The modelling of these approaches facilitates detailed experimentation without the associated costs and risks of setting up real-life prototypes.

In line with this approach, this dissertation presents an integrated resource network model that includes a bioenergy supply chain and a polygeneration hub. The objective is to optimally allocate renewable fuel, and a fossil fuel backup, to the polygeneration hub while optimally distributing the utilities produced to supply industrial and residential demand. The method used involves a 3-layer superstructure. The first layer consists of a supply chain network that includes seasonally available renewable and non-renewable energy sources, linked to the second layer through a transport system made up of railways, roads, and pipelines. The second layer, the polygeneration hub, contains a boiler for generating high-pressure steam, steam turbines for power production, a multi-effect evaporation system for desalinating seawater, and an absorption refrigeration system to produce chilled water. This layer also includes the option of connecting the boiler to a solar-thermal and heat storage subnetwork for preheating boiler feedwater. Piping and electrical cables connect the polygeneration hub to the third layer, which meets industrial heat demand through a heat exchanger network and electrical power demand. The generated model, which is a mixed-integer non-linear program, is applied to two case studies. The first case study provides valuable insights into the impact of weighting factors on cost and emissions, highlighting the model's decision-making process under varying renewable fuel availability and objective preferences. The second case study extends the model's applicability by incorporating cooperative game theory, showcasing its potential to enhance industrial symbiosis and achieve significant cost savings through strategic collaboration. In the first case, a multi-objective function with an equal weighting between total annual cost and CO_2 emissions is used. A total annual cost of 40.2 $\times 10^6$ \$/y and emissions of 73.7 $\times$ 10^6 t/y CO_2 is obtained. Furthermore, a sensitivity analysis is conducted to determine the effect of changes in biomass availability and weighting factors in the multi-objective function on the solution. The solution reveals that the model prefers to exhaust the supply capacity of the

cheapest biomass with lowest carbon composition, before moving on to the next. As a last resort, the model uses fossil fuel to meet the set energy demand. A change in weighting factors in the multi-objective function in favour of economics results in lower total annual cost values, achieved by using cheaper fuel and transport, and reducing number of units in the heat exchanger network and multi-effect evaporation system. When the weighting factor is changed to favour of emission reduction, lower CO_2 emission values are obtained by the incorporation of solar thermal energy and increasing the number of units in the heat exchanger network and multi-effect evaporation system.

In the second case study, the subnetworks in the superstructure from the first case are treated as individual participants within an industrial symbiosis network, with the potential to engage in a cooperative game. The objective function for this scenario aims to minimise the sum of the marginal contributions of each participant, assigning equal weighting to each, toward the coalition's total annual cost. The results indicate a preference for forming a coalition among the combined heat and power, multi-effect evaporation, and the heat exchanger network. This had the highest cost savings of 465.5×10^5 \$/y.

Table of Contents

Plagiarism Declaration i
Publication Disclosure ii
Acknowledgements iii
Chidimbu v
Abstract vii
List of Figures iii
List of Tables iv
Chapter 1: Introduction 1
1.1 Background 1
1.2 Modelling and Optimisation 3
1.3 Motivation 4
1.4 Research Objective 5
1.5 Methodology 6
1.6 Scope and Limitations 6
1.7 Thesis structure 7
2.0 Literature Review 10
2.1 Renewable Energy Supply Chain Optimisation 10
2.1.1 Harvesting and Pre-Processing 10
2.1.2 Transportation and Storage 11
2.1.3 Emissions 12
2.1.4 SCN Objective Function 14
2.2 Utility Hub 15
2.2.1 Power generation 15
2.2.2 Solar Energy 18
2.2.3 Absorption Refrigeration System 20
2.2.4 Multi-effect Evaporation 23
2.2.5 Capital Costing 26
2.3 Utility Demand 27
2.3.1 Residential Demand 27
2.3.2 Industrial Demand 28
2.4 Process Integration in Energy Systems 28
2.4.1 Advantages of integration and optimisation of energy systems 29
2.4.2 Polygeneration networks 29
2.4.3 Game Theory 30

2.4.4 Application of Game Theory in Polygeneration Networks 33
2.5 Conclusion 34
3.0 Methodology 36
3.1 Problem Statement 37
3.2 Assumptions 38
3.3 Model formulation 38
3.3.1 SCN Model Equations 38
3.3.2 CHP model equations 40
3.3.3 MEE model equations 45
3.3.4 ARS model equations 47
3.3.5 HEN model equations 51
4.0 Multi-Objective Optimisation Case Study 56
4.1 Case Description 56
4.2 Model Solution 59
4.2.1 Objective function 59
4.2.2 Results 60
4.2.3 Sensitivity analysis 68
5.0 Case Study Illustrating Industrial Symbiosis 73
5.1 Case Description 73
5.2 Model Solution 75
5.2.1 Objective function 75
5.2.2 Results 76
5.2.3 Sensitivity Analysis 81
Nomenclature 85
References 89
Appendix A 97
Appendix B 99
Appendix C 100

List of Figures

Figure 1.1: World fuel consumption in exajoules (BP, 2021) 2
Figure 1.2: Superstructure scope 7
Figure 2.1: Biogenic vs non-biogenic CO2 (IEA Bioenergy, 2018) 17
Figure 2.2: Single effect absorption cycle (Ren et al., 2019) 20
Figure 2.3: Effect of generator temperature on COP and QE for a single-effect absorber (Herold et al., 2016) 22
Figure 2.4: Single HTFFE unit (El-Halwagi, 2017) 24
Figure 2.5: Forward-feed configuration (El-Halwagi, 2017) 25
Figure 3.1: Detailed integrated model superstructure 37
Figure 3.2: Lithium-bromide absorption refrigeration system 48
Figure 4.1: Total emissions 61
Figure 4.2: Emission distribution for the three scenarios 62
Figure 4.3: TAC Analysis 64
Figure 4.4: Optimal biomass distribution 65
Figure 4.5: Pareto frontier plot: Cost vs Emissions 65
Figure 4.6: Superstructure solution – Case 1 67
Figure 4.7: Sensitivity analysis on weighting. 69
Figure 4.8: Sensitivity analysis on biomass supply capacity 71
Figure 5.1: Superstructure solution – Case 2 80
Figure 5.2: SCN sensitivity analysis 81

List of Tables

Table 4.1: Supply chain feedstock data 57
Table 4.2: Fuel LHVs 57
Table 4.3: Supply chain transport data (adopted from Cowen et al., 2019) 57
Table 4.4: Estimates of the CO2-intensity of Freight Transport Modes (g CO2 per tonne-km) 58
Table 4.5: Process plant's HEN stream data (adopted from Isafiade and Short (2022)).....58
Table 4.6: ARS subnetwork input parameters (adopted from Florides et al., (2003)) 59
Table 4.7: Superheated steam properties (adopted from Edgar, Himmelblau & Lasdon, (2001)).....59
Table 4.8: SCN-CHP energy supply and emissions 63
Table 4.9: Additional SCN-CHP variables.....63
Table 5.1: Bioenergy supply chain feedstock data 75
Table 5.2: HEN stream data (adopted from (Isafiade & Short, 2022)).....75
Table 5.3: Cost savings for each coalition.....76
Table 5.4: Player contributions for each coalition permutation in grand coalition ($/y $\times 10^5$) 77
Table 5.5: Marginal contributions for a coalition between players 1, 2 and 3 ($/y ×105) 78
Table 5.6: Optimal SCN configuration.....79

Chapter 1: Introduction

1.1 Background

The world is currently experiencing growing concerns over increasing global temperatures, and rates of climate change, due to greenhouse gas (GHG) emissions. The emission of GHGs is mostly resultant from five sectors i.e., industry, buildings, energy systems, transport and agriculture and forestry (Lamb et al., 2021). The energy sector is one of the biggest contributors to GHG emissions, with coal generated power producing over 40% of global CO_2 emissions (Karakurt et al., 2024) .This has given rise to the need for climate action and sourcing of cleaner renewable resources, such as the 2015 Paris convention, where it was agreed to limit global temperature increase to below 2 ℃ (Edenhofer et al., 2018).

Apart from environmental concerns, energy security is another concerning aspect that has given rise to the need for renewable energy alternatives. In Africa, energy shortages are an aspect of great concern. About 2-4% of the GDP is lost due to energy shortages alone, and with the continental population expected to increase to over 2 billion by 2050, energy shortages will only worsen (Schwerhoff & Sy, 2015). Several studies show that there is a positive correlation between energy production/consumption, and a country's GDP. This is supported by a study conducted on Pakistan's GDP, which showed that an increase in energy consumption by 1 kilo ton of oil would result in a $2.517 million increase in GDP (Naseem & Khan, 2015). This is a clear indication of the importance of energy to the economic survival of the world.

Figure 1.1 shows a comparison in the world's usage of the different fuel types in exajoules from the year 1995 to 2020. The graph shows that the world's largest fuel consumption is in oil, natural gas and coal, which all happen to be non-renewable energy sources. The graph also shows a general upward trend in energy consumption as the years go by. Simply put, this means the world will continue to need increasing quantities of fuel in the future (BP, 2021). It would therefore be ideal for the world to pursue renewable and/or clean energy sources, as they are vital for environmental conservation and contribute to sustained economic growth, though their integration must consider reliability and efficiency challenges.

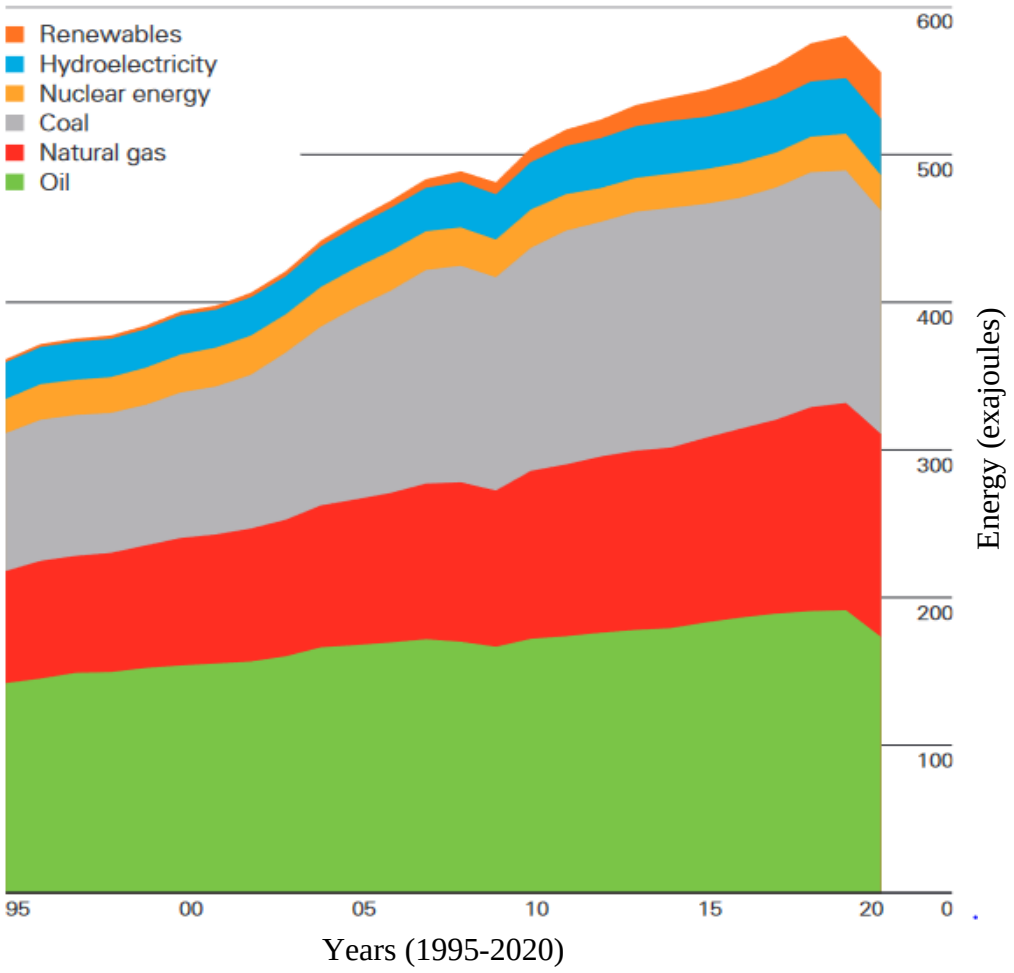

Figure 1.1: World fuel consumption in exajoules ***(BP, 2021)***

A complete transition to renewable energy may not be immediately possible, however, renewable energy may be integrated with existing forms of power generation (Yang et al., 2011). Once integration has been achieved, there is then the need for optimisation to ensure minimised use of fossil fuel (hence minimised emissions) and maximised renewable fuel usage. Various renewable energy sources, including solar, wind, hydropower, and biomass, can be integrated into these systems. Solar energy, while reducing greenhouse gas emissions compared to fossil fuels, requires substantial land areas for photovoltaic installations, potentially impacting local ecosystems (Kumar et al., 2020). Biomass energy, derived from organic materials, can contribute to carbon neutrality; however, its production may involve significant land use and lifecycle emissions associated with cultivation, harvesting, and processing (Chowdhury et al., 2025). Renewable energy technologies generally have lower lifecycle greenhouse gas emissions than fossil fuels, but factors such as land use and ecosystem disruption must be considered. Therefore, integrating renewable energy sources necessitates careful planning to balance environmental impacts, land footprint, and lifecycle emissions.

Apart from optimisation of integrated energy systems, optimising energy usage in general can go a long way in fuel usage reduction and hence emission reduction. This can be seen with heat exchanger network (HEN) synthesis, where the aim is to minimise utility usage and other costs related to heating and cooling in industrial plants (Onishi et al., 2018).

Beyond individual process optimization, a broader systemic approach, such as industrial symbiosis, offers a viable strategy for reducing emissions and enhancing energy security. Industrial symbiosis enables industries to share resources, by-products, and energy, fostering closed-loop systems that minimize waste and greenhouse gas emissions. For example, the Kalundborg Industrial Symbiosis in Denmark demonstrates how industrial symbiosis can effectively lower emissions through resource efficiency and energy integration (Hald-Mortensen, 2025). Additionally, industrial symbiosis strengthens energy security by promoting inter-industry energy exchanges, reducing dependency on external sources, and improving overall resilience (Marinelli et al., 2020). Thus, industrial symbiosis complements energy optimization efforts by creating sustainable and interconnected industrial networks.

1.2 Modelling and Optimisation

A mathematical model is a simplified representation of real-world phenomenon that can either be descriptive or predictive in nature and is described in mathematical concepts. Models allow detailed experimentation without associated costs and risks of the object being modelled (Gonzalez, Karelin & Tarasenko, 2014). Mathematical models can be presented as a linear program (LP), nonlinear program (NLP), mixed integer linear program (MILP), and mixed integer nonlinear program (MINLP). Each of these models can be set to achieve optimum solutions subject to sets of constraints and input parameters. An objective function contains the variable to be maximised or minimised in the optimisation model (Edgar, Himmelblau & Lasdon, 2001). Different types of objective functions will be discussed further in chapter two.

Several studies have used mathematical modelling in optimisation, with the aim of minimising variables such as costs or environmental emissions. Leão et al., (2011) designed a model to optimise a biodiesel supply chain with castor oil as a feedstock. Their model included the agricultural production of seeds, the crushing, and the ultimate production of biodiesel. Variables optimised included transport costs from farms to crushing sites, and from crushing sites to diesel production sites. In addition, the model included a binary variable denoting the decision to place a crushing plant at a particular location and period of operation. The model allowed purchasing of supplementary seed oil to meet the biodiesel demand.

Isafiade & Short, (2022) designed an integrated network that included a supply chain aspect for renewable biomass feedstocks, combined heat and power generation, and a heat exchanger network. This was optimised for minimum total annual cost (TAC) and environmental emissions, using the multi-objective approach. Their model, which is a MINLP was solved in General Algebraic Modelling System (GAMS), and this allowed use of integer variables to determine supply chain route selection and stream pairing in the heat exchanger network. Their model also allowed purchasing of supplementary electricity to meet the specified power demand.

In a similar manner, modelling is used in this study to simulate integration of renewable energy feedstocks with a polygeneration hub to meet demand for heating, cooling, power, and fresh water. The goal is to build investor confidence in such integrations and to pave the way for future studies and prototypes.

1.3 Motivation

The model in this study represents resource sharing among co-located plant networks for increased efficiency, cost reduction and improved environmental sustainability. Some of the benefits of such industrial symbiosis are analysed using cooperative game theory to outline the advantages for each industrial player. Modelling such networks allows careful planning to address challenges of resource sharing, such as logistical complexities, and resource compatibility between technologies.

Additionally, in a bid to reduce carbon emissions and their resulting effects, substitution of fossil fuel with biomass has been suggested (Ali et al., 2024a). Integration of solar thermal energy into the conventional Rankine cycle has also been brought forward as a solution (Qin, Hu & Li, 2020). Combining biomass combustion, or cofiring, with solar aided power generation would further reduce carbon emissions and their resulting effects. This proposed solution would also be a step towards rectifying the energy security problem identified in literature.

Whilst there are existing models of a similar nature, these have certain gaps as they do not account for some crucial variables that make the simulation as realistic as possible. A study by Cowen et al., (2019) proposed the integration of renewable energy supply chain with multiperiod heat demand of co-located process plants. Similarly, Isafiade & Short, (2022) modelled a renewable energy supply chain integrated with power generation and heat demand.

These studies minimised total annual cost but neglected key technologies and associated criteria to evaluate potentially more detailed integrated networks. For example, Cowen et al., (2019) did not include a utility generation hub detailing the generation of high pressure steam. Isafiade & Short, (2022) did not account for the desuperheating of excess steam supplied as hot utility. In both studies, technologies such as multi-effect evaporation and absorption refrigeration were not included to fully utilise excess steam. A study by Qiu & Entchev, (2024) developed an optimization model for integrated renewable energy systems, incorporating solar, wind, biomass, and battery storage to minimize net present cost and levelized cost of electricity. This study advanced modelling approaches but overlooked key aspects of process integration and thermal energy storage as it did not account for the dynamic interactions between industrial heat demand and renewable energy fluctuations. A study by (Lotfi et al., 2024) proposed a robust stochastic optimization model for designing net-zero, resilient, and agile closed-loop supply chain networks. The model integrated renewable energy sources, such as solar power and hybrid trucks, to supply energy for facilities and transportation. While the study advanced the concept of circular economy and sustainability, it did not address the dynamic interactions between renewable energy generation and industrial heat demand. Additionally, the model lacked detailed frameworks for incorporating thermal energy storage systems, which are critical for managing energy fluctuations.

To the best of the researcher's knowledge there are no studies that have considered a detailed integration that includes a polygeneration utility hub involving absorption refrigeration, water purification technology and combined heat and power technologies, whilst accounting for transport emissions, and total annual cost of the integrated network. This research therefore addresses the gaps identified in existing models whilst extending integration to include more technologies such as absorption refrigeration, multi-effect evaporation, and solar aided power generation. In addition, this work incorporates game theory to better outline the benefits of industrial symbiosis.

1.4 Research Objective

The main objective of this research is to develop an integrated model that optimally allocates renewable fuel, with the option of a fossil fuel backup, to a polygeneration hub while optimally distributing the utilities produced to supply industrial and residential demand. This is achieved by establishing interconnections within the polygeneration hub, between the steam turbines, multi-effect evaporation and absorption refrigeration for utilisation of waste heat to generate other utilities within the hub. Additionally, the research aims to incorporate game theory to

analyse the benefits of resource sharing among co-located industries, assessing how cooperative strategies can enhance overall efficiency, cost savings, and emissions reduction within the polygeneration network.

1.5 Methodology

The model was setup as a MINLP using GAMS. The multi-objective approach was used in the first case study to minimise total annual cost and CO_2 emissions. Cooperative game theory was used in the second case study, to calculate the marginal cost contributions of each player in coalition and the resultant cost savings. All costs, distances, and other parameters used in the model are obtained from literature. Assumptions have been made to simplify the model where necessary; these include negligible energy losses and known efficiencies for all turbines and other equipment. Detailed assumptions are listed in the respective sections.

1.6 Scope and Limitations

The superstructure model in this work involves the integration of a biomass supply chain network, with networks such as, combined heat and power generation (CHP) network, solar thermal energy network, multi-effect evaporation (MEE) system, absorption refrigeration system (ARS) and heat exchanger network. Figure 1.2 illustrates the scope of the proposed work. The model was applied to two hypothetical case studies with parameters adopted from literature such as Cowen et al., (2019) and Isafiade & Short, (2022). In the first case study, the model is solved for 3 scenarios. In scenario 1, the objective is to minimise the TAC of the network, and this is inclusive of all capital and operating costs for the units shown in Figure 1.2. In the second scenario, the objective is to minimise CO_2 emissions from combustion in the boiler and transportation of fuel. In the third scenario, the multi-objective approach similar to that used by Isafiade & Short, (2022) is used to simultaneously optimise both objectives, economics and environmental impact, with equal prioritisation or weighting. Included in the scope of this work is the selection of optimum feedstock quantities based on cost, heating values and emission factors; selection of the optimum transport modes based on cost per unit distance and emission factors; optimum distribution of steam between electricity generation and utility supply to the polygeneration hub; and determining the cost versus benefit of including solar preheating of boiler feed water. A sensitivity analysis is done to determine the effect of different objective weightings on these variables.

In the second case study, the supply cain network and combined heat and power generation system (SCN-CHP), MEE, HEN and ARS are considered as independent players that can form coalitions depending on the cost savings associated with each coalition. A game theoretical approach is used to determine the optimum coalition, with an objective function based on the Shapely values of each player. The cost estimations in this research are done using methods from (Towler & Sinnott, 2021), and the operating conditions are obtained from the respective literature sources referenced for each section of the model.

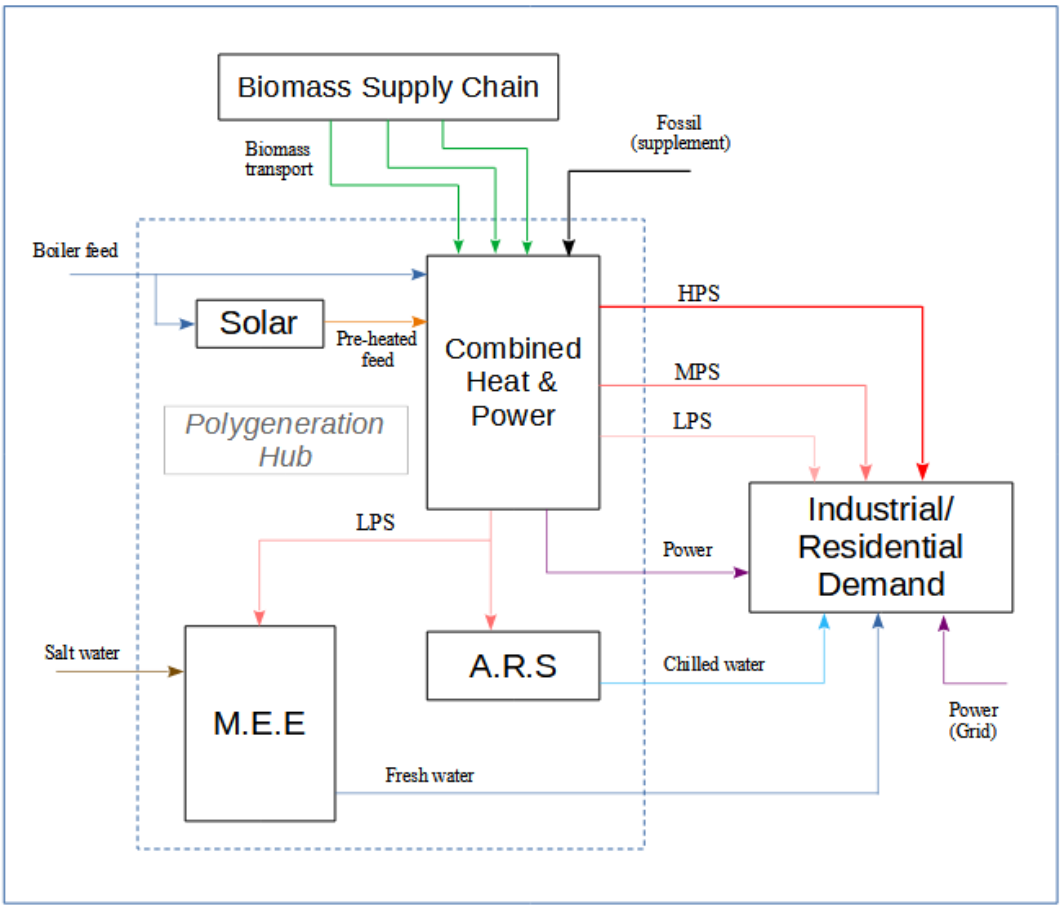

Figure 1.2: Superstructure scope

1.7 Thesis structure

Chapter 2

This chapter includes a thorough survey of relevant literature. It presents the different types of biomasses available and their energy values, and transportation modes and their emission

factors. In addition, various utility generation technologies are analysed and the existing application of modelling to optimise utility generation is explored.

Chapter 3

The equations making up the model are displayed in this chapter. The chapter also explains how the different parts of the model are integrated and states all relevant assumptions.

Chapter 4

This chapter details the application of the designed model to the first hypothetical case study. The input parameters for the model are specified with reference to the source literature where applicable. The model is run for different optimisation scenarios; economic, environmental, and multi-objective.

Chapter 5

In this chapter, the subnetworks of the superstructure, i.e., SCN-CHP, MEE, ARS and HEN, are considered individual players that can form coalitions for cost saving. Game theoretical analysis is applied to determine the most optimal coalition.

Chapter 6

This chapter outlines the conclusions of this study and the recommendations for possible future work.

Chapter 2

Literature Review

2.0 Literature Review

This chapter outlines the literature reviewed during the development of the various sections of the model, namely: renewable energy supply chain optimisation, combined heat and power generation, solar aided power generation, multi-effect evaporation, absorption refrigeration system, and the industrial and residential heat and power demand.

2.1 Renewable Energy Supply Chain Optimisation

Renewable resources refer to resources that can be naturally replenished at a rate that is equal to, or faster than that of their usage and depletion. Alternatively, a renewable resource can be one that is durable and readily available in nature. Examples include biomass, geothermal, wind, and solar (Maradin, 2021). Biomass can be defined as any organic material that can be used as a source of energy. Examples of biomass include agricultural waste, animal waste and wood (Ali et al., 2024b). Biomass can be combusted to generate steam and electrical energy and given its high availability, it may contribute to meeting the increasing renewable energy demand (Fatihah Salleh et al., 2019). Supply chain is the movement of biomass from the point of generation to the point of use and all other processes involved in between, such as harvesting, storage and pre-processing. Supply chain costs have a very high significance with regards to biomass as the biomass itself is usually low-cost material. Logistical costs tend to be a considerable fraction of the price per ton of biomass (Wang et al., 2024). The primary factors in the supply chain of biomass that affect logistic effectiveness are the raw materials' widespread production, their periodical availability, and their frequent handling as bulky goods. Biomass supply chain can be divided into harvesting, pre-processing, transportation, and storage.

2.1.1 Harvesting and Pre-Processing

Harvesting involves the collection of biomass from the point of generation or primary source, this can be a farming or forestry area. Pre-processing is done when necessary to make the biomass easier to handle and transport. This can be through dewatering, briquetting, or pelletising. This allows economic transportation over long distances (Maradin, 2021). The dewatering of biomass reduces the moisture content in biomass and therefore enhances the calorific value, which has a positive effect on combustion efficiencies (Atashbar, Labadie & Prins, 2016). Dewatering or drying can be done through torrefaction, which is the heating of biomass at atmospheric pressure, in the absence of oxygen, at temperatures from 200 to 300°C.

This yields a low moisture content solid. This method is mainly used for lignocellulosic materials (Niu et al., 2019). Pyrolysis is also a method that can be employed for the drying of biomass, it is the thermal breakdown of biomass under oxygen-free conditions at temperatures of about 400 to 800℃. This process yields gas, liquid, solid and solid char in proportions that are dependent on the properties of the biomass (Amjed et al., 2024).

2.1.2 Transportation and Storage

Different modes of transport can be used for biomass, depending on distance from destination, type, form, and quantity of biomass. When local suppliers are the source of the biomass, the most appropriate mode of transportation is by road since it allows flexibility when relatively short distances need to be covered. Ships are ideal for long-distance bulk transport because very big users of biomass, such as power plants or large-scale manufacturing facilities for biofuels, may have annual demand ranges between several hundred thousand and a million tons. Railway is an alternative mode of transport for long distances however it requires already existing infrastructure lest the capital cost would be high (Tumuluru et al., 2024).

For road and railway transport, the complexity of the existing network is typically important and is taken into consideration during the planning and designing stage of a biomass supply chain. This complexity is denoted by the tortuosity factor which can be defined as the proportion of actual road/rail trip distance to the shortest linear distance (Ranta, 2005). This factor is used to calculate the approximate distance travelled by road/rail between the locations where biomass is collected and the facility where it is utilised. This is a crucial factor in precisely estimating the cost of transportation to any facility using biomass as fuel. Assuming all other factors are held constant, the tortuosity factor should be kept minimal. Several studies have used different values of tortuosity factor, ranging between 1 and 3, however, none of these studies have justified the values or shown their determination methods (Sultana & Kumar, 2014). For example, Sultana et al. (2010) used a value of 1.27 as the tortuosity factor to estimate transport costs for straw and woody biomass by road. Leduc et al. (2009) used values of 1.45 and 1.50 to estimate transport cost for similar material. Isafiade and Short (2022) used values of 1.10 and 1.27 for transportation of corn stover, glycerine and wood by railway and road respectively. A recent study by Sohaib et al. (2024) utilized an integrated framework combining Building Information Modeling (BIM) and Geographic Information Systems (GIS) to analyze urban road infrastructure (Sohaib et al., 2024). The study included the assessment of tortuosity

factors for road intersections, leveraging GIS-based traffic microsimulation to optimize design and functionality.The total cost of transportation for biomass can be determined as the sum of the fixed transport cost in currency unit per unit mass and the variable transport cost in currency units per unit mass-distance.

Fixed transport costs are derived from the logistics of loading and offloading a vehicle, whereas variable costs are incurred in driver wages, fuel, and vehicle maintenance and are therefore dependant on the distance travelled. The fixed cost for trucks in North America is $5.45 per green tonne, and the variable cost is $0.22 per green tonne (Sultana & Kumar, 2014). For rail, Searcy et al. (2007) stated distance variable costs for woodchips and corn stover as 0.023 and 0.017 US dollars per tonne-kilometre respectively. Distance fixed costs for the same material were stated as 14.15 and 5.48 US dollars per tonne.

The investment cost associated with transport infrastructure can be factored into the total cost of transportation as a value in currency units per unit distance, that can be multiplied by the tortuosity factor and distance travelled to establish the total investment cost (Isafiade et al., 2022).

Storage of biomass often needs to be done from the point of harvesting to the point of usage. This is done to reduces loss of dry matter and to shield the biomass from elemental conditions. Depending on the climate and the biomass, storage may be outside or under a roof with an air fan. Location of the storage area can be at the harvesting site or centralised elsewhere. An intermediate storage area may also be required at the point of use to ensure a constant supply of fuel, this is dependent on harvesting patterns, demand levels and biomass availability (Atashbar, Labadie & Prins, 2016).

2.1.3 Emissions

Another factor to consider regarding supply chain is the emissions that result from the transportation of goods. All freight transportation is directly driven by fossil fuels, apart from a very limited amount of electric propulsion used by freight trains (Sohaib et al., 2024). Electric-powered road vehicles or freight trains are rarely used to transport freight in most countries. In these situations, pollution is created at the site of power generation, and the type of pollution depends on the primary energy source used (McKinnon et al., 2010). Carbon monoxide CO, aliphatic and aromatic hydrocarbons (including benzo(a)pyrene), sulphur dioxide SO2, nitric oxide NOx, particulate matter PM (soot, tar), and heavy metals are the

principal toxic pollutants released into the environment by the burning of fuels. Environmental concerns mostly address pollutant emissions, especially carbon dioxide and other greenhouse gases such as CH_4 and N_2O (Kijewska, Konicki & Iwan, 2016). Road transport emissions result from various processes, such as exhaust emissions from the internal combustion engines of cars, motor fuel evaporation, and tyre and brake wear (Klein et al., 2018).

With regards to emissions, this study will focus on carbon dioxide emissions. Estimates of the carbon footprint of different modes of transport are inconsistent, and official values may differ for the same region. Differences partially reflect fundamental assumptions about fleet composition, fuel economy, and vehicle load factors as well as global variations in power sources, transport network quality, and the types of freight transported by specific modes (Zhang, 2024).

Carbon emissions from the transport sector can be calculated in different ways. According to Klein et al (2018), for a particular country for fossil fuel powered vehicles, one way is to quantify the amount of fuel sales and multiply this by the heating value of the fuel and the emission factor. The heating values and CO_2 emission factors differ between countries (Klein et al., 2018).

This method sums up an estimate of the overall CO_2 emissions for an entire country that originate from internal combustion engine (ICE) vehicles and does not differentiate between emissions from freight and passenger transport.

Alan McKinnon (2007) proposed that there are two types of emission factors, one based directly on the fuel used i.e., input- based measures, such as the one used by Klein et al. (2018). An example is the emission per litre of diesel. The input-based factor is more specific because it accounts for every litre of fuel used. From an organisational perspective, this is the most appropriate factor to use for direct sources of emissions such as company owned vehicles and indirect sources such as purchased power. Data for the fuel used in these sources of emissions can easily be obtained.

The second type of factor is the activity-based factor which relates more to the trip output for example distance travelled. This can be used when fuel input data is not available, it makes a general assumption of the fuel used per kilometre of travel. Activity based factors are most useful when accounting for emissions from third party sources such as contracted vehicles (Hendricks, 2010). Activity-based emission factors can be used in combination with distance travelled and vehicle load to calculate the total CO_2 emissions in kg per tonne-kilometre.

2.1.4 SCN Objective Function

The optimisation of supply chain networks can be done through different objective functions. An objective function can be defined as an expression of a business goal into mathematical form for the purpose of decision analysis or optimisation studying (Atashbar, Labadie & Prins, 2016). A common method is to minimise annual cost, for example Leao et al. (2011) developed a method to optimise the supply chain of a diesel plant with an objective function that minimised logistical, industrial and agricultural chain costs. Another method is to maximise profit. For processes that include sale of goods, the objective function can be set to maximise the profit made. An et al. (2011) introduce a mathematical approach for designing a supply chain system that utilises lignocellulosic biofuel and apply it to a specific area in Central Texas to optimise profit generation.

More recently a method that has seen increasing attention is the multi-objective approach, where the goal is to optimize two conflicting parameters. Santibanes-Aguilar et al. (2014) undertook a study on the optimal planning of biorefineries in Mexico. They took both economic and environmental factors into account when looking at different types of agricultural biomass, such as sawdust and wood chips, to create ethanol, hydrogen, and biodiesel. To select the feedstock, processing technology, and product range in a bio-refinery supply chain, the researchers suggested a multi-objective model. Their primary objectives were to maximise overall profits and reduce the environmental impact during the life cycle. They also proposed a multi-objective optimisation of biomass-to-liquids processing networks, which focused on minimising the total annualised cost and assessing environmental performance and greenhouse gas emissions throughout the life cycle.

For this work, both economic and environmental objectives will be considered in the first case study and hence will be added to the individual overall objective functions for simultaneous optimisation.

Building on the multi-objective optimisation approach discussed, it is essential to consider the integration of renewable energy sources within a broader utility framework. This can be done through the concept of a utility hub, which serves as a centralised system for managing and optimising the distribution of various energy forms, including electricity, heat, and cooling. The utility Hub not only enhances the efficiency of energy use but also facilitates the incorporation of renewable energy sources into the existing energy infrastructure.

2.2 Utility Hub

The integrated and simultaneous generation of utilities such as electricity, process heat, and cooling through the heat management of an energy system can be referred to as polygeneration. The polygeneration method has the potential to lower the capital costs of each utility generation system and enhance the overall performance and reliability (Sahoo et al., 2015). The use of excess heat that would typically be lost is what makes polygeneration a more efficient process. This energy efficiency enables the lowering of CO_2 emissions. Thermally activated technologies such as absorption refrigeration, can be used to provide cooling (Rong & Lahdelma, 2016). Fresh water can be produced by desalination through multi-effect evaporation units (Sahoo et al., 2015).

2.2.1 Power generation

The generation of electricity in thermal power plants is mostly done using steam turbines, which are driven by steam primarily from combustion of fossil fuel. Several cycles can be adopted to explain the function of steam turbine power plants, these include the Carnot, Rankine, reheat and the regenerative cycles. The Carnot cycle has limited applicability in practice due to the assumption of isentropic and reversible processes which are not achievable in reality. As a result, the Rankine cycle is used as the standard cycle for steam turbines (Tanuma, 2017).

The energy used to drive Rankine cycles is typically generated by the combustion of fossil fuels. In 2021, 36.28% of the world's electricity generation was driven by coal, whilst 23.08% was from natural gas and 2.55% was from oil. The remaining 38.09% was split between hydro, nuclear and renewables (Meana-Fernández et al., 2022). The high calorific value of fossil fuels contributes to their widespread use. The heating value of a fuel has a substantial impact on and is directly proportional to the thermal efficiency of a thermodynamic cycle (Tanuma, 2017). Energy content of a fuel can be defined in terms of the higher heating value (HHV) or the lower heating value (LHV). HHV is also known as gross calorific value (GCV) and LHV is also known as net calorific value (NCV). The HHV of a fuel is the energy released when combusting a known amount of fuel initially at 25℃ and then returning the products to the initial temperature. This implies that the water produced in the reaction is in liquid form. LHV, also known as net calorific value, is similar, however, the water produced is accounted for in vapour form i.e., products are not returned to the initial temperature of 25℃ (Sanchumpu et al., 2024). According to Nunes et al., (2020) coal can have a LHV ranging from 16.10 MJ/kg for lignite

to 30.1 MJ/kg for anthracite. Natural gas and oil have LHVs of 50 and 41 MJ/kg respectively (Kuparinen & Vakkilainen, 2017). On the other hand, renewables such as forest wood chips have a LHV of about 11.86 MJ/kg (Stolarski et al., 2019).

In addition, fossil fuels have been in use since the last two centuries and drove the industrial revolution. As a result, most systems in place from logistics to infrastructure have been design with an orientation towards fossil fuel. It is argued that abandoning fossil fuels would upset the current balance of socio-economic aspects (Halkos & Gkampoura, 2023).

Aside from the depletion of fossil fuels and the need to address climate change, the abundance and low cost of biomass make it an appealing alternative energy source. Converting waste to energy can be an economical and environmentally responsible approach to dispose of waste while also producing energy (Siwal et al., 2021). A good example is sewage sludge. On average, a human being produces about 50g of dry matter waste per day. This makes municipal waste treatment a continuous activity with a perpetual supply of waste in possibly increasing quantities over time. There are several ways of converting sewage sludge to energy including incineration and co-firing with coal to produce electricity. Energy recovery from sewage sludge is largely dependent on the water content and therefore there is need for mechanical dewatering or drying before burning, to increase the energy efficiency of the process. Waste heat from exhaust gases can be used for the drying process. Potential environmental problems arising from combustion of sewage sludge include the release of pollutants in the exhaust gas and this would need to be addressed. Another potential problem is the heavy metals present in the sludge which would ultimately be in the ash, however, due to the combination of high incineration temperatures and the organic substances present in the sludge, the heavy metals would be stabilised and unaffected by leaching. Economically, incineration of sewage sludge alone can be costly due to the need to setup new technologies for pollution abatement. A study by Rahmanta et al., (2024) analyzed the techno-economic aspects of biomass co-firing in existing coal-fired power plants. The research highlighted that co-firing leverages existing infrastructure, significantly reducing capital costs compared to dedicated biomass power plants. The study also emphasized that co-firing enables high-efficiency power generation while minimizing greenhouse gas emissions. However, it noted challenges such as fuel compatibility and the need for operational adjustments to accommodate biomass (Rahmanta et al., 2024). Biomass can also be converted to other forms of fuel such as biogas and biodiesel which may have more uses than just power generation.

The combustion of biomass in place of fossil fuels for power generation is an arguable subject. One argument is that combustion of biomass similarly produces large quantities of CO_2 and therefore does not aid in the fight against climate change. Biomass in fact produces higher CO_2 volume per unit energy (Partnership for Policy Integrity, 2011). On the other hand, there is contrasting argument stating that the planet's carbon mass balance can be divided into a biogenic cycle which is short term, and an overall cycle which is long term. The biogenic cycle includes plants, water bodies, daily emissions, and soil. The overall cycle includes the biogenic cycle and the carbon trapped in fossil fuels. Whilst combustion of biomass produces CO_2, this is within the biogenic cycle and is managed by sequestration through farming activities, thereby maintaining a balance in the CO_2 cycle. When fossil fuels are combusted, more CO_2 is fed into the biogenic cycle upsetting the balance and thereby affecting the climate (IEA Bioenergy, 2018). Figure 2.3 shows the difference between biogenic and non-biogenic CO_2. The second argument is sound but highlights the importance of strict regulations regarding the sourcing and harvesting of biomass. With addition of pollution abatement technology at power generation sites, zero net emission of CO_2 can be achieved.

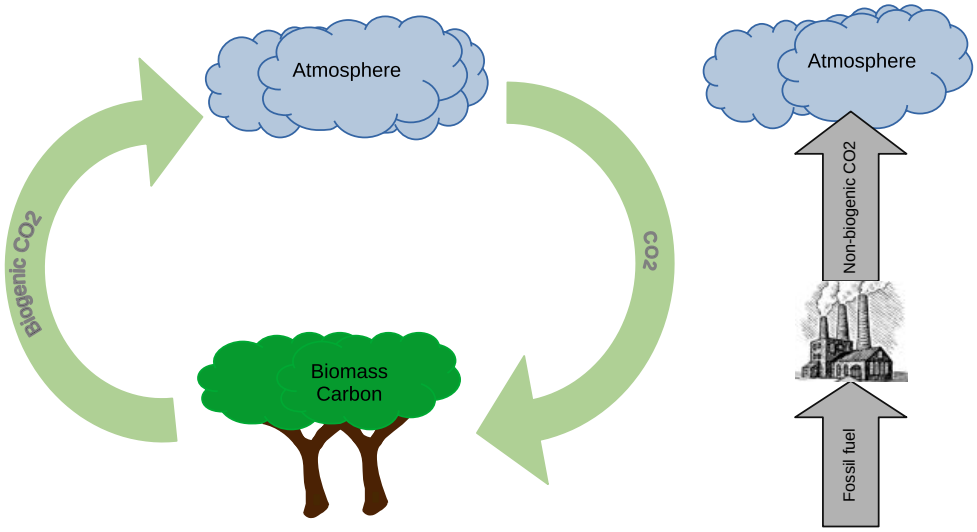

Figure 2.1: Biogenic vs non-biogenic CO2 ***(IEA Bioenergy, 2018)***

Input based emission factors can be used to calculate the emissions from the power generation, since the properties of the fuel are usually known. Isafiade and Short (2022) calculated power generation emissions using the energy produced in kW, the combustion efficiency, the lower heating value of the fuel expressed in kWh/kg, the weight percent of the non-oxidised pollutant, the number of operating hours, and the ratio of the molecular mass of CO_2 to that of carbon. A study by Mahlia et al., (2018) also presents utilisation of input-based emission factors to

calculate emissions from power generation. This study outlines a general emission estimation formula for power plants, considering factors such as the amount of fuel burned, the emission reduction efficiency of the power plant, and the specific emission factors of the fuel used. It provides detailed calculations for emission factors of carbon dioxide from gas-fired and oil-fired power plants, incorporating fuel composition and combustion efficiency. The method of input-based emission factors is adopted from (Shenoy, 1995).

2.2.2 Solar Energy

Solar energy is one of the most significant renewable sources of energy and is available worldwide. Solar energy can be harnessed in two ways, photovoltaic (PV) and solar thermal technologies. Solar PV involves the conversion of solar energy to electricity whilst solar thermal is conversion to heat that can be applied to different processes (Baljit, Chan & Sopian, 2016). Generation capacity of Solar PV has seen a significant increase globally, from 483.1 GW to 580.2 GW between 2018 and 2019. The efficiency of PV systems is affected by meteorological conditions such as ambient temperature, solar radiation, wind velocity and dust storms. Several technologies have been developed to counteract meteorological effects, and these include cooling systems for temperature regulation, power storage devices for irregular solar radiation availability, and self-cleaning technology for dust removal. Advantages of PV technology include low operating and maintenance cost and the feasibility of small-scale installations (Allouhi et al., 2022).

Solar thermal energy has received a lot of attention in recent decades, owing to its high efficiency and low cost. Solar thermal systems can be divided into two types: large scale and small scale. The former can be used in industrial scale activities such as domestic hot water, process industry hot utility, and integration into power generation. Small scale systems are most applicable to individual homes where energy is stored in hot water tanks, i.e., solar geysers. Large scale solar thermal systems have more sophisticated technologies that enhance their efficiency. Whilst this gives them a higher installation cost, the higher efficiency and CO_2 emission reduction are an important trade-off (Evangelisti, De Lieto Vollaro & Asdrubali, 2019). There are different types of Solar thermal collectors currently in use and these can be described as follows.

Flat-plate collectors(liquid): these are commonly used to provide domestic hot water. A dark surface is heated by solar radiation and subsequently heats up the water. A typical unit consists of a dark surface for incident solar radiation absorption, usually made of steel, copper or

aluminium; a glazing transparent cover that transfers radiation to the absorber; internal channels containing the heat transfer fluid; a frame capable of protecting and stabilising the components; and an insulation for minimising collector heat losses (Rommel, Kovács & Kramer, 2010).

Unglazed collectors: these do not have a transparent cover for the absorber, this enables them to absorb more solar radiation, however, the lack of insulation greatly reduces their efficiency due to heat losses. They are typically applicable where the required temperature is below 30℃, such as the heating of swimming pools outdoors (Kalogirou, 2004).

Another type of solar thermal collectors is the concentrating collectors. These focus the incident radiation on a smaller area than the receiving surface by use of optical concentrators. These can be further grouped by shaped and method of function into flat concentrator collectors, compound parabolic collectors, parabolic trough collectors, and heliostat field collectors. Concentrating collectors can generate a considerably higher amount of energy for example, a parabolic trough collector can operate at temperatures of up to 400℃. As a result, high temperature heat transfer fluid such as diathermic oils and molten salts can be used (Evangelisti, De Lieto Vollaro & Asdrubali, 2019). Advances in collectors have led to the development of solar tracking collectors which move to face the direction of the sun as the day progresses. Their advantages include higher thermal efficiency per unit area due to an uninterrupted radiation supply during the day and minimal heat losses (Kalogirou, 2004). A hybrid system of solar PV and solar thermal energy has been developed to allow the simultaneous generation of electricity and heat from solar. A working fluid is used to cool down the system and thus generating useful heat. This improves the overall solar conversion efficiency (Evangelisti et al. 2019).

Research on the optimisation and integration of solar thermal energy into industrial processes has been conducted extensively. For example, Isafiade et al. (2016) developed a mathematical model to integrate solar thermal energy with the heat exchanger network of a process plant. Their model accounted for the periodical (day and night) and seasonal variations in solar energy availability while also incorporating fossil fuel as an alternative energy source. Their findings demonstrated a 13% reduction in TAC through solar-thermal integration, highlighting its significant cost-saving potential. Similarly, Walmsley et al. (2014) proposed a hybrid system combining solar thermal energy and a heat recovery loop. This design utilised solar thermal energy and stored it in a series of vessel loops to mitigate heat losses caused by the intermittent

nature of solar energy supply. This was applied to the case study of a dairy industry with a multi-plant setup to show the potential of hot utility conservation. Solar thermal energy has been used to pre-heat boiler feed water in a process known as solar-aided power generation. This has the benefit of either using less fossil fuel and emitting less pollutants or utilising the same amount of fuel to generate more steam and hence more electricity. In solar-aided power generation, solar thermal energy replaces the regenerative steam that would otherwise be diverted from a turbine for feedwater preheating (Hu, et al., 2012). The installation cost of solar systems is largely dependent on the collector area and the collector type. These are subsequently affected by the desired application, geographical location and resultant meteorological conditions, specifically solar radiation available (Kalogirou, 2004).

2.2.3 Absorption Refrigeration System

This term refers to a system that transfers heat from a low temperature medium to a high temperature medium. The transfer is facilitated by heat or work input and is applied in refrigeration and heating systems. Absorption refrigeration systems, in particular, rely on heat input to operate the refrigeration cycle, enabling applications such as solar cooling and steam-powered refrigeration (Herold et al., 2016). Consequently, surplus steam from the Rankine cycle can be harnessed to power an absorption refrigeration system. Figure 2.4 shows a simple illustration of an absorption refrigeration system.

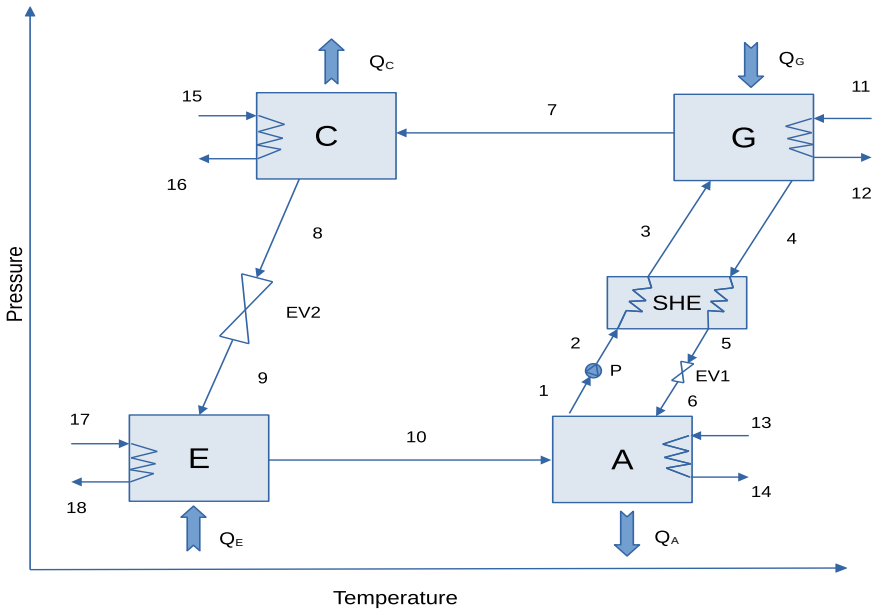

Figure 2.2: Single effect absorption cycle ***(Ren et al., 2019)***

The cycle has two pressure levels, the absorber (A) and evaporator (E) operate at low pressure whilst the condenser (C) and generator (G) work at high pressure. The heat input is applied to the generator as steam (stream 11-12), and this boils refrigerant out of the solution allowing it to enter the condenser as a vapour (stream 7) and leaves a strong absorbent solution (stream 4). The refrigerant is then cooled by cooling water from stream 15-16 in the condenser and then passes through an expansion valve (EV2) and enters the evaporator where it vaporises at saturation temperature, as it absorbs heat from the chilled water (stream 17-18). The refrigerant vapor flows to the absorber (stream 10) where it is reabsorbed by the strong solution from stream 6 (from an expansion valve) to form a weak solution. The absorption process is cooled with cooling water from stream 13-14. Lastly, the weak solution at the absorber outlet is pumped, from stream 1, to the generator, through a solution heat exchanger (SHE). The SHE allows the pressurised weak solution (stream 2-3) to be preheated by the high-temperature strong solution (stream 4-5) (Ren et al., 2019). The measure of efficiency for an absorption refrigeration cycle is the coefficient of performance (COP) which can be defined as the ratio of refrigeration capacity to driving heat input.

The operating variables of an absorption cycle are interdependent, and a typical plot of COP and cooling capacity vs generator temperature can exhibit this. Figure 2.5 shows that COP has a maximum value of 0.75 at a driving temperature of 75℃ and refrigeration capacity of 7kW. An increase in temperature results in an increase in cooling capacity but also an increase in Q_G and all other heat transfers in the cycle, for this reason increasing the generator input temperature by a great margin in a single effect absorber, has a small effect on the COP. Therefore, a cycle design that can fully harness the energy from high temperature generator input is needed to improve cycle performance. A double effect absorption cycle can achieve this as it exhibits a similarly flat COP trend line but with higher values due to a step change in the COP values. As a result, single effect technology is most applicable when the generator input source is waste heat at low temperature (Herold et al., 2016).

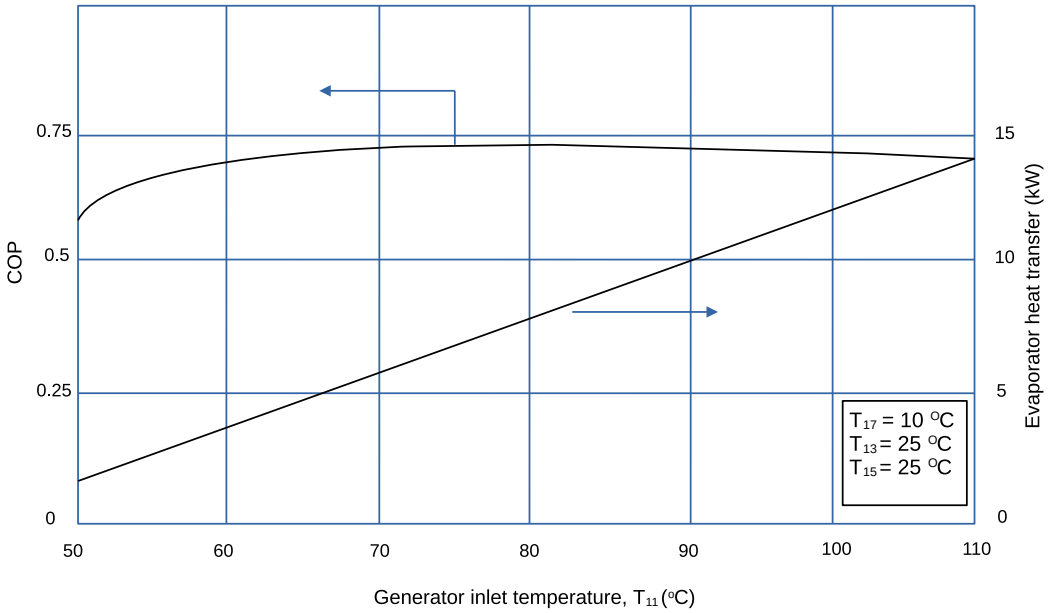

Figure 2.3: Effect of generator temperature on COP and QE for a single-effect absorber ***(Herold et al., 2016)***

Apart from the driving temperature, the performance of an absorption cycle is also affected by the chosen working fluid. The working fluid is comprised of the refrigerant and the absorbent and different pairs of fluids have been studied and used for example, water/sodium hydroxide, water/calcium chloride, ammonia/lithium nitrate, etc. The ideal properties of a working fluid include the following:

1) A large difference in boiling points between the pure refrigerant and the combined fluids at the same pressure
2) To maintain low circulation rate between the generator and the absorber per unit of cooling capacity, the refrigerant should have a high heat of vaporisation and a high concentration inside the absorbent.
3) Favourable transport properties that influence heat and mass transfer, such as diffusion coefficients, viscosity, and thermal conductivity.
4) Both fluids should be low-cost, non-corrosive, and environmentally friendly (Sun, Fu & Zhang, 2012).

The conventional working fluids currently being used in industry are ammonia/water and water/lithium bromide. These fluids both have their trade-offs regarding ideal properties and the ultimate choice would be dependent on application. The non-volatility of lithium bromide makes it an ideal absorbent as it eliminates the need for a rectifier in the cycle design. Water

would be an ideal absorbent as its crystallisation points falls outside the property ranges of interest. The use of water as a refrigerant (and hence water/lithium bromide as a working fluid), is limited by the freezing point of water, and can only be done for cooling processes above 0℃ (Herold et al., 2016). Whilst water/lithium bromide results in higher efficiency and lower installation costs, ammonia/water would be a more practical working fluid for processes below 0℃ as the freezing point of ammonia is -77℃ (Sun, Fu & Zhang, 2012).

Various methods have been employed to perform thermodynamic analysis of absorption refrigeration cycles. These approaches typically involve conducting mass and energy balances across the different components of the cycle, with some researchers extending this analysis to include an exergy balance of the system. For instance, Mendiburu et al., (2023) developed a thermodynamic model for a NH_3-H_2O absorption refrigeration system integrated with solar thermal power from parabolic collectors. Their model, implemented in Matlab, utilised the Newton-Raphson method to solve nonlinear algebraic equations and was applied to a case study in Porto Alegre, Brazil. The system achieved cooling loads of 18.89 kW during summer and 11.31 kW in spring, highlighting the potential for combining solar thermal energy with cooling technologies to promote sustainable cooling solutions. Similarly, Rubio-Maya et al., (2011) developed a non-linear programming model of LiBr-H_2O absorption refrigeration system to minimise total annual operating costs. created a nonlinear programming model for a LiBr-H_2O absorption refrigeration system aimed at minimising total annual operating costs. Their work also included a thermodynamic analysis with an exergy balance to evaluate the fuel-related operating costs. Florides et al (2003) designed a LiBr-H_2O absorption system clearly outlining the sizing of equipment and the material used. Both studies utilised correlations to determine the various fluid state properties within the absorption cycle. Ren et al., (2019) developed a Matlab-based thermodynamic model for analysing LiCl-H_2O and LiBr-H_2O absorption refrigeration systems. Their findings revealed that reducing the temperatures of the absorber and generator led to improved coefficient of performance (COP) values.

2.2.4 Multi-effect Evaporation

Nearly 97% of the water on Earth is saltwater in the oceans, with the remaining 3% being fresh water. Almost 70% of this fresh water is in the form of ice in the arctic regions and mountain ranges. Underground water accounts for 27% of fresh water, with surface water in lakes and rivers accounting for about 1%. Rapid changes in human lifestyle and industrialisation have put a strain on the world's finite freshwater resources (Hossein Davood Abadi Farahani,

Vatanpour & Hooshang Taheri, 2020). Water and energy have an interconnection that cannot be separated, for example, water is required in power generation and energy is required in the purification and distribution of water. This relationship is called the water-energy nexus.

The energy from steam can be used to desalinate sea water by use of multi-effect evaporation. The horizontal-tube falling film evaporator (HTFFE) is commonly used at industrial scale for desalination. Figure 2.6 shows a typical HTFFE. Mass flowrates of seawater feed, brine and distillate are represented by F, *B* and *D* respectively, while $x_{F,}$ x_B and x_D refer to the respective mole fractions of salt in these streams. M_S is the flowrate of heating steam. Pumped seawater is sprayed over the tube bundle. Inside the tubes, condensing steam is fed. Evaporation happens as a thin film of seawater forms on the exterior surface of the heating tubes. The boiling seawater vapor collected on the exterior surface of the heating tubes is collected and condensed to give the high-purity distillate. The concentrated liquor is collected in the form of brine.

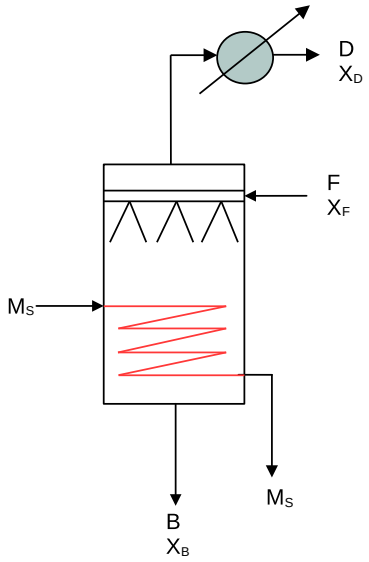

Figure 2.4: Single HTFFE unit ***(El-Halwagi, 2017)***

In multi-effect evaporation, several units (effects) are used together. These can be connected in different configurations, with the most common being forward feed. Figure 2.7 shows a simplified illustration of the forward-feed configuration. Preheated seawater and heating steam are fed to the first effect, brine from this effect serves as feed for the next effect. Succeeding effects use distillate vapor as a heating medium instead of steam. The temperature of the brine from the first effect is higher than the corresponding distillate vapour temperature, and because of the increased salted concentration, the boiling point of brine in the second effect would be even higher than that in the first, given constant pressure. It is therefore necessary to lower the boiling point of brine in succeeding units by progressively reducing the operating pressure to

a point lower than the preceding effect and enough to lower the boiling point. Other ways to make the desalination process more energy efficient include preheating of feed using waste heat from power plants and industrial facilities (El-Halwagi, 2017).

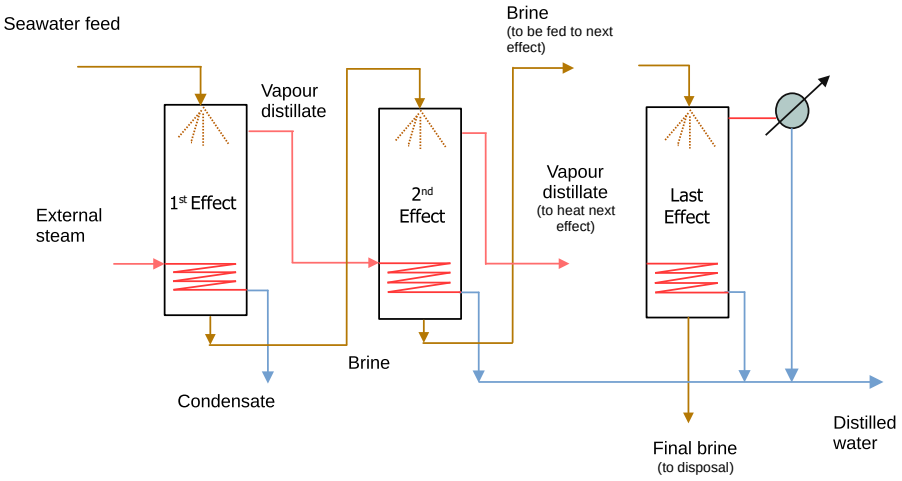

Figure 2.5: Forward-feed configuration ***(El-Halwagi, 2017)***

Aguilar-Jiménez et al., (2020) developed a simulation integrating a multiple-effect desalination (MED) system with an organic Rankine cycle (ORC). The MED system included an evaporator to provide thermal energy, while the ORC utilised the latent heat of condensation from the water vapor produced in the first effect. The effects were modelled as heat exchangers. Their findings indicated that this integration enhanced system performance with only a minimal increase in the heat transfer area. Similarly, Zhou et al., (2019) proposed a detailed mathematical model to compare the performance of a MEE system with and without thermal vapor compression (TVC). Their results demonstrated that coupling MEE with TVC improved the gained output ratio while having a minimal impact on the heat transfer area. Typically, the vapor generated in each effect is utilised to heat the next effect, but it eventually condenses and is wasted. By incorporating TVC, the vapor from the last effect is compressed and recycled back into the system. This allows it to be reused as a heating medium in the preceding effects. This recycling minimises the demand for additional steam supply, hence increasing the gained output ratio (GOR).

When evaluating various utility generation technologies, such as multi-effect evaporation and power generation, it is crucial to consider the economic implications of each option. The capital cost of equipment plays a significant role in determining the feasibility and selection of these technologies. High initial investment costs can be a barrier to the adoption of advanced and

efficient technologies, even if they offer long-term benefits in terms of energy savings and environmental impact. A detailed capital cost assessment is crucial to weighing initial investments against possible operational savings and environmental benefits. This evaluation supports well-informed decision-making that aligns with financial and sustainability objectives, facilitating the effective implementation of utility generation technologies.

2.2.5 Capital Costing

Capital costing is an important aspect of engineering design. With profit being a key objective in processing plants and industrial businesses, it is important to estimate the amount of investment required before financial viability can be determined. Detailed cost estimation is a specialised field that requires trained professionals, however, a rough estimation to be used as a guideline can be done by the design engineer. Capital costs can be divided into fixed capital investment and working capital. The former incorporates costs associated with design, construction, installation, and modification of plant equipment. Working capital is the investment made to sustain plant operations, catering for costs such as feed inventory and spare parts.

There are several methods that can be used to determine the investment cost of a plant. The cost curve method can be applied when published data of a plant with similar technology is available. The unknown capital cost of a plant can be related to that with published data through scaling the plant capacities and applying an exponent of about 0.6 to the ratio. This is commonly known as the six tenths rule. The step count method can also be applied to estimate overall plant capital costs. This is based on the number of processing steps in the proposed plant, the conversion rate of feed to products, and the degree of conversion. An exponent is also included and varies based on whether the plant processes solids or liquids.

Alternatively, capital cost estimation can be based on individual pieces of equipment purchased. This is derived from actual prices paid for similar equipment. This method can be affected by bulk purchasing and the confidentiality of business information such as discounts. There are several cost correlations and costing software that can be used. For academic purposes, access to high-quality cost data may be limited and correlations must be used (Towler & Sinnott, 2021)nience (Towler & Sinnott, 2021).

An annualised (amortized) capital cost is determined by computing the annual payment required to repay the initial investment, as well as the projected return on capital in the form of

compound interest. Multiplying the capital cost by the annualization factor gives the regular annual payment that needs to be made for n years (Towler & Sinnott, 2013).

2.3 Utility Demand

The key drivers of energy consumption include social and economic modernisation in terms of globalisation, trade openness, industrial and agricultural expansion, population increase, urbanisation, and infrastructural development, as well as other development strategies (Hussain & Zhou, 2022). It is important that the use of energy and other utilities in residential and industrial applications be as optimal as possible to minimize energy waste and environmental emissions. For instance, in industrial settings, heat exchanger network synthesis can be employed to optimize utility demand by designing a network that maximizes heat recovery and minimizes the need for external heating and cooling, as is done in this research.

2.3.1 Residential Demand

Residential and commercial buildings are responsible for a significant share of the world's energy consumption and resultantly contributor to CO_2 emissions and climate change (Lu & Lai, 2020). The use of energy in buildings accounts for about 30% of total world energy consumption and 27% of emissions from the energy sector (IEA, 2022). Depending on the specific climate zone, about 60 to 80% of this energy is applied to water heating, space heating and cooking. Currently the source of this energy can mostly be traced back to non-renewable fuels (Abikoye et al., 2019). With floor area expected to increase by almost 20% by the year 2030, it is important that energy intensity in the building sector be reduced in order to align with the Net Zero goal (IEA, 2022).

Abikoye et al., (2019) developed a solar thermal network for utilisation in domestic heating. Their work resulted in an optimised solar heat network applicable to a cluster of buildings. The method used accounted for variations in meteorological parameters such as solar irradiation with time of day and seasons. The goal was to minimise dependency on a fossil fuel energy backup and the obtained results for their case study in Slovenia showed that solar energy could cater for 7.4% of required heating with considerable panel sizes. This value has potential to increase when considering seasons and geographical locations with higher solar irradiation levels. Maximov et al. (2021) simulated a multi-objective optimisation of the use of solar energy incorporating seasonal thermal storage. They considered the design cost and the

greenhouse gas emissions of the system, and their results revealed that solar thermal networks were almost equally as cost-efficient as conventional heating methods, with an added advantage of reduced emissions.

2.3.2 Industrial Demand

Excessive energy usage is one of the most common issues in manufacturing facilities. It contributes the most to the composition of the worldwide cost of industrialised goods (Ravagnani et al., 2005). Utility costs are among the key operating costs in manufacturing industries and are often the second largest contribution to a plant's operating costs after raw materials. Utilities can be purchased or generated on-site, resulting in an operational expense. Heating and cooling are used in process industries to guarantee that process stream temperatures meet the target set points. Heat exchange with process streams and/or hot/cold utilities can be used to achieve such heating/cooling (Cowen et al., 2019).

Isafiade et al., (2022) developed a model that included a supply chain network and a multi-period interplant stage-wise superstructure. Their model included a heat exchanger network that represented multiple processing plants with process streams that required heating and cooling. Hot and cold utility streams were available for heating and cooling, and these were supplied by a utility hub connected to a renewable energy supply chain. The objective was to minimise the total annual cost of the superstructure, hence energy saving was a key aspect. The model was solved as a MINLP model. Their solution showed a preference for intra-plant heat exchangers i.e., process stream to process stream exchange, with 8 out of 14 exchangers being intra-plant process stream heat exchangers. Cowen et al., (2019) solved a similar model as a MINLP however, their superstructure did not include inter-plant heat integration.

2.4 Process Integration in Energy Systems

Process integration involves the strategic alignment and optimisation of interconnected processes by combining technologies, equipment and flows to reduce energy consumption, waste generation, and maximise resource usage (El-Halwagi, 2017). Energy efficiency in processing plants can be achieved through Heat Exchanger Network Synthesis using heuristic approaches (such as Pinch technology) and mathematical programming. Whilst Pinch technology has been widely used in minimising capital costs and energy usage (Smith, 2005), the mathematical programming approach has proven easier to optimise networks that include multi-period heat demand (Isafiade et al., 2022). Overall, several authors have used

mathematical programming to develop resource sharing networks and outline the benefits of process integration.

2.4.1 Advantages of integration and optimisation of energy systems

Isafiade et al., (2022) developed a composite superstructure that combined a bioenergy supply chain network and a multi-period interplant HEN model. Their superstructure allowed intra-plant and interplant heat exchange among three co-located process plants, with hot utility generated by an energy hub, using renewable fuel. Their model was solved as a MINLP to minimise the total annual cost of the superstructure. Chitsiga & Isafiade, (2023) designed a polygeneration hub that combined a renewable energy supply chain network, a combined heat and power plant, an absorption refrigeration system, and a HEN. Their work outlined the benefits of integrating processes to make use of excess heat and minimise energy waste. The integration of HENs with renewable energy supply chain networks including industrial and municipal waste can contribute towards achieving some of the sustainable development goals (7, 11, 12 and 13) (Isafiade et al., 2022).

2.4.2 Polygeneration networks

Polygeneration networks represent a shift from traditional single-output energy systems to multi-output setups that generate multiple utilities, such as electricity, heat, cooling, and water, simultaneously from a shared input (Murugan & Horák, 2016). This integrated production approach significantly increases energy efficiency and facilitates industrial symbiosis by enabling facilities to exchange resources, share by-products, and minimise waste. Such networks have gained traction in industries aiming to enhance sustainability and resilience, particularly through resource-sharing and cost-reduction mechanisms that optimise the use of both conventional and renewable energy sources (Pang et al., 2023). Two key components of a polygeneration system are a prime mover and an energy conversion device. Various prime movers, including Stirling engines, reciprocating engines, steam engines, gas turbines, micro-gas turbines, and the organic Rankine cycle, are commonly utilised to produce power and heat. Additionally, renewable energy sources like biomass, solar power, wind energy, and fuel cells can be integrated into polygeneration systems to generate either electrical or mechanical energy (Murugan & Horák, 2016).

Several authors have modelled polygeneration networks integrated with renewable energy sources. Calise et al., (2014) presented an innovative renewable polygeneration system that

produces energy and water for use in a small Mediterranean volcanic island. The system, which included concentrated photovoltaic-thermal collectors, geothermal wells, and multi-effect distillation, was modelled with TRANSYS simulation software. A case study was carried out on Pantelleria, a volcanic island in the southern Mediterranean, to test the system's potential to meet local energy demand. The simulation results showed exceptional performance, particularly in summer when high solar radiation facilitated the production of space cooling, domestic hot water, electricity, and desalinated water using a combination of solar and low-enthalpy geothermal energy. However, in winter, the efficiency of the concentrating photovoltaic-thermal collectors declined significantly, reducing the system's capacity to provide space heating. The study highlighted the system's potential for Mediterranean volcanic islands, where demand for energy and water is high. Economic analysis suggested a short payback period under optimal thermal energy use. However, reduced utilisation of thermal energy could extend the payback period to 10 years. Overall, the system demonstrated economic feasibility and suitability for addressing resource challenges in such regions.

Pang et al., (2023) developed a MINLP model for a renewable multi-energy system (RMES), aimed at reducing both cost and environmental impact. The model integrates renewable solar energy, using photovoltaic solar panels for electricity and solar thermal collectors for heat. To manage supply-demand fluctuations and address intermittency, thermal, battery, and hydrogen energy storage systems (ESS) are included. A comparative analysis was done to evaluate each storage type's effectiveness based on economic and environmental goals, with findings showing that the ESS performs better when the environmental objective is considered, with a 45% increase in usage. Multi-objective optimisation, using the ϵ-constraint method, produced Pareto-optimal solutions, with the fourth solution achieving a balanced approach. This solution maintained a high profit and considerable carbon emissions reduction, meeting both objectives at a 0.75 satisfaction level. Their RMES model demonstrates economic and environmental feasibility, and advances energy recovery and technology optimisation for urban-industrial systems, aiming to reduce carbon emissions and minimise energy costs.

2.4.3 Game Theory

Game Theory (GT) is a tool used to analyse models that involve decision-making among different parties in a competitive scenario. GT considers the profit or cost obtained by each party should a certain decision be made. The key elements found in a GT model include a set of players, with each having a set of strategies (decisions) to choose from. In addition, each

player in the game has an objective or goal, which can be expressed m(Muggy & L. Heier Stamm, 2014) (Muggy & L. Heier Stamm, 2014). Games can be classified as cooperative or non-cooperative. In a cooperative game, the model is based on the decisions of groups of players in which improved profits may be obtained from strategic alliances and cooperation. In non-cooperative games, players independently make decisions to optimise their own objectives (Osborne, 2004).

Game theory has been extensively applied in energy systems and industrial symbiosis to optimize resource allocation, cost-sharing, and decision-making among multiple stakeholders. Various game-theoretic approaches exist, including cooperative and non-cooperative methods. The Nash equilibrium, a key concept in non-cooperative game theory, identifies stable strategies where no participant can gain by unilaterally changing their strategy. This method has been applied in industrial symbiosis to model stakeholder behaviour and predict stable, mutually beneficial collaborations. For example, a study by Emmons et al., (2022) demonstrated that in symmetric team settings, locally optimal strategies correspond to global Nash equilibria, providing insights into stable collaborative behaviours. However, while the Nash equilibrium provides strategic stability, it does not necessarily ensure fairness in benefit distribution, which is crucial in shared energy systems. In contrast, cooperative game theory methods, particularly the Shapley value, offer a fair allocation of costs and benefits based on each participant's marginal contribution. The Shapley value guarantees a unique and equitable distribution while considering the impact of every possible coalition (Shapley, 1953). In polygeneration networks and industrial symbiosis, where multiple entities contribute resources and share benefits, this ensures proportional and justifiable cost-sharing, making it a robust tool for sustainable collaboration (Tan et al., 2016). Moreover, its axiomatic properties of efficiency, symmetry, and additivity align well with the fairness principles required in energy-sharing systems. Thus, while Nash equilibrium is valuable for strategic interaction analysis, the Shapley value stands out as the best choice for ensuring fair and stable cooperation in industrial symbiosis and energy networks.

Ahmad Fadzil et al., (2022) designed a game theory-based model that had three plants as different players with the ability to form coalitions to share carbon permits in IS. Emission factors were associated with utility purchases, and the overall emissions generated were calculated for each player. In their model, a player required a carbon permit to gain additional emission allowance and therefore increase production and profit, which was the objective to be maximised. They used the Shapley value (Shapley, 1953), to distribute the profits obtained

amongst players in coalition. Their results showed that each player had an average increase of 25% in profit when working in a coalition. Tan et al., (2016) designed a linear cooperative game theory model for the allocation of benefits obtained from inter-plant integration. Their model considered a case study in which three plants could form a coalition to share utilities such as steam and chilled water, instead of purchasing them externally, and the sharing of waste material that can be reused. They made use of the Maali's method and the Shapley value (Shapley, 1953) to allocate the cost savings. Their results showed that both methods yielded the same results and that each of the plants had an added advantage when working in a coalition. There are several other studies in which GT has (Chew et al., 2009; Piluso & Hu(Chew et al., 2009; Piluso & Huang, 2009; Lozano et al., 2013)(Chew et al., 2009; Piluso & Huang, 2009; Lozano et al., 2013), and this is testament to the benefits of GT in industrial symbiosis.

The marginal contribution and Shapley value of each player are calculated to identify the coalition that benefits a player the most. The marginal contribution refers to the additional value a player adds to a coalition upon joining it (Ahmad Fadzil et al., 2022). This can be determined using Equation (2.1).

$$MC_a(\mathrm{z}) = \nu(\mathrm{z} \cup \{a\}) - \nu(\mathrm{z}) \tag{2.1}$$

In this equation, $MC_a(\mathrm{z})$ represents the marginal contribution of player a to coalition z, where $\nu(\mathrm{z} \cup \{a\})$ denotes the value of the coalition with player a included, and $\nu(\mathrm{z})$ is the value of the coalition without player a. Consequently, a player's marginal contribution varies based on the order in which the coalition is formed. For instance, in the coalition (2:3:4) player 2 could occupy the second or third position, such as in (3:2:4) or (3:4:2). The total number of possible permutations of the coalition is the factorial of the number of players, including single-player coalitions. To ensure a fair distribution of coalition value among the players, the Shapley value is computed. This value is the average of a player's marginal contributions across all possible permutations involving that player (Ahmad Fadzil et al., 2022). It can be calculated from Equation (2.2).

$$\phi_a(\nu) = \sum_{c \epsilon \mathrm{C}} \frac{1}{C} \left(\nu\left(\{a\} \cup \mathrm{z}_{c(a)}\right) - \nu\left(\mathrm{z}_{c(a)}\right) \right) \tag{2.2}$$

$\phi_a(\nu)$ is the Shapely value for player a, C is the set of all possible coalitions, $\mathrm{z}_{c(a)}$ is the coalition formed by the first player c(a) in the permutation κ. The term $\nu\left(\{a\} \cup \mathrm{z}_{c(a)}\right) - \nu\left(\mathrm{z}_{c(a)}\right)$ is the marginal contribution of player a in the coalition $\mathrm{z}_{c(a)}$.

2.4.4 Application of Game Theory in Polygeneration Networks

Game theory has emerged as a critical tool for modelling the complex, interdependent decisions made within polygeneration networks. Lozano et al., (2022) used a MINLP model to optimise the configuration of a trigeneration system for meeting the electricity, heating, and cooling demands of a residential complex in Zaragoza, Spain. The model compares different technologies inside a superstructure and optimises operations over a typical meteorological year. Its primary objective is to lower the total annual cost. Their findings show that the optimal trigeneration system offers significant cost reductions over individual consumer systems. Cooperative game theory analysis validates benefits for all consumers, and the Shapley value technique ensures equitable cost distribution. The method highlights significant savings in electricity, heating, and cooling demands, demonstrating the economic benefits of shared energy systems. Overall, the study emphasises the potential of trigeneration systems to improve cost-effectiveness and promote fair distribution of resources in managing residential energy needs.

Párraga et al., (2024) proposed a model that integrates the operation and dispatch of isolated water-energy microgrids (IWEMGs). The concept uses game theory to optimise resource management by modelling interactions among players (such as consumers, producers, and prosumers) using a non-cooperative Cournot competition. This technique offers an effective mechanism for allocating resources while taking into account the strategic behaviour of all players. The model is used in a case study in Ranchería, a rural community in La Guajira, Colombia, to meet water and energy demand. It is implemented and solved using GAMS software, which demonstrates optimal resource management and allows for informed decision-making. Quantitative results highlight its effectiveness in optimising water and energy transactions, achieving substantial net benefits for all players. This research emphasises the potential of game theory to enhance the operational efficiency of IWEMGs. Furthermore, it provides valuable insights into sustainable resource management, offering a foundation for developing policies and strategies for implementing IWEMGs in similar rural settings worldwide. The study showcases how such systems can effectively meet resource needs while fostering sustainable and equitable practices.

Studies have demonstrated that game theory in polygeneration networks facilitates optimal resource distribution, aligns stakeholder objectives, and ensures system stability. Cooperative game models, like coalition games and Shapley value approaches, allow stakeholders to

leverage shared resources, achieve greater cost efficiency, and reduce emissions by maximising synergy among participants. Non-cooperative models also show distinct advantages, especially in contexts where stakeholders maintain separate interests. These models help balance competitive interactions, ensuring that each participant can operate efficiently without compromising overall network stability.

2.5 Conclusion

The reviewed literature emphasises the importance of optimising renewable energy systems for efficiency and sustainability across supply chains, utility hubs, and energy demand. The effective management of harvesting, pre-processing, shipping, storage, and emissions is critical to optimising supply chain performance. Utility hubs, which use technologies such as solar energy, absorption refrigeration systems, and multi-effect evaporation, provide efficient resource conversion to meet residential and industrial demands. Process integration enhances energy systems by promoting economic and environmental benefits, while polygeneration networks provide a versatile approach to simultaneous utility production. Combining these aspects with game theory promotes effective optimisation of resource allocation and stakeholder interactions. The application of game theory demonstrates improved operational performance, equitable resource distribution, and informed decision-making, supporting the transition to sustainable energy systems. Collectively, these advancements reinforce the potential of integrated and optimised energy systems to address global energy challenges effectively, hence the need for this study. The technologies described in this chapter involve complex mechanisms and phenomena that can be modelled with specific mathematical equations which are subject to logical constraints and assumptions, to simplify their simulation. It is important to limit assumptions and include as much detail in the modelling as possible, to make it more robust and realistic.

Chapter 3

Methodology

3.0 Methodology

This chapter details the method used in developing the superstructure model. The literature in chapter two highlighted the need for energy efficiency and optimisation and hence the model described in this chapter aims to address those aspects.

The model is designed to select the optimum transport mode and biomass fuel considering emissions and cost, to supply a solar aided combined heat and power generation plant. This in turn supplies steam to the MEE, ARS and HEN. Overall, the objective is to simultaneously minimise total annual cost and emissions of the integrated network. Figure 3.1 outlines the detailed network in the model. The SCN can supply 3 types of renewable fuel to the CHP and fossil fuel as a backup through rail, road or pipeline. The CHP is comprised of a boiler for high pressure steam generation and turbines that generate electricity whilst releasing low and medium pressure steam. A solar thermal energy system is connected to the CHP for boiler feedwater preheating, and this is specified as an optional alternative in the model. The CHP is connected to the MEE, ARS, and HEN through pipes and supplies LPS to the ARS and MEE, as well as LPS, MPS and HPS to the HEN. Electrical cables connect the CHP to a residential and industrial area to meet a set power demand. The MEE is connected by pipeline to a saltwater feed and produces fresh water, whilst the ARS produces chilled water.

The model is similar to the work of Isafiade & Short, (2022) and Isafiade et al., (2022), but includes other units such as the ARS and MEE. In addition, the said authors did not account for emissions from transportation of biomass, and the de-superheating of steam produced in the combined heat and power generation plant. In addition, the model in this work accounts for turbine and boiler capital costs, and transmission costs, to make it as realistic as possible. Cooperative game theory is also used in this study to better outline the benefits of symbiosis, as one of the case studies considers the SCN-CHP, MEE, ARS, and HEN as four individual players that can opt to form coalitions.

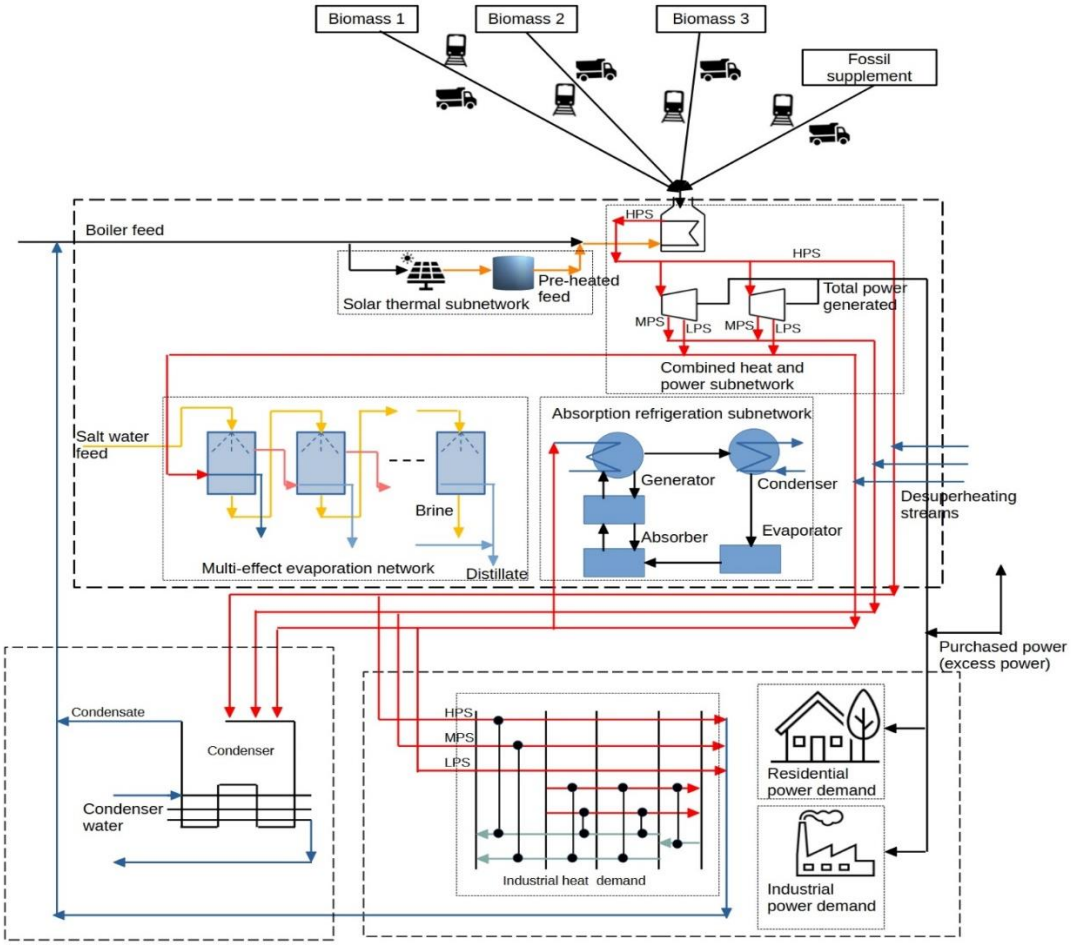

Figure 3.1: Detailed integrated model superstructure

3.1 Problem Statement

The problem statement is as follows: Given a set of biomass energy sources *sp*, that can supply feedstock to be transported by a set of freight modes *f*, to a polygeneration hub located at a distance *D* from the supply points. Each feedstock has a seasonal availability, represented by the set *s*, and corresponding unit costs. The polygeneration hub is required to generate heating and cooling utilities to meet the heat demand of a set of hot *H* and cold *C* process streams which are defined by their heat capacity flowrates *FCP* and heat transfer coefficients *h*. Integrated with the combined heat and power subnetwork of the polygeneration hub is solar aided power generation to preheat the boiler feedwater. Additionally, the hub includes an absorption refrigeration system, which is a subnetwork, that comprises a set of units denoted by *ars*, and a multi-effect evaporator which is another subnetwork of the polygeneration hub denoted by *MEE*. This subnetwork desalinates saltwater to provide fresh water as a utility. Additional parameters given in the problem include transport costs for the energy feedstocks, heat exchanger installation and area costs, and unit-based costs for the utilities. The aim is to design

an integrated network that optimally distributes resources and energy to satisfy demand for heat, cooling, fresh water, and electricity considering both economic and environmental objectives. Additionally, subnetworks are treated as individual players that decide whether to join the integrated network based on the benefits they receive. A game-theoretical analysis is employed to identify the most optimal coalition.

3.2 Assumptions

A superstructure that integrates 4 different networks and heat exchange is a complex system that necessitates the use of simplifying assumptions. The following general assumptions were made in generating the superstructure in this model:

1. No loss of water in any part of the system and hence no need for boiler feed makeup.
2. All heat exchangers operate isothermally and in an isobaric manner except in the MEE.
3. Distillate and vapour are the same temperature in the MEE.
4. The seasons considered for renewable energy feedstock availability have equal duration of 4 months each.
5. The LHV of renewable energy feedstock remains unchanged during transportation to the CHP subnetwork within the polygeneration hub.
6. The stream properties, such as density and heat capacity, are assumed to be independent of temperature.
7. Heat exchangers with a counter-current configuration, featuring single shell passes and single tube passes, are utilised.
8. There is isothermal mixing for split streams in the HEN.
9. Utility pipes are equipped with insulation, ensuring that no heat is lost during operation.
10. Boiler feedwater is recycled and cooled back to its original feed temperature following condensation.

3.3 Model formulation

This section details the equations used in formulating the different parts of the model, including logical constraints.

3.3.1 SCN Model Equations

The total cost of the supply chain network is calculated as the combination of fixed costs, variable cost and investment cost for the infrastructure as shown in Equation (3.1a). The fixed

cost is the cost of purchasing feedstock and the variable cost is associated with transportation costs.

$$C_{SCN}^{F,V,I} = \sum_{s\in S}\sum_{f\in F}\sum_{sp\in SP}\left[C_{sp,s}^{F} + C_{f}^{V}\cdot\tau_f\cdot r_f\cdot D_{sp}\right]\left[\frac{x_{sp,f,s}}{\frac{\eta^{bl}\cdot NCV_{sp}}{n\cdot DS_s}}\right] + \sum_{f\in F}\sum_{sp\in SP}\left[AF_{SCN}\cdot C_f^{I}\cdot\tau_f\cdot z_{sp,f}.D_{sp}\right] \quad f\in F, sp\in SP, s\in S \tag{3.1a}$$

The first term on the right-hand side of Equation (3.1a) represents the fixed and variable costs. $C_{sp,s}^{F}$ ($/kg) is the cost of acquiring feedstock from supply point sp during season s. C_f^V ($/kg.km) accounts for transportation costs for feedstock from sp using freight mode f in season s. The straight-line distance from supply points sp to the utility hub is D_{sp} (km), which is adjusted by the tortuosity factor τ_f and the return trip factor r_f to represent the actual travel distance, including the return leg. $x_{sp,f,s}$ (kW) represents the quantity of feedstock transported from sp via freight mode f during season s. This is converted to an annual mass using the feedstock's net calorific value NCV_{sp} (kWh/kg), boiler efficiency η^{bl}, annual operating hours n (h/y), and the season duration (DS_s) as a fraction of the year. The second term represents the investment cost for the supply chain infrastructure. AF_{SCN} is the capital cost annualisation factor, which can be calculated using Equation (3.1b). The annualization factor AF for an amount P invested over a period of n years at an interest rate i can be calculated as shown below.

$$AF = \frac{[i(1+i)^n]}{[(1+i)^n - 1]} \tag{3.1b}$$

Multiplying the capital cost by the annualization factor gives the regular annual payment (Towler & Sinnott, 2013).

C_f^I ($/km) represents the capital cost per kilometre for freight mode f, and $z_{sp,f}$ is a binary variable indicating whether the model selects freight mode f to transport feedstock from supply point sp.

Equation (3.2) was developed to account for the CO_2 emissions resulting from the transportation of feedstock. In the equation, the quantity of feedstock is multiplied by the total

distance travelled and the emission factor EF_f (gCO_2/kg·km) for each transport mode, summed over all supply points sp and all seasons s.

$$E_{SCN} = \sum_{sp \in SP} \sum_{s \in S} \left[\frac{x_{sp,f,s}}{\frac{\eta^{bl} \cdot NCV_{sp}}{n}} \right] \cdot \tau_f \cdot D_{sp} \cdot EF_f \qquad sp \in SP, s \in S \qquad (3.2)$$

The integration of the supply chain network with the CHP subnetwork of the polygeneration hub was modelled using Equation (3.3). The demand of feedstock by the boiler, $bd_{sp,s}$ (kW), in the CHP serves as the link.

$$\sum_{f \in F} x_{sp,f,s} \geq bd_{sp,s} \qquad f \in F, sp \in SP, s \in S \qquad (3.3)$$

Equation (3.4) introduces a logical constraint to ensure that the total feedstock quantity $x_{sp,f,s}$ transported from supply point sp via freight mode f during season s does not exceed the feedstock capacity $Cap_{sp,s}$ (kg) available at sp in that season.

$$\sum_{f \in F} x_{sp,f,s} \leq Cap_{sp,s} \left[\frac{\eta^{bl} \cdot NCV_{sp}}{n \cdot DS_s} \right] \qquad f \in F, sp \in SP, s \in S \qquad (3.4)$$

3.3.2 CHP model equations

The combined heat and power generation model is based on the work of (Edgar, Himmelblau & Lasdon, 2001). This model incorporates two turbines: turbine 1 is a double-extraction turbine, while turbine 2 features a single extraction. Several operational constraints are considered, including the maximum internal and exit flow rates for the turbines. Equation (3.5) represents the mass balance for the CHP fuel, where HPS_{Tot} (kg/s) denotes the total high-pressure steam produced, and ΔH_{sp} (kW) represents the energy demand of the boiler. Additionally, Equation (3.6) establishes a connection between the boiler's energy requirement and the fuel supply for the SCN.

$$\Delta H_{sp} = \sum_{s \in S} bd_{sp,s} \qquad sp \in SP, s \in S \qquad (3.6)$$

$$HPS_{Tot} = \sum_{sp \in SP} \frac{\Delta H_{sp}}{NCV_{sp} \cdot 3600} \qquad sp \in SP \qquad (3.5)$$

Equation (3.7) represents the steam mass balance between the boiler and the turbines. In this balance, HEN_{Fin}^{1} denotes the high-pressure steam supplied to the heat exchanger network, while *MPS* and *LPS* refer to the medium-pressure steam and low-pressure steam exiting the turbines, respectively. All quantities in this equation are expressed in kg/s.

$$HPS_{Tot} = HEN_{Fin}^{1} + MPS + LPS \tag{3.7}$$

In Equation (3.8a), *P* represents power, with the superscripts T1, and T2 indicating power generated by turbine 1 and turbine 2, respectively. $P^{Purchased}$ denotes additional power procured from the grid, while P^{Demand} represents the total power requirement. This equation ensures that the total power supply satisfies the demand. To satisfy the electricity demand, power can be procured from an external producer, with a minimum purchase requirement, base-purchased power (BSSP), of 12,000 kW. If the system's demand falls below this threshold, any unused electricity will incur a penalty cost. This constraint is represented in equation (3.8b), where *EP* is excess power.

$$P^{T1} + P^{T2} + P^{Purchased} \geq P^{Demand} \tag{3.8a}$$

$$EP + P^{Purchased} \geq BSSP \tag{3.8b}$$

The model presented in Edgar et al., (2001) assumes that the LPS and MPS leaving the turbines is at superheated conditions. To make this steam suitable for other heating applications, it must be desuperheated to saturated conditions. This adjustment enables the use of the latent heat of condensation for heating other streams. In this model, desuperheating is achieved by injecting a water spray, with the water assumed to be at 25 ℃. The quantity of water required for this process is calculated using a method outlined in Donohue, (2001), as described in Equation (3.9). W^{F} is the mass flowrate (kg/s) of spray water, H^{LPS} and H^{LPSd} denote the enthalpy (kJ/kg) of superheated and desuperheated steam, this notation is similar for MPS and HPS. H^{W} is the enthalpy (kJ/kg) of spray water at 25℃. Desuperheated LPS can be supplied to the absorption refrigeration unit and the heat exchanger network, whilst desuperheated HPS and MPS can be supplied to the heat exchanger network.

$$W^{F} = \left[LPS \cdot \frac{H^{LPS} - H^{LPSd}}{H^{LPSd} - H^{W}}\right] + \left[MPS \cdot \frac{H^{MPS} - H^{MPSd}}{H^{MPSd} - H^{W}}\right] + \left[HEN_{Fin}^{1} \cdot \frac{H^{HPS} - H^{HPSd}}{H^{HPSd} - H^{W}}\right] \tag{3.9}$$

Edgar, Himmelblau & Lasdon, (2001) did not account for the condensation of spend steam to complete the Rankine cycle. In this study, Equations (3.10) to (3.12) detail the calculation of the condensation cost for the CHP's excess steam. The first step, shown in Equation (3.10), determines the required flowrate of cooling water. Here, FCL_{LPS} represents the cooling water flowrate needed to condense the LPS, while F_{LPS} denotes the LPS flowrate. The enthalpy of vaporisation of LPS at its specific temperature and pressure is $\mathrm{H_{vap}}$. The cooling water's heat capacity and temperature change are denoted as $\mathrm{CP_{wt}}$ and ΔT_{wt} respectively.

$$FCL_{LPS} = \frac{F_{LPS} \cdot H_{vap}}{CP_{wt} \cdot \Delta T_{wt}} \tag{3.10}$$

The second step involves calculating the area of the condenser heat exchangers, as shown in Equation (3.11). Here, A_{LPS} represents the heat exchanger area for the LPS condenser, $\mathrm{U_{Cnd}}$ is the heat transfer coefficient, and ΔT_{lm} is the logarithmic mean temperature difference, determined using Chen's approximation (Chen, 1987).

$$A_{LPS} = \frac{FCL_{LPS} \cdot \Delta T_{wt} \cdot CP_{wt}}{U_{Cnd} \cdot \Delta T_{lm}} \tag{3.11}$$

Equations (3.10) and (3.11) are similarly applied to determine the cooling water flowrate and heat exchanger area required for condensing MPS and HPS. The overall capital cost for condensation is evaluated by Equation (3.12). CI_{cnd} denotes the capital cost for the condensers, $\mathrm{FI_{cnd}}$ is the fixed investment cost, EcndL , EcndM, and EcndH are the area cost indices, and $\mathrm{VI_{cnd}}$ is the variable investment cost.

$$CI_{cnd} = FI_{cnd} + \left(A_{LPS}{}^{EcndL} + A_{MPS}{}^{EcndM} + A_{HPS}{}^{EcndH}\right) \cdot VI_{cnd} \tag{3.12}$$

An enhancement to the CHP model incorporates solar aided pre-heating of the boiler feed water. In this setup, a solar collector heats a capture fluid, which then transfers heat to the feedwater. Equation (3.13) calculates the required area of the solar collector. This is an empirical second order expression based on the Hottel Whillier - Bliss equation. The equation compensates for nonlinearities in heat loss and is originally adopted from Smith & Weiss, (1977). Where A_{sc} is the area of the collector, Q_{SA} is the heat (kW) exchanged between the working fluid and process stream where solar is applied. η_0 is the collector efficiency, Global horizontal irradiation (GHI) represents the amount of solar radiation accessible at a

specific installation site. T_c is the average of temperatures of the boiler feed water before and after pre-heating. T_a is the ambient temperature. a_1 and a_2 are thermal loss coefficients

$$A_{sc} \geq \frac{Q_{SA}}{\eta_0(GHI) - a_1(T_c - T_a) - a_2(T_c - T_a)^2} \tag{3.13}$$

Equation (3.14) calculates the heat, Q_{SA} (kW) transferred from the solar collector to the capture fluid. In this equation, F_{SA} represents the mass flowrate (kg/s), C_p denotes the heat capacity (kJ/kg·°C), and T_{2SA} and T_{1SA} are the final and initial temperatures (°C) of the boiler feed water that has been preheated by solar thermal energy. The binary variable z_{SA} indicates whether solar thermal energy will be included in the model solution.

$$Q_{SA} = F_{SA} \cdot C_{pf} \cdot (T_{2SA} - T_{1SA}) \cdot z_{SA} \tag{3.14}$$

Equation (3.15) calculates the volume of thermal storage tank, V_{TS} (m^3) for the capture fluid. In this equation, C_p, ρ, T^s and T^t represent the heat capacity (kJ/kg.°C), density (kg/m^3), and the supply and target temperatures (°C) for the capture fluid respectively. The term Q_{SA} is divided by two based on the assumption that only half of the solar energy is used to regenerate the thermal storage tank. Furthermore, the thermal storage tank is assumed to provide the necessary pre-heating during periods when solar energy is unavailable.

$$V_{TS} \geq \frac{\left(Q_{SA}/_2\right)}{C_p \cdot \rho \cdot (T^s - T^t)} \tag{3.15}$$

Equation (3.16) calculates the area of the heat exchanger between the capture fluid and the feedwater. Here, A_{SA} is the area (m^3) of the heat exchanger, $LMTD_{SA}$ is the logarithmic mean temperature difference (°C) between the capture fluid and the feedwater, and U_{SA} is the heat transfer coefficient ($kW/(m^2.°C)$) between the capture fluid and feedwater.

$$A_{SA} \geq \frac{Q_{SA}}{LMTD_{SA} \cdot U_{SA}} \tag{3.16}$$

To incorporate the effect of solar pre-heating, Equation (3.6) is modified to Equation (3.17). This adjustment ensures that only the amount of fuel required to meet the reduced boiler demand, after accounting for the solar pre-heating, is transported through the supply chain network.

$$\Delta H_{sp} - \frac{Q_{SA}}{2} = \sum_{s \in S} bd_{sp,s} \qquad sp \in SP, s \in S \qquad (3.17)$$

Equation (3.18) calculates the capital cost for the solar aided power generation, CI_{SA} (\$/y). In this equation, AF_{SA} denotes the annualization factor, C_{SC} is the capital cost per unit area (\$/m^2) for the solar collector, and C_{TS} represents the capital cost per unit volume (\$/m^3) for the thermal storage tank. C_H is the cost per unit area (\$/m^2) for the heat exchanger, and CI is the cost index.

$$CI_{SA} = AF_{SA} \cdot [(A_{SC} \cdot C_{SC}) + (V_{TS} \cdot C_{TS}) + (C_H \cdot {A_{SA}}^{CI})] \qquad (3.18)$$

Equation (3.19) is used to compute the capital cost of the CHP, denoted as CI_{CHP} (\$/y). The first term calculates the boiler's investment cost, where a_{Bl} and b_{Bl} are boiler-related constants and e1 is the corresponding exponent with values of 130 000, 53 and 0.9 respectively. The second term calculates the investment cost for the turbines, with a_T and b_T as constants with values of -14 000 and 1 900, P^T is power generated by the turbine and e2 as the exponent, 0.75 (Towler & Sinnott, 2021). This is summed over both turbines in the model. AF_{CHP} represents an annualization factor for the CHP.

$$CI_{CHP} = \Bigg\{ [a_{Bl} + b_{Bl} \cdot (HPS_{Tot} \cdot 3600)^{e1}] + \left[\sum_T a_T + b_T \cdot (P^T)^{e2} + CI_{cnd} \right] \Bigg\} \cdot AF_{CHP} + CI_{SA} \qquad (3.19)$$

Equation (3.20) calculates the total annual cost for the combined SCN and CHP. In this equation, $C_{SCN}^{F,V,I}$, represents the total annual cost (\$/y) for the supply chain network, and CI_{CHP}, is the annualized investment cost (\$/y) for the CHP subnetwork. *WTC* denotes the total cost of water used in the polygeneration hub, which is calculated as the product of the sum of HPS_{Tot} and W^F, and the unit cost of water. The cost of purchased power, $P^{Purchased}$ is 0.0239 \$/(kW·h) and the penalty cost per unit of unused purchased power, *EP* is 0.00983 \$/(kW·h). The annual number of operating hours (8,160) is denoted by n. The unit costs of *PP* and *EP* are adapted from (Edgar, Himmelblau & Lasdon, 2001).

$$\dot{TAC_{CHP}} = C_{SCN}^{F,V,I} + CI_{CHP} + WTC + \{(0.0239 \cdot P^{Purchased} \cdot n) + (0.00983 \cdot EP \cdot n)\} \qquad (3.20)$$

Equation (3.21) calculates the carbon emissions from the combustion of fuel in the boiler, E_{CHP}. The quantity of feedstock, converted to kilograms, is multiplied by the percentage composition of non-oxidised carbon in the fuel, C^{comp}, and the ratio of the molecular mass of CO_2 to that of carbon, 3.67.

$$E_{CHP} = \sum_{f \in F} \sum_{s \in S} \left[\frac{x_{sp,f,s}}{\frac{\eta^{bl} \cdot NCV_{sp}}{n}} \right] \cdot C^{comp} \cdot 3.67 \qquad f \in F, s \in S, sp \in SP \tag{3.21}$$

3.3.3 MEE model equations

The multi-effect evaporation unit is modelled based on the work by El-Halwagi, (2017). The overall heat load of the MEE is calculated using Equations (3.22a) and (3.22b).

$$Q_{MEE} = F^{dist} \times \lambda_{ave} \tag{3.22a}$$

In Equation (3.22a), Q_{MEE} (kW) is the total heat load of the MEE, F^{dist} is the distillate flowrate (kg/s) and λ_{ave} is the average latent heat of condensation (kJ/kg) for the distillate.

$$Q_{MEE} = N^{EFF} \times U^{HTFFE} \times A_{HTFFE} \times \Delta T_{ave} \tag{3.22b}$$

In Equation (3.22b), N^{EFF} is the total number of effects and must be an integer, U^{HTFFE} is the overall heat transfer coefficient (kW/m^{2}K) of the heating tubes, A_{HTFFE} is the area (m^2) of heat exchange and ΔT_{ave} is the average distillate temperature (K) over all the effects.

Equations (3.23) to (3.25) detail the calculation of λ_{ave}, U^{HTFFE}, and ΔT_{VAC}.

$$\lambda_{ave} = -2.7532 \times TV_{ave} + 3278.8 \tag{3.23}$$

$$U^{HTFFE} = 0.8552 + 0.0047 \times TV_{ave} \tag{3.24}$$

$$\Delta T_{ave} = \frac{TV_1 - TV_f}{N^{EFF}} \tag{3.25}$$

TV_{ave} is the average distillate temperature (K), TV_1 is the temperature of the first distillate and TV_f is the condensation temperature (K) of the final distillate. *AFC*, the evaporator's fixed cost, and *AOC*, the annual operating cost, are evaluated using Equations (3.26) and (3.27).

$$AFC = N^{EFF} \times 600 \times A_{HTFFE}^{0.6} \tag{3.26}$$

$$AOC = C^{Stm} \times F^{Stm} \times A_{HTFFE}^{0.6} \times 3600 \times n \tag{3.27}$$

Where C^{Stm} is the cost of steam ($/kg), F^{Stm} is the flowrate of MEE feed steam (kg/s) and n is the number of operating hours in a year.

Equation (3.28) shows the calculation of steam feed flowrate, F^{Stm} to the MEE. Where F^{dist} is the distillate flowrate (kg/s), and GOR is the gained output ratio.

$$F^{Stm} = \frac{F^{dist}}{GOR} \tag{3.28}$$

A mass and component balance of the MEE is shown by Equation (3.29) and (3.30).

$$F^{dist} = F^{SwF} - F^{Brine} \tag{3.29}$$

$$x_F F^{SwF} = x_B F^{Brine} \tag{3.30}$$

F^{SwF} and F^{Brine} are the flowrates of saltwater feed and brine whilst x_F and x_B are the mass fractions of brine in the feed and in the brine solution.

Installation costs for piping for the subnetworks were evaluated using equations modified from Chang et al., (2018). MEE, ARS, and HEN can be connected to the CHP via pipes for hot utility supply, and the HEN can be connected to the ARS for cold utility as shown in Figure 3.1. Alternatively, these subnetworks could connect to an external utility source. Equations (3.31) through (3.34) are applied to the MEE seawater feed stream, and the MEE, HEN and ARS utility feed streams. First, the internal pipe diameter (m) is calculated using Equation (3.31). In this equation, D^{in} is the internal diameter, F, CP and ρ denote the flowrate (kg/s), heat capacity and density (kg/m^3) of fluid in the pipe, in this case LPS, MPS and HPS for utility, and chilled water for cold utility.

$$D^{in} \geq F^{0.45} \cdot CP^{-0.45} \cdot \rho^{-0.32} \tag{3.31}$$

The external diameter D^{ext} is evaluated from Equation (3.32).

$$D^{ext} \geq 1.101 \cdot D^{in} + 0.006349 \tag{3.32}$$

Equations (3.33) and (3.34) calculate the pipe weight per unit length, W (kg/m) and cost of piping per unit length, P_{cst} ($/m).

$$W = 1330 \cdot D^{in^2} + 75.18 \cdot D^{in} + 0.9268 \quad (3.33)$$

$$P_{cst} = A_1 \cdot W + A_2 \cdot D^{ext^{0.48}} + A_3 + A_4 \cdot D^{ext} \quad (3.34)$$

Where A_1, A_2, A_3 and A_4 are cost parameters obtained from (Chang et al., 2018). The respective annualized piping capital costs are calculated from respective annualization factors and piping distances.

The total annual cost for the MEE is calculated using Equation (3.35), where AF_{MEE} is the annualization factor for the MEE and P_{MEE} is the piping cost for the MEE.

$$TAC_{MEE} = (AFC \cdot AF_{MEE}) + AOC + P_{MEE} \quad (3.35)$$

3.3.4 ARS model equations

The absorption refrigeration model was developed from correlations outlined in Florides et al., (2003) and it is based on Figure 3.1 which depicts the streams referred to in the equations evaluating the different state points. A detailed model of the absorption refrigeration system is essential for accurately assessing its integration within the broader energy network. Absorption refrigeration operates through intricate thermodynamic mechanisms, which encompass concurrent heat and mass transfer alongside phase transitions of the working fluids. These detailed interactions play a crucial role in determining the system's overall efficiency and functionality. Accurate modelling is essential to effectively capture these processes, allowing for energy flow optimization and enhancing the reliability of performance forecasts (Madu et al., 2020). Equations (3.36) to (3.45) demonstrate the calculation of mass and energy balance, and properties of internal streams i.e., 1 to 11. m_{10} denotes the mass flowrate (kg/s) in stream 10 and H_{10} is the enthalpy of stream 10 in kJ/kg, T_{10} is the temperature of stream 10 in ℃ and P_{10} is the pressure of stream 10 in kPa. This nomenclature applies to all streams described in the ARS model. In order to perform calculations for the different stream properties, the model needed input parameters for Q_{evap}, T_{10}, T_4, T_7, T_3, x_1, x_3, and x_4. Where Q_{evap} is the overall heat duty of the evaporator, and T and x are the temperature and mole fraction of Li-Br for the respective streams. The following assumptions are made to assess the performance of the ARS, and approximate unit sizes.

1. There are no heat losses to the environment.
2. Streams, 1, 4, 8 and 11 contain saturated liquid.
3. Stream 10 is purely saturated vapour.

4. Pure water serves as the refrigerant.
5. Significant pressure changes only occur through flow restrictors and the pump.
6. Flow restrictors are adiabatic.
7. The pump follows an isentropic model.

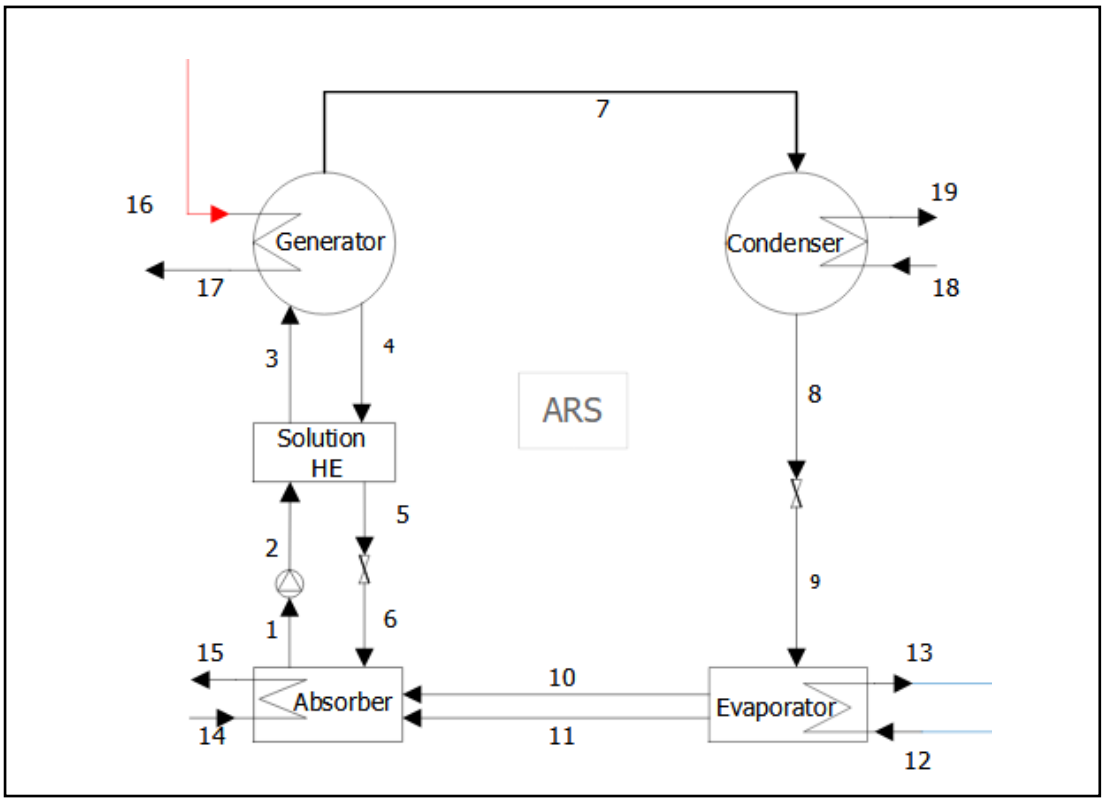

Figure 3.2: Lithium-bromide absorption refrigeration system

For the analysis around the evaporator, T_{10} is known, and the enthalpy of saturated water vapor in stream 10, H_{10} is calculated from Equation (A1.1) in the appendices. Stream 11 contains condensed vapor and is therefore a liquid at the temperature of stream 10. H_{11} is determined by subtracting the latent heat of condensation from the vapor enthalpy, as described in Equation (A1.2). For stream 9, the enthalpy, H_9, is assumed to be equal to H_8 based on the adiabatic nature of the throttling process. To calculate H_8, the pressure P_8 is first determined. With x_4 and T_4 known, P_4 and H_4 are obtained from Equations (A2.1) and (A3.1) respectively. Since P_4 is equal to P_8, H_8 is obtained by subtracting the enthalpy of condensation from H_7 as shown in Equation (A1.1).

Equations (3.36) and (3.37) show the mass and energy balance around the evaporator. m_{11} is assumed to be 2.5% of m_{10} hence with all other values known, it can be calculated.

$$m_9 = m_{10} + m_{11} \tag{3.36}$$

$$Q_{evap} = \ m_{10}H_{10} + m_{11}H_{11} - m_9H_9 \tag{3.37}$$

For the analysis around the absorber, the mass and component balance around the unit is shown by Equations (3.38) and (3.39), with x_6 equal to x_4.

$$x_1m_1 = \ x_6m_6 \tag{3.39}$$

$$m_1 = \ m_{10} + m_{11} + m_6 \tag{3.38}$$

An energy balance is required to evaluate the rate of heat transfer in the absorber. H_1 is obtained using x_1 through Equations (A2.3), (A2.2) with T_1 as T_{sol} and (A3.1). P_1 is assumed to be equal to P_{10}. Based on the adiabatic throttling process, H_6 is equal to H_5, and H_5 can be obtained from the solution heat exchanger energy balance in Equation (3.40).

$$m_2H_2 + m_4H_4 = \ m_3H_3 + m_5H_5 \tag{3.40}$$

Given that T_3 is a known input value, and mass fraction is constant from stream 1 to 3, Equation (A3.1) can be used to evaluate H_3. Since T_1 is equal to T_2, H_2 can also be evaluated from (A3.1) and is found to be equal to H_1. This allows Equation (3.40) to be solved for H_5, and T_5 to be calculated from Equation (A3.1). The pump's power requirements are computed using Equation (3.41) where w is the minimum work input (W) and v_1 is the specific volume calculated using Equation (A4.1).

$$w = \ m_1v_1(P_2 - P_1) \tag{3.41}$$

Equation (3.42) shows the total energy balance around the absorber. Where Q_{abs} is the absorber's heat duty in kW.

$$Q_{abs} = \ m_{10}H_{10} + m_{11}H_{11} + m_6H_6 - m_1H_1 \tag{3.42}$$

The overall heat balance on the generator is shown by Equation (3.43), with Q_{gen} as the generator heat duty in kW.

$$Q_{gen} = \ m_4H_4 + m_7H_7 - m_3H_3 \tag{3.43}$$

For the condenser and solution heat exchanger, the heat duty Q_{con} and Q_{SHX} is calculated from Equations (3.44) and (3.45).

$$Q_{con} = \ m_7(H_7 - H_8) \tag{3.44}$$

$$Q_{SHX} = \ m_3(H_3 - H_2) \tag{3.45}$$

For the external streams (12 to 19) T_{12} to T_{19} are input parameters and therefore the respective enthalpies can be obtained from steam tables with known pressure values. T_{12} and T_{13} are obtained from the inlet and outlet temperature of the cold utility in the heat exchanger network. T_{14} and T_{18} are arbitrary input values for cooling water. T_{16} is obtained from the temperature of desuperheated LPS from the combined heat and power generation plant. The mass flow rates of these streams are calculated from the unit energy balance Equations, (3.46) - (3.48).

$$m_{14} = \frac{Q_{abs}}{(H_{15} - H_{14})} \tag{3.46}$$

$$m_{16} = \frac{Q_{gen}}{(H_{16} - H_{17})} \tag{3.47}$$

$$m_{18} = \frac{Q_{con}}{(H_{19} - H_{18})} \tag{3.48}$$

The ARS units were designed as heat exchangers using Equation (3.49), where A_{ARS} represents the heat transfer area in m^2, U is the overall heat transfer coefficient and ΔT_{lm} is the log mean temperature difference determined by Equation (3.50). Here, ΔT_{in} and ΔT_{out} refer to the temperature differences between the hot stream and cold stream at the heat exchanger's inlet and outlet. By using heat transfer coefficient values obtained from literature, the model can calculate the heat transfer area as a variable.

$$Q = A_{ARS} \cdot U \cdot \Delta T_{lm} \tag{3.49}$$

$$\Delta T_{lm} = \frac{\Delta T_{in} - \Delta T_{out}}{\ln\left(\frac{\Delta T_{in}}{\Delta T_{out}}\right)} \tag{3.50}$$

For the absorber, the hot fluid inlet temperature depends on the temperatures of streams 6, 10 and 11. This is determined using Equation (A2.2) using x_6 with T_{10} as T_{ref} and the combined solution temperature as T_{sol}. A similar calculation can be done to determine the temperature of the cold fluid exiting the generator.

The total annual cost for the ARS is calculated using Equation (3.51).

$$C_{ARS} = AF_{ars} \cdot \left(5C_{HI} + \sum_{ars} A^{CI} \cdot C_H \right) + P_{ars} \qquad ars \in ARS \qquad (3.51)$$

In this equation, AF_{ars} represents the annualization factor for the ARS, C_{HI} denotes the fixed installation cost of the heat exchanger ($), A is the heat transfer area (m^2), CI denotes the cost index for heat exchanger area, C_H is the cost per unit area of the heat exchanger ($/m^2$), and P_{ars} represents the piping cost for the ARS in $.

A mass balance on LPS that links the ARS, MEE, HEN, and the CHP is shown in Equation (3.52). Where m_{LPS}, m_{16}, m_{HEN3} and F^{Stm} are the flow rates of LPS from the CHP to the ARS, HEN and MEE respectively.

$$m_{LPS} - m_{16} - m_{HEN3} - F^{Stm} = 0 \qquad (3.52)$$

3.3.5 HEN model equations

The heat exchanger network model, adapted from Isafiade et al., (2015), incorporates three indices, i for hot streams, j for cold streams, and k for superstructure stages. These indices are denoted as sets within the model. The overall stream energy balance is shown in Equations (3.53) for hot streams and (3.54) for cold streams.

$$\left(T_i^{in} - T_i^{out}\right) \cdot F_i = \sum_{j=J} \sum_{k=K} q_{i,j,k} \qquad i \in I, \qquad (3.53)$$

$$\left(T_j^{in} - T_j^{out}\right) \cdot F_j = \sum_{i=I} \sum_{k=K} q_{i,j,k} \qquad j \in J, \qquad (3.54)$$

T_i^{in} and T_i^{out} denote the inlet and outlet temperatures of hot stream i, while T_j^{in} and T_j^{out} represent the inlet and outlet temperatures of cold stream j. F_i and F_j represent the heat capacity flowrates of the respective streams. The variable $q_{i,j,k}$ represents the heat exchanged between hot stream i, and cold stream j, at stage k of the stagewise superstructure described by (Yee & Grossmann, 1990).

Equations (3.55) and (3.56) show the heat balance for each stage or temperature location k. Where $t_{i,k}$ and $t_{i,k+1}$ represent the temperature of hot stream i, in stage k, and in the following stage k + 1. This is similar for cold stream j with $t_{j,k}$ and $t_{j,k+1}$.

$$\left(t_{i,k} - t_{i,k+1}\right) \cdot F_i = \sum_{j=J} q_{i,j,k} \qquad i \in I, k \in K \qquad (3.55)$$

$$\left(t_{j,k} - t_{j,k+1}\right) \cdot F_j = \sum_{i=I} q_{i,j,k} \qquad j \in J, k \in K \qquad (3.56)$$

The HEN model requires assignment of inlet temperatures to the superstructure for both hot and cold streams. In the initial stage (k = 1), the supply temperatures of hot streams i, are assigned, while in the final stage (k = NOK + 1), the supply temperatures of the cold streams j, are assigned. These temperature assignments are defined by Equations (3.57) and (3.58).

$$T_i^{in} = t_{i,1} \qquad i \in I \qquad (3.57)$$

$$T_j^{in} = t_{j,NOK+1} \qquad j \in J \qquad (3.58)$$

To maintain feasibility, the temperatures of hot streams are constrained to decrease progressively from left to right, while the temperatures of cold streams are set to increase from right to left. This ensures monotonicity in the temperature profiles as outlined in Equations (3.59) and (3.60).

$$t_{i,k} \geq t_{i,k+1} \qquad i \in I, k \in K \qquad (3.59)$$

$$t_{j,k} \geq t_{j,k+1} \qquad j \in J, k \in K \qquad (3.60)$$

For heat exchange to take place between a hot and cold stream at a given stage, the streams must be matched. This matching is governed by the binary variable $y_{i,j,k}$ along with a logical constraint that restricts the amount of heat exchanged. The heat transfer is limited to the minimum available heat (Ω) in the participating streams. This relationship is described by the logical constraint in Equation (3.61).

$$\Omega \cdot y_{i,j,k} \leq 0 \qquad i \in I, j \in J, k \in K \qquad (3.61)$$

To guarantee feasible matches between streams, the minimum approach temperatures of heat exchangers must be constrained. These constraints determine the driving force for heat

exchange and are activated in the model by the binary variable $y_{i,j,k}$. Equations (3.62) and (3.63) detail the calculations for the minimum approach temperature at the hot and cold ends.

$$dt_{i,j,k} \leq t_{i,k} - t_{j,k} + \gamma(1 - y_{i,j,k}) \qquad i \in I, j \in J, k \in K \tag{3.62}$$

$$dt_{i,j,k+1} \leq t_{i,k+1} - t_{j,k+1} + \gamma(1 - y_{i,j,k}) \qquad i \in I, j \in J, k \in K \tag{3.63}$$

In these equations, γ represents the upper bound for the approach temperature. This bound, in conjunction with the binary variable $y_{i,j,k}$, ensures that all driving forces within the network remain non-negative, thereby maintaining feasibility. When no match exists between a hot stream and a cold stream, $y_{i,j,k}$ is set to zero and γ is the value of the approach temperature. To prevent an infinitely large heat exchanger area, a lower bound for the approach temperatures must also be defined. This minimum approach temperature bound, Emat, is expressed in Equation (3.64).

$$dt_{i,j,k+1} \geq Emat \qquad i \in I, j \in J, k \in K \tag{3.64}$$

An approximation of the *LMTD* is needed to calculate the heat exchanger area. For this section, Chen's approximation (Chen, 1987) shown in Equation (3.65) is used.

$$LMTD_{i,j,k} = \left[\frac{(dt_{i,j,k}) \cdot (dt_{i,j,k+1}) \cdot (dt_{i,j,k} + dt_{i,j,k+1})}{2}\right]^{\frac{1}{3}} \tag{3.65}$$

The total annual cost for the HEN, C_{HEN}, is calculated from Equation (3.66).

$$C_{HEN} = AF_{HEN}\left\{CF\sum_{i\in I}\sum_{j\in J}\sum_{k\in K} y_{i,j,k} + AC\sum_{i\in I}\sum_{j\in J}\sum_{k\in K} A^{AE}\right\} + \left\{\sum_{i\in I}\sum_{j\in J}\sum_{k\in K} C_j \cdot q_{i,j,k}\right\} + \left\{\sum_{i\in I}\sum_{j\in J}\sum_{k\in K} C_i \cdot q_{i,j,k}\right\} \tag{3.66}$$

In this equation, AF_{HEN} represents the annualization factor for the heat exchanger capital costs. CF is the fixed installation cost for heat exchangers ($), and AC is the variable cost for heat exchanger units ($/m^2). A (m^2) is the heat exchanger area, AE is the cost exponent for heat exchangers, and C_j and C_i are the costs for cold and hot utility ($/kW). The HEN is connected

to a source of hot utility by Equations (3.67) and (3.68). This can be the CHP, or an alternative external source.

$$HEN^{Huin} = \sum_{j \in J} \sum_{k \in K} q_{i(hu),j,k} \tag{3.67}$$

$$HEN^{Huin} = m_{HEN} \cdot H_{HEN} \tag{3.69}$$

HEN^{Huin} represents the energy (kW) in the steam supplied as hot utility to the HEN, and m_{HEN} and H_{HEN} are the flowrate (kg/s) and enthalpy (kJ/kg) of steam supplied to the HEN. $q_{i(hu),j,k}$ denotes the heat exchanged between hot utility stream i(hu), and cold stream j, at stage k of the superstructure. This equation is applied to the LPS, MPS, and HPS supplied to the HEN. A similar equation connects the HEN to a source of chilled water (cold utility), which can be the ARS or an external supply.

Chapter 4

Multi-objective Optimisation Case Study

4.0 Multi-Objective Optimisation Case Study

4.1 Case Description

In this case study the model was applied to a scenario involving four feedstocks: sewage sludge, forestry residue, biogas, and coal. Each renewable feedstock is situated at a specific distance from the polygeneration hub and exhibits varying costs and seasonal availability across 3 agricultural periods as detailed in Table 4.1. The lower heating value, LHV, or net calorific value of each feedstock is measured in kWh/kg. These values are obtained from Table 4.2 and converted to kWh/kg. Throughout the seasons, coal acts as a backup fuel to address any shortfalls in renewable feedstock supply. The carbon composition for the feedstocks is shown in Table B1 in the appendices. Table 4.3 outlines available transportation modes and their associated cost parameters, tortuosity, and return trip factors. The annualization factor, AF, is used to calculate investment costs for the transport network, T_f^{FC} (\$/t) and T_f^{VC} (\$/t·km) are the fixed and variable costs associated with transportation. T_f^{IC} (\$/km) is the investment cost for the transportation network, τ_f is the tortuosity factor that accounts for route curvature, and t_{RF} is the return trip factor which considers the distance for return trips to the supply points. In this case, the polygeneration hub is owned by a single entity that purchases feedstock and supplies utilities to industrial and residential demand.

The polygeneration hub is comprised of a boiler for high pressure steam generation, a set of turbines for power generation, an MEE for saltwater desalination, and an ARS for cold utility generation. The demand node is a set power demand and a HEN that requires hot and cold utility. The HEN in the hypothetical process plant includes 2 hot process streams and 2 cold process streams. The hot utilities consist of LPS and MPS from the two turbines in the polygeneration hub, along with a branch of HPS that is diverted directly from the boiler to the HEN via a desuperheater. The LPS stream is divided, with on portion feeding into the generator of the ARS and MEE subnetworks while the other portion supplies the HEN. The HEN incorporates 3 cold utility streams, sourced externally. Cooling for the ARS absorber and condenser (streams 15 and 19) is assumed to be facilitated through a system connected to a cooling tower. The connection between the polygeneration hub and the HEN consists of the three hot utility streams. Specifications of the process plant streams are detailed in Table 4.5. The initial input parameters of the ARS are provided in Table 4.6, where the liquid carryover from the evaporator is assumed to be 2.5 % of the vapor leaving the evaporator (m_{10}), which is treated as a variable.

Table 4.1: Supply chain feedstock data

Feedstock		Season 1		Season 2		Season 3	
	LHV (kWh/kg)	Cost ($/kg)	Capacity ($\times 10^6$ kg)	Cost ($/kg)	Capacity ($\times 10^6$ kg)	Cost ($/kg)	Capacity ($\times 10^6$ kg)
Sewage sludge	4.52	0.024	3	0.022	4.5	0.027	2
Forestry residue	4.95	0.040	250	0.045	210	0.025	30
Biogas	5.08	0.050	450	0.03	500	0.07	2,000
Coal	7.20	0.900	50	0.9	50	0.9	50

Table 4.2: Fuel LHVs

Fuel	**LHV (MJ/kg)**
Sewage sludge	12.51 (Zakaria, Hassan & Nor, 2015)
Forestry industry waste (bark)	5.9 (Gavrilescu, 2008)
Industrial sludge (pulp industry)	8.73 (Kurniawan, Hakiki & Sidjabat, 2018)
Sawdust	7.89 (Fleischman, Botha & Germanis, 2014)
Shredded bagasse	7.58 (Fleischman, Botha & Germanis, 2014)
Biogas	35 - 37 (Ferrer et al., 2011)

Table 4.3: Supply chain transport data (adopted from Cowen et al., 2019)

Transport mode	Transport Parameters					
	AF	T_f^{FC}($/t)	T_f^{VC}($/t·km)	T_f^{IC}($/km)	τ_f	t_{RF}
Truck	0.20	2	0.0900	5,000	1.27	2
Railway	0.25	5	0.0070	50,000	1.10	2
Pipeline	0.50	0	0.0001	1.5×10^5	1.27	1

AF in Table 4.3 is calculated from the discount rates 10 %, 15 % and 23 % for road, railway, and pipeline, whilst annualization is done over 10 y, 7 y, and 3 y. A discount rate of 30 % was used for the heat exchangers, boiler, and turbines over 10 y. The emission factors, EF_f (gCO_2/kg·km) for road and rail are 72 and 35 respectively based on the range of values presented in Table 4.4.

Table 4.4: Estimates of the CO2-intensity of Freight Transport Modes (g CO2 per tonne-km)

	Air (short haul<452 km)	**Air (medium haul 452-1600 km)**	**Air (long haul >1600 km)**	**Inland Water way**	**Sea (short sea)**	**Sea (Ocean ship)**	**Road (>35t)**	**Rail (Diesel)**	**Rail (Electric)**
Dings and Dijkstra 1997	1420	800	-	40	13	-	100	69	38
WBCSD-WRI GHG Protocol	1580	800	570	-	35	10	72	20	40
INFRAS/ IWW 2004	-	673	-	-	31	-	91	38	19
NTM	1925	867	633	-	-	15	51	17	-
IFEU 2005	-	-	-	10	-	4	69	-	34

Sources: Dings and Dijkstra, 1997; INFRAS / IWW, 2004; IFEU, 2005; online calculators were used to derive average values for NTM (www.ntm.a.se) and WBCSD-WRI GHG Protocol (http://www.ghgprotocol.org/calculation-tools).

The streams in the HEN were assumed to have a uniform heat transfer coefficient of 0.5 (kW/(m^{2}·°C)) whilst the ARS heat transfer coefficients of 0.85, 1.50, 1.10, 0.85, and 1.40 (kW/(m^{2}·°C)) for the absorber, evaporator, solution heat exchanger, generator and condenser were adopted from DiPippo, (2008). To ensure maximum heating efficiency, the HPS leaving the boiler and the MPS and LPS from the turbines were desuperheated by addition of water using calculations in Equations (3.9) adopted from (Donohue, 2001).

Table 4.5: Process plant's HEN stream data (adopted from Isafiade and Short (2022))

Hot streams	T_i^s (°C)	T_i^t (°C)	FCP_i (kW/°C)	Cold streams	T_j^s (°C)	T_i^t (°C)	FCP_j (kW/°C)
HU1 (HPS)	257	257	-	C1	25	240	140
HU2 (MPS)	197	197	-	C2	20	250	150
HU3 (LPS)	150	150	-	CU1	50	180	70
H1	155	85	150	CU2	70	100	120
H2	230	40	285	CU3	6.5	10	-

Table 4.6: ARS subnetwork input parameters (adopted from Florides et al., (2003))

Parameter	Symbol	Input Value
Capacity	Q_{evap}	40 kW
Evaporator temperature	T_{10}	6 ℃
Exit temperature of generator solution	T_4	90 ℃
Mass fraction of weak solution	x_1	55% LiBr
Mass fraction of strong solution	x_4	60% LiBr
Exit temperature of solution heat exchanger	T_3	65℃
Generator vapor exit temperature	T_7	85℃
Evaporator liquid carryover	m_{11}	$0.025m_{10}$

Table 4.7 shows the steam properties of superheated steam. Desuperheating is conducted at constant pressure and the desuperheated HPS fed to the HEN has an enthalpy of 2,798.9 kJ/kg, while the desuperheated LPS has an enthalpy of 2,752.78 kJ/kg. The LPS is assumed to be cooled to the desired feed temperatures of 100℃ and 150℃ for the MEE and ARS respectively.

Table 4.7: Superheated steam properties (adopted from Edgar, Himmelblau & Lasdon, (2001))

	Enthalpy (kJ/kg)	**Temp (℃)**	**Pressure (bar)**
HPS	3,162.9	382.2	43.83
MPS	2,948.9	154.4	13.4
LPS	2,910.8	154.4	4.3

4.2 Model Solution

4.2.1 Objective function

The overall model employs a multi-objective function that incorporates both economic and environmental objectives. The economic objective accounts for the total annual operating and capital costs for the SCN, polygeneration network and the HEN. Equation (4.1) shows the economic objective function. $C_{SCN}^{F,V,I}$, C_{ARS}, and C_{HEN} represent the total annual costs (\$/y) for the supply chain network, absorption refrigeration system and heat exchanger network respectively, and CI_{CHP}, represents the annualized investment cost (\$/y) for the combined heat and power generation subnetwork. *WTC* is the total cost of water used in the poly-generation network which is the sum of HPS_{Tot} and W^F multiplied by the unit cost of water. 0.0239 \$/(kW·h) is the unit cost of purchased power *PP*, 0.00983 \$/(kW·h) is the unit cost of the penalty for unused excess power *EP*, while OH is the number of annual operating hours (8,160 h). The values for unit costs of *PP* and *EP* are adapted from Edgar et al., (2001).

$$Min\ TAC = C_{SCN}^{F,V,I} + CI_{CHP} + CI_{SA} + C_{MEE} + C_{ARS} + C_{HEN} + WTC + \{(0.0239 * PP * OH) + (0.00983 * EP * OH)\} \quad (4.1)$$

Equation (4.2) shows the environmental objective function. The environmental impact, EI, is a summation of the transport and boiler emissions and is calculated in kgCO_2/y.

$$Min\ EI = E_{CHP} + E_{SCN} \quad (4.2)$$

Equation (4.3) shows the multi-objective function. The weighted sum method adopted from (Gxavu & Smail, 2012) is used in this model. R_g is a weighting factor between 0 and 1, that determines the model's prioritisation when minimising the multi-objective variable, MO. The model is solved for three scenarios, firstly only TAC is minimised (scenario 1), secondly, only Environmental impact is minimised (scenario 2), and lastly, both TAC and environmental impact are minimised with equal weighting (scenario 3). TAC_{min} and EI_{min} are the most optimal values for total annual cost and environmental impact, obtained by individually minimising the variables.

$$Min\ \dot{M}O = R_g \cdot \left(\frac{TAC}{TAC_{min}}\right) + (1 - R_g) \cdot \left(\frac{EI}{EI_{min}}\right) \quad (4.3)$$

The model comprised of 559 single equations and was solved in General Algebraic Modelling System (GAMS) version 24.4.6. CPLEX and CONOPT solvers, working in conjunction with DICOPT, were used for MIP and NLP respectively and the solution was obtained in 4.73 seconds on an 11th Gen Intel(R) Core (TM) i5-1135G7 @ 2.40GHz processor with 8GB RAM.

4.2.2 Results

Solutions to key variables in the model were extracted to a spreadsheet and analysed. Figure 4.1 shows the distribution of emissions generated in the three scenarios described. Notably, scenario 1 has the highest emissions of 106.69×10^6 (t/y CO_2), as the model prioritises economics whilst neglecting emission reduction. Scenario 2 has the lowest, 69.58×10^6 (t/y CO_2), as emission reduction is the priority, and scenario 3 gives an intermediate value of 73.74×10^6 (t/y CO_2), as there is a trade-off between cost and emissions.

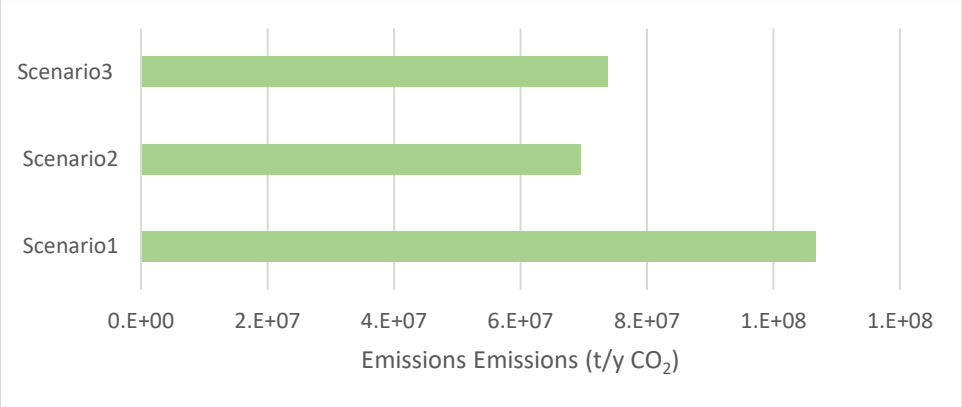

Figure 4.1: Total emissions

Figure 4.2 shows the distribution of emissions in the three scenarios. Transport emissions (T) are highest in scenario 1, with 95.31 % (2.53×10^7 t/y CO_2) resulting from road transport. In scenario 2, road transport emissions are significantly lower, by a margin of 99.90 % with 2.52×10^4 (t/y CO_2). In the third scenario, road transport emissions are 93.10 % lower than scenario 1 and 6,843 % higher than scenario 2. Rail emissions have smaller fluctuations with values of 1.24×10^6, 1.48×10^6 and 1.61×10^6 (t/y CO_2) respectively for the three scenarios. The change in transport emission distribution is subject to the respective emission factors for the transport modes. Road transport has a much higher factor of 72 gCO_2/ton-km compared to rail transport, with 35 gCO_2/ton-km. Scenario 1 uses more of road transport as emissions are not considered in the optimisation and conversely, in scenario 2, there is a decrease in road transport usage and an increase in rail usage.

For boiler emissions (B), forestry residue is the largest contributor in scenario 1, with 4.91×10^7 (t/y CO_2), followed by biogas with 2.94×10^7 (t/y CO_2) and sewage sludge has the lowest contribution with 1.62×10^6 (t/y CO_2). In the second scenario there is a 31.11 % increase in emissions from sewage sludge to 2.13×10^6 t/y CO_2), and a 34.30 % increase in emissions from forestry residue. In the third scenario, sewage sludge-derived emissions have the same value as in scenario 2, forestry residue emissions are 39.03 % and 3.49 % higher than scenarios 1 and 2. Biogas was not used in scenario 2 and 3. The significant decrease in boiler emissions in the second scenario is due to the incorporation of solar aided power generation in the SCN-CHP. The carbon composition of biomass plays a significant role in the selection of energy source. When emission reduction is prioritised, sewage sludge emissions increase as it is used more, due to its lower carbon composition. Biogas, which has the highest carbon composition after coal, is not used at all in scenarios 2 and 3 where emission reduction is part of the objective function.

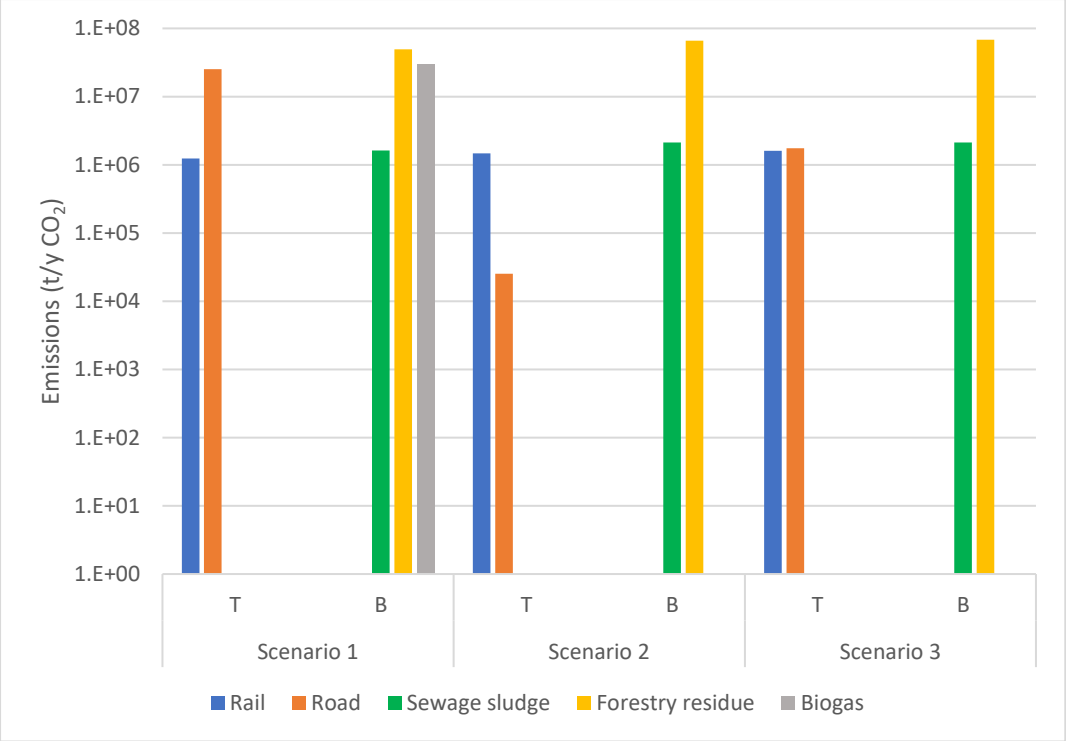

Figure 4.2: Emission distribution for the three scenarios

Table 4.8 shows the energy supplied and the resultant emissions from different energy sources, and Table 4.9 shows solutions to additional SCN-CHP variables for the three scenarios. Scenario 1 has the highest energy, 889,085.59 kW supplied from biomass combustion to generate 50.0 kg/s of HPS, which corresponds to the highest boiler emissions. Scenario 2 has 15.01 % less emissions resulting from the use of solar aided power generation to supply 3068 kW of clean energy, and lower HPS production (48.70 kg/s). It is evident that the model prioritises emission reduction in scenario 2 by lowering HPS production and using solar thermal energy in boiler feed preheating. Additionally, this is shown in the reduction in power generated by the turbines (56.18 % and 52.18 % less than scenario 1 and 3), with the model resorting to purchasing more power externally. In the third scenario, a trade-off between cost and emissions occurs, and solar thermal energy is excluded from the solution. This results in boiler emissions being 3.39 % higher than scenario 2 and 12.19 % lower than scenario 1, showing an intermediate optimal solution. The exclusion of solar thermal energy from the optimal scenario can be attributed to the high surface area required for the solar collector, which results in a higher TAC value for the SCN-CHP. In all scenarios, there was no excess unused power as this was allocated a penalty fee which the model avoided.

Table 4.8: SCN-CHP energy supply and emissions

	Scenario 1		Scenario 2		Scenario 3	
	Energy supplied (kW)	Emissions $\times 10^6$ (t/y CO_2)	Energy supplied (kW)	Emissions $\times 10^6$ (t/y CO_2)	Energy supplied (kW)	Emissions $\times 10^6$ (t/y CO_2)
Sewage sludge	89,023	1.62	116,719	2.13	116,719	2.13
Forestry residue	542,296	49.09	728,508	65.95	753,970	68.25
Biogas	257,766	29.44	0	0	0	0
Solar	0	0	3,068	0	0	0
Total	889,085	80.15	848,295	68.08	870,689	70.38

The total energy used in the three scenarios presented in Table 4.8 varies due to the different objective functions applied in each case. The model optimises the outcomes based on the specific objective function for each scenario while meeting the energy demand. As a result, there may be instances where excess energy is supplied, since the primary focus of the optimisation is not directly on minimising or balancing energy supply. The comparison of the three scenarios remains fair, since the demand is the same in all three scenarios.

Table 4.9: Additional SCN-CHP variables

	Scenario 1	Scenario 2	Scenario 3
HPS (kg/s)	50.00	48.70	49.48
Power (kW)	12,550.00	5,500.00	11,500.00
Purchased Power(kW)	12,000.00	19050.00	13,050.00
Excess Power (kW)	0.00	0.00	0.00
Collector area (m^2)	0.00	10,432	0.00

Figure 4.3 shows an analysis of the TAC for the different scenarios, and the unit numbers in the HEN and MEE. HE represents the heat exchangers in the HEN and Neff represents the number of effects in the MEE. The first scenario has the lowest TAC value of 38.05 $\times 10^6$ \$/y. The model achieves this in part, by minimising the number of effects in the MEE to 4 units, and the HEs in the HEN to 7 units. In addition, the model prioritises use of the cheapest energy source first, in this case, sewage sludge, as it has the lowest feed cost and shortest supply distance (Tables 4.1 and B1). TAC is highest in the second scenario, 41.02 % and 33.35 % greater than in scenario 1 and 3. This is largely due to the increase in number of units in the HEN and MEE to 10 HEs and 7 effects. In addition, the inclusion of solar thermal energy

contributes to the increase in TAC. An 8.63% increase is observed in SCN-CHP TAC, 943.57 % in HEN TAC, and 16.83 % in MEE TAC relative to scenario 1. These show the significance of change in number of heat exchanger units in determining the TAC value. In the third scenario, the total TAC is 5.76 % higher and 25.0 % lower than scenario 1 and 2. This is explained by the exclusion of solar thermal energy in the optimal solution, and reduction in the number of units in the HEN and MEE. The ARS TAC remained constant across all scenarios, as this section of the model had a fixed chilled water demand.

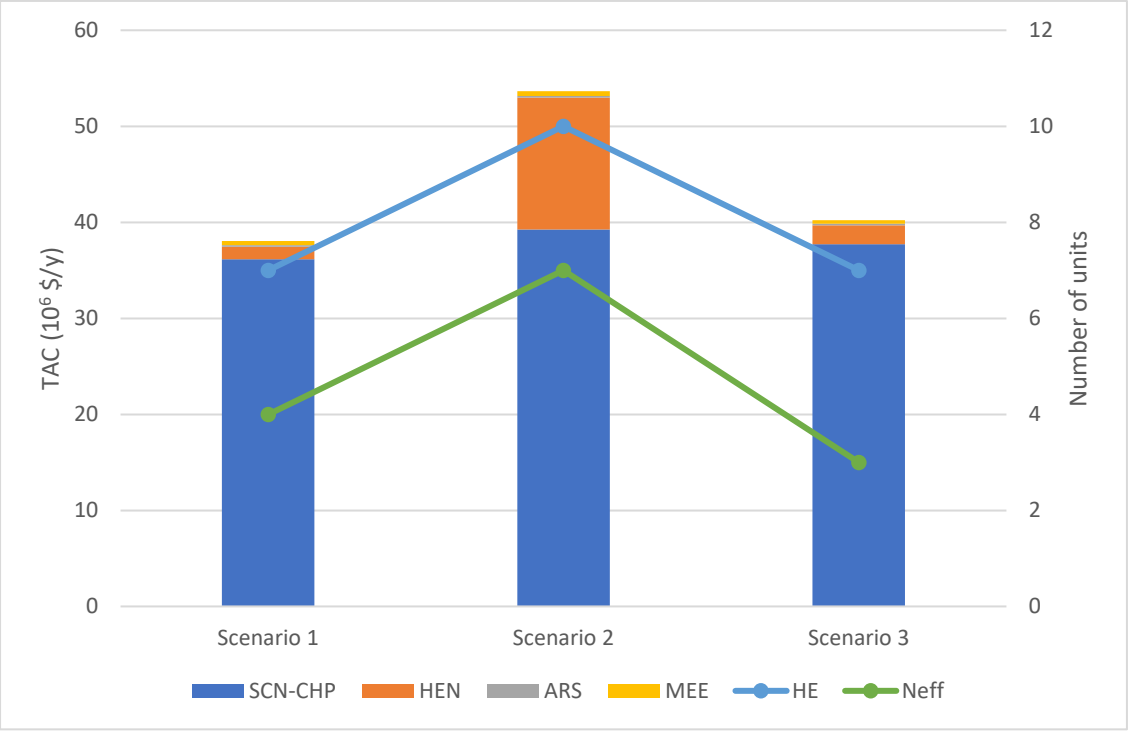

Figure 4.3: TAC Analysis

Figure 4.4 shows biomass distribution in the optimal solution (scenario 3). In season 1, 87.3 % of the fuel used was forestry residue transported by rail, with the rest being sewage sludge transported by road. In the season 2 forestry residue usage decreases by 6.2 % and increases to 88.5 % in season 3. Figure 4.5 shows the Pareto frontier plot of cost against emissions for the three scenarios. The plot clearly shows the inverse relationship between the two objectives. The overall superstructure of the optimal solution is shown in Figure 4.6.

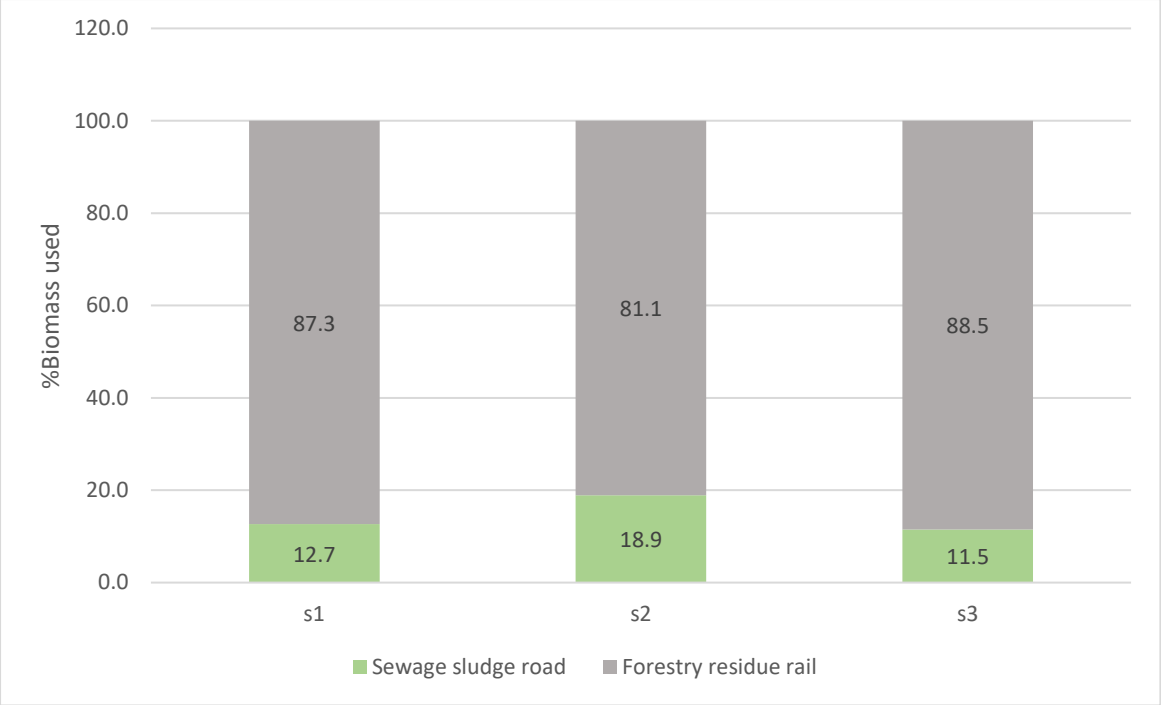

Figure 4.4: Optimal biomass distribution

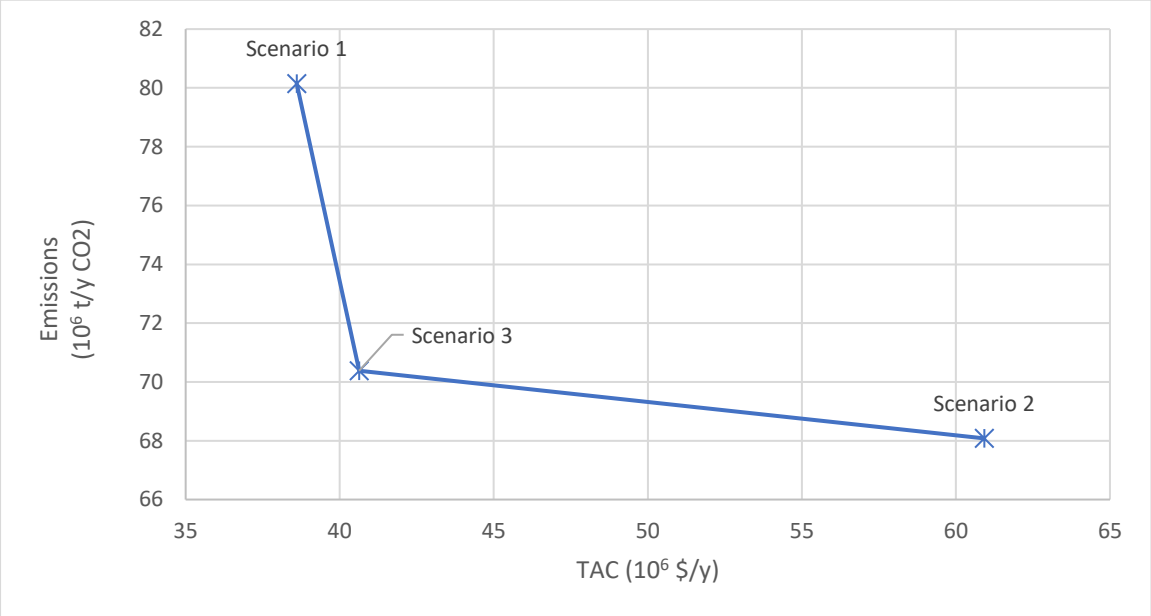

Figure 4.5: Pareto frontier plot: Cost vs Emissions

In the optimal solution shown in Figure 4.6, the boiler produces 49.48 kg/s of HPS. Turbines 1 and 2 produce 6.10 kg/s and 24.27 kg/s of LPS and MPS respectively. Furthermore, an additional 6.58 kg/s of LPS and 16.50 kg/s of MPS is obtained from the MPS and HPS bypass streams. 3.01 kg/s of desuperheating water is added to the HPS, MPS, and LPS streams. 2.59 kg/s of desuperheated HPS is directed to the HEN, 1.2 kg/s and 10.63 kg/s are directed to the

ARS and MEE respectively. 60 kg/s of saltwater feed is supplied to the MEE at 25 ℃ and 30 kg/s of distillate at 35 ℃ is produced. The ARS produces 0.18 kg/s of chilled water at 6 ℃.

The selection of energy source and transport mode is dependent on intricate trade-offs between TAC and emissions. The model considers several factors including the weight assigned to each objective in the multi-objective function, fuel cost, available supply capacity and distance, carbon composition and net calorific value of energy sources. Regarding transport, factors such as tortuosity, investment cost, and associated emissions are considered. A sensitivity analysis was conducted to further explore the effects of some of these factors on the model solution.

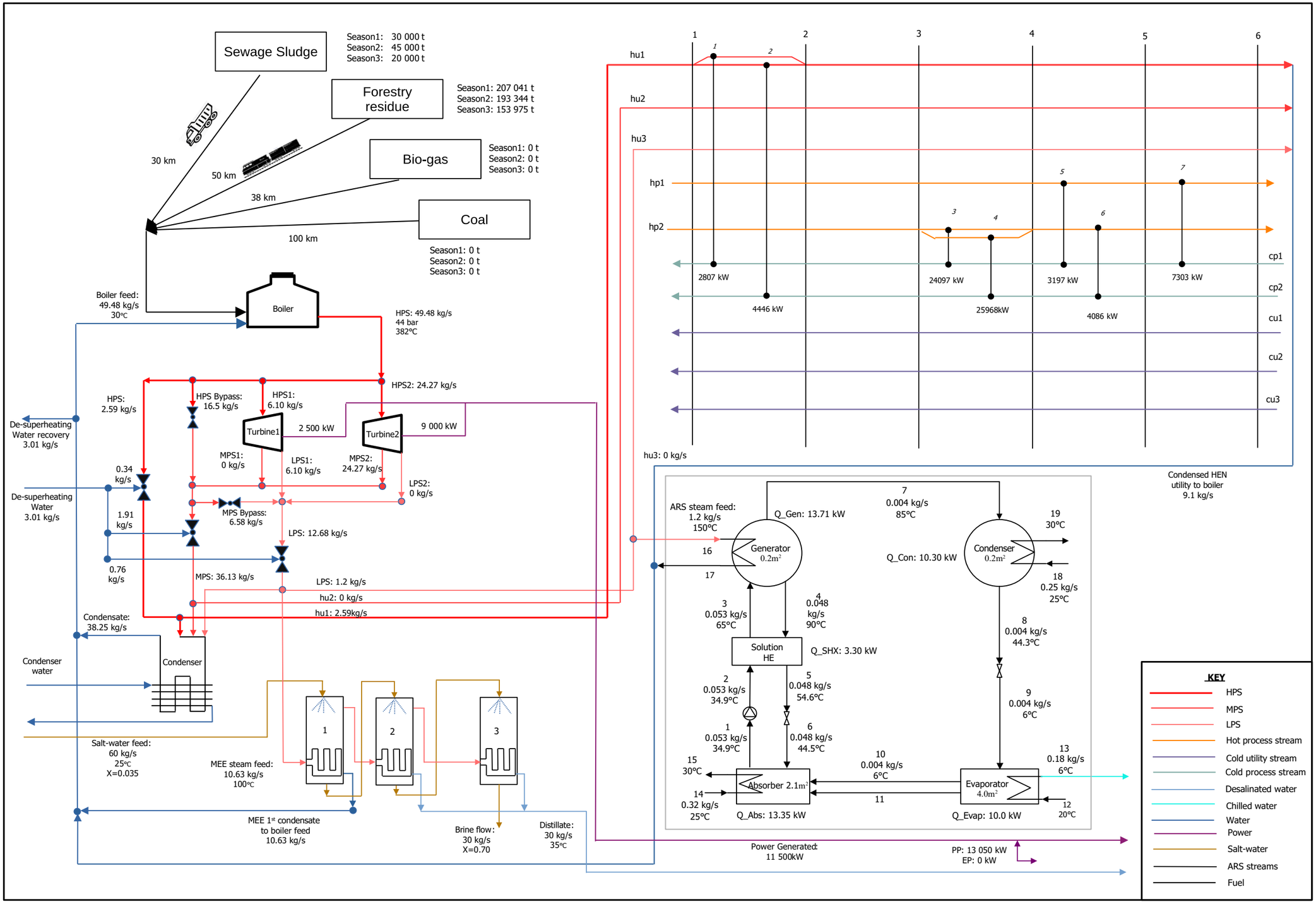

Figure 4.6: Superstructure solution – Case 1

4.2.3 Sensitivity analysis

Figure 4.6 shows a sensitivity analysis conducted on the weighting factor in the multi-objective function. This process ensures that the optimization is not overly influenced by specific weights, leading to a more balanced and reliable outcome, given that the model is nonlinear. The primary vertical axis refers to values of emissions, power generated, and power purchased on a logarithmic scale. The secondary vertical axis refers to the TAC, HPS, HEs and Neff. The horizontal axis shows the respective weighting factors on a TAC basis. The first point, with a TAC weighting factor of 0 corresponds to the minimising of carbon emissions only, just as in scenario 2, and the last point corresponds to scenario 1 where only TAC was minimised. As weighting increases in favour of TAC, HE and effects in the HEN and MEE reduce in number from 10 and 7 at a weighting of 0, to 7 and 4 at a weighting of 1. This leads to gradual decrease in TAC from 53.65 $\times 10^6$ (\$/y) to 38.05 $\times 10^6$ (\$/y). Conversely, there is a gradual increase in emissions, as weighting changes in favour of TAC, from 69.58 $\times 10^6$ (t/y CO_2) to 106.69 $\times 10^6$ (t/y CO_2). The sharp decrease in TAC between the weighting of 0 and 0.1 can be explained by the trade-off between purchasing 19,050 kW of power and generating 5,055 kW on one hand to purchasing 13,050 kW and generating 11,500 kW on the other hand. In addition, whilst sewage sludge and forestry residue were used in both cases, at 0 weighting, 1.59 $\times 10^6$ kg of sludge were transported by road and 93.41 $\times 10^6$ kg by rail, only rail was used to transport the entire 95.0 $\times 10^6$ kg of sludge at 0.1 weighting. All forestry residue used was transported by rail and no change in transport mode was observed at 0.1 weighting. The variable freight costs and tortuosity factor for rail are 1,185.71 % and 13.39 % lower than road transport, and this explains why rail transport was preferred when the model considered minimising TAC. There were minimal changes in the HPS produced, within the range of 48.7 kg/s to 50.0 kg/s. The minimal changes in HPS produced can be explained by the turbine specifications which constrain the model to ensure a minimum generative capacity of 2,500 kW and 3,000 kW for turbine 1 and 2 respectively. Solar thermal energy is included in the solution from 0 to 0.4 weighting. As prioritisation of TAC increases, costs associated with solar thermal energy outweigh the benefit of emission reduction and hence the model resorts to using more biomass, which is a cheaper alternative.

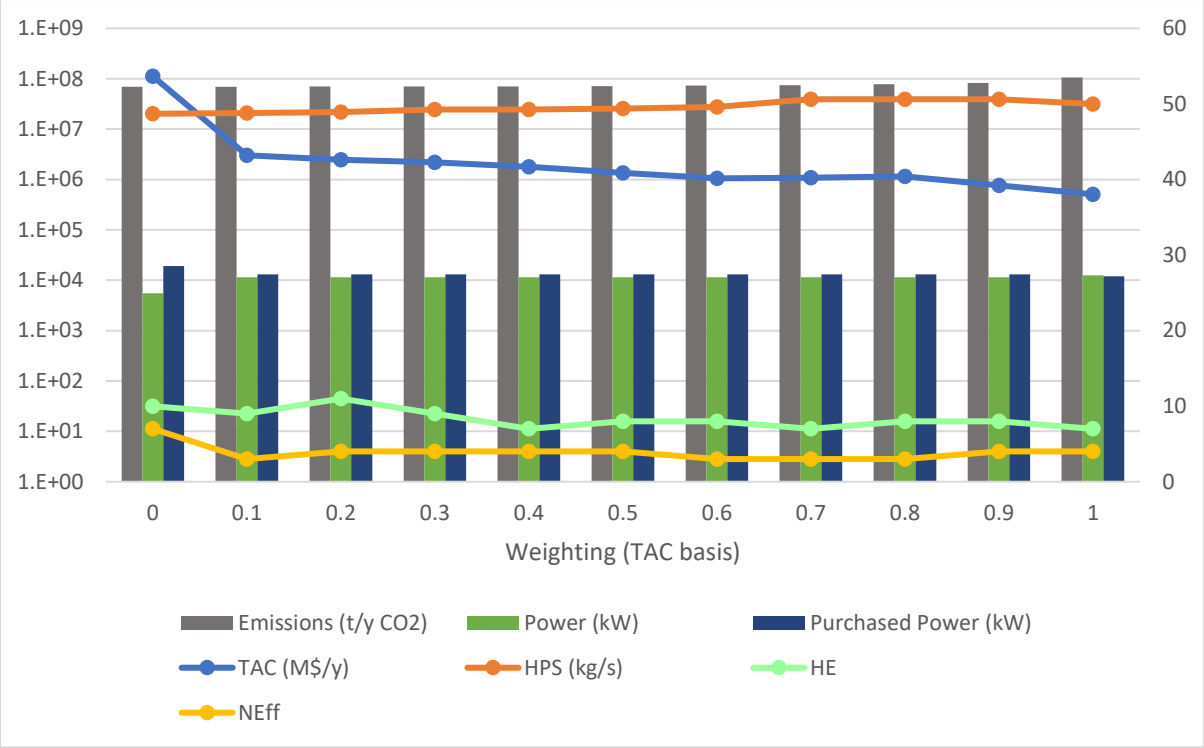

Figure 4.7: Sensitivity analysis on weighting.

The availability of biomass, and the distance from the supply point, combined with other specifications such as lower heating value and carbon composition play a vital role in the optimisation of this model. Figure 4.7 show a sensitivity analysis conducted based on the availability of forestry residue in season 2. This analysis was conducted with an equal weighting on minimisation of TAC and emissions, to show effects on the optimal solution. The forestry residue available in season 2 was gradually decreased by up to 57.1 %. Of the biomass considered in the case study, forestry residue has the second lowest LHV, second longest supply distance, third highest carbon composition and second highest cost. Sewage sludge, which has the lowest LHV, supply distance, carbon composition and purchase cost, is first exhausted by the model and hence there is no change in the sludge used, as forestry residue supply capacity is reduced. At 9.5 % forestry residue reduction, energy supplied from biogas increases from zero to 4,321.16 kW. Biogas has the third lowest LHV, second highest carbon composition, second lowest supply distance, and the third highest purchase cost. It is therefore the next preferred available fuel after sewage sludge and forestry residue. The biogas used gradually increases from 4,321.16 kW at 9.5 % to 66,701.68 kW at 38.1 % decrease in forestry residue. After this point, the biogas used remains constant as this is the maximum available biogas. At 38.1% decrease in forestry residue availability, the model resorts to using coal despite it having the highest carbon composition, longest supply distance and highest purchase

cost per kilogram. To counteract the high emissions from the use of coal, the model also introduces solar thermal power. The 3,068.19 kW supplied by solar thermal energy would have been supplied by coal leading to an additional 13,187 (t/y CO_2). This however resulted in a sharp increase of 16.6% in TAC value and only 1.63 % increase in emissions. As forestry residue continued to decrease after 38.1 %, a larger increase in emissions is observed; by 8.54 % and 6.61 % at 47.6 % and 57.1 % reduction in forestry residue supply. This increase in emissions is explained by the continued increase in use of coal from 10,790 kW to 69,113.3 kW, without an increase in solar thermal energy used due to feasibility constraints on collector area in the model.

Regarding transport mode, rail has the second lowest variable freight costs ($/t.km), second highest investment cost ($/km), highest fixed freight cost ($/t), lowest tortuosity factor, and the second lowest emission factor. Road transport has the highest variable freight cost, lowest investment cost in ($/km), second highest fixed freight cost ($/t), highest tortuosity factor, and the highest emission factor. Pipeline has the lowest variable freight costs, highest investment cost, lowest fixed costs and highest tortuosity factor tied with road transport. For these reasons, rail transport was preferred over road for transporting forestry residue due to the large quantities required, which would result in combined higher variable and fixed freight charges. For example, at 0% reduction in forestry residue supply, use of road transport would have resulted in combined variable and fixed freight charges 27.65 % higher than the use of rail. The resultant transport emissions for road use would be 105.71 % higher than rail use. For similar reasons, road transport is preferred for smaller quantities of fuel, due to the resulting lower fixed and variable freight costs which are dependent on weight only. The distance from the supply point did not seem to have much effect on the selection of transport modes as there are smaller differences between the supply point distances compared to other factors such as emission factor and fixed and variable charges. For example, there is a 100 % difference in supply distances for forestry residue and coal, and a 1,185 % difference in the variable freight costs ($/t.km) for the modes of transport available for these energy sources. This suggests that the selection of transport mode is more sensitive to the quantity of fuel to be transported than the distance from the supplier.

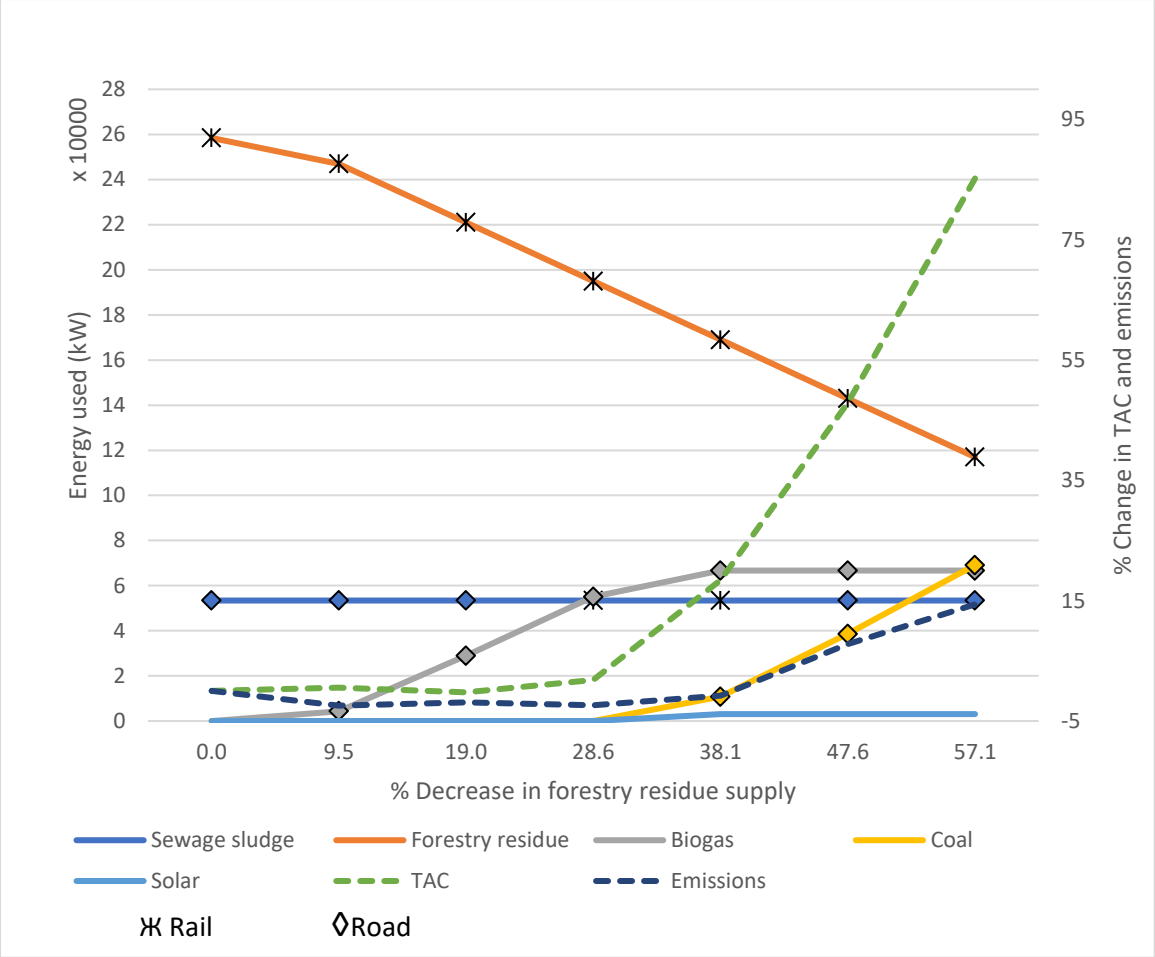

Figure 4.8: Sensitivity analysis on biomass supply capacity

This case study showed the different trade-offs in integrating renewable energy sources and technologies whilst considering different weighting between TAC and carbon emissions. In reality, a single organisation or industry may not have the resources to establish such an integrated network. It is therefore necessary to consider the possibility of industrial symbiosis, involving the different networks and technologies being considered as different industrial players.

Chapter 5

Industrial Symbiosis Case Study

5.0 Case Study Illustrating Industrial Symbiosis

5.1 Case Description

In this case study, the integrated superstructure is composed of four distinct subnetworks, each operating independently with specific functional objectives. The subnetworks are treated as four distinct players: SCN-CHP (Player 1), MEE (Player 2), HEN (Player 3), and ARS (Player 4). The SCN-CHP focuses on generating electricity while having the potential to produce various grades of heat as waste steam. The MEE's objective is to produce desalinated water, which requires a heat source. Similarly, the ARS aims to produce chilled water and also depends on a heat source. The HEN is designed for industrial heating and cooling of process streams and relies on hot and cold utilities. Two or more players can form coalitions to achieve a combined TAC, with the benefits shared among the coalition members. A game-theoretical approach is applied to analyse potential coalitions involving one or more players, determining which coalition minimises the TAC. The possible coalitions are described as follows:

SCN-CHP and MEE (player 1 and 2): In this coalition the SCN-CHP provides surplus desuperheated LPS to drive evaporation in the MEE. In turn the MEE seawater feed substitutes the water required for condensation of LPS in the power cycle of the SCN-CHP. This implies that the running costs of the MEE, which are dependent on the steam fed to it, are excluded from the TAC of the SCN-CHP and MEE coalition.

SCN-CHP and HEN (player 1 and 3): In this coalition the HEN receives hot utilities as desuperheated LPS, MPS and HPS from the SCN-CHP. In this process, the steam is condensed and returned to the SCN-CHP to continue the steam generation cycle. This means that the cost of hot utilities for the HEN is included in the supply chain network's energy feedstock costs and hence should be excluded in the computation of the HEN's TAC.

MEE and HEN (player 2 and 3): In this coalition, the MEE seawater feed is included in the HEN serving as a process stream that requires heating. In turn it substitutes some of the cold utility required by the HEN. This coalition's TAC excludes utility costs for the MEE and accounts for the reduced cold utility costs for the HEN. The HEN is supplied with hot utility from an external source.

SCN-CHP and ARS (player 1 and 4): The CHP provides excess desuperheated LPS to the ARS, which is condensed and recycled back to the boiler in the SCN-CHP for further steam generation. This coalition's TAC excludes hot utility costs for the ARS as the demand is satisfied by LPS from the SCN-CHP, and condensation costs for the SCN-CHP are adjusted to account for the LPS diverted to meet ARS demand.

MEE and ARS (player 2 and 4): Both the MEE and the ARS require hot utilities and can form a coalition to procure discounted steam from an external supplier.

HEN and ARS (player 3 and 4): In this coalition, the ARS's hot utility demand is included into the HEN and serves as a cold process stream that requires heating. An external supply meets the hot utility requirement of both the ARS and the HEN.

In addition to the two-player coalitions, players can also choose to be in three-player coalitions (player 1, 2, and 3), (player 1, 2, and 4), (player 1, 3, and 4), (player 2, 3, and 4) or a four-player coalition (player 1, 2, 3, and 4). The 3 player and 4 player coalitions are based on the same principle as the 2 player coalitions, for example in the three-player coalition shown below.

SCN-CHP, MEE, and HEN (player 1, 2, and 3): This coalition enables the MEE and HEN to obtain hot utility supply from the CHP. Piping expenses are modified accordingly and distributed between the two utility recipients based on their distance from the SCN-CHP. The TAC for this coalition excludes hot utility costs for the MEE and HEN and is adjusted to reduce the cost of condensation for the SCN-CHP, accounting for steam redirected to the MEE and HEN.

The specific data used in this case study is similar to that used in the first one, with any differences specified. Table 5.1 shows amended seasonal cost and supply capacity data, LHVs, and supply distances. Table 5.2 shows the properties of the HEN process streams used in this case study. In the HEN, there are 5 cold and 2 hot process streams. The hot utility demand of the HEN can be met by one or more of LPS, MPS and HPS exiting the boiler and turbines in the CHP subnetwork, while the cold utility demand can be satisfied by chilled water from the ARS subnetwork.

Table 5.1: Bioenergy supply chain feedstock data

Feedstock			Season 1		Season 2		Season 3	
	LHV_{sp} (kWh/kg)	D (km)	Cost ($/kg)	Capacity ($\times 10^6$ kg)	Cost ($/kg)	Capacity ($\times 10^6$ kg)	Cost ($/kg)	Capacity ($\times 10^6$ kg)
Sewage sludge	4.52	30	0.024	38	0.22	440	0.27	20
Forestry residue	4.95	50	0.004	78	0.045	210	0.025	50
Biogas	5.08	38	0.050	78	0.03	50	0.07	50
Coal	7.20	100	0.9	50	0.9	4.7	0.9	21.5

Table 5.2: HEN stream data (adopted from (Isafiade & Short, 2022))

Hot streams	T_i^s (°C)	T_i^t (°C)	FCP_i (kW/°C)	Cold streams	T_j^s (°C)	T_i^t (°C)	FCP_j (kW/°C)
HU1 (HPS)	257	257	-	C1	25	240	140
HU2 (MPS)	197	197	-	C2	20	250	150
HU3 (LPS)	150	150	-	C3	50	180	70
H1	155	85	150	C4	70	100	120
H2	230	40	285	C5	25	100	209
				CU1	6.5	10	-

The model comprised of 820 single equations and was solved in General Algebraic Modelling System (GAMS) version 24.4.6. CPLEX and CONOPT solvers, working in conjunction with DICOPT, were used for MIP and NLP respectively and the solution was obtained in 1.673 seconds on an 11th Gen Intel(R) Core (TM) i5-1135G7 @ 2.40GHz processor with 8GB RAM.

5.2 Model Solution

5.2.1 Objective function

The objective function of this model is shown in Equation (5.1), in this equation R1, R2, R3, R4 are weighting factors and a value of 0.25 was used to ensure equal weighting among the four players and to maintain the fairness of the game theory aspect. Unlike in the first case study, emissions were not considered in this objective function.

$$Obj = Min\left(\mathrm{R1}\cdot\phi_1(\nu) + \mathrm{R2}\cdot\phi_2(\nu) + \mathrm{R3}\cdot\phi_3(\nu) + \mathrm{R4}\cdot\phi_4(\nu)\right) \quad (5.1)$$

$\phi_1(\nu)$ to $\phi_4(\nu)$ are the shapely values of the individual players as determined from Equation (2.1) but with each element of the set C multiplied by a binary variable, CL_c that denotes the existence of a coalition as illustrated in Equation (5.2). Additionally, the binary variable is included in Equation (3.52) to account for the formation of coalitions. The introduction of this

binary variable allows the model to only be solved once rather than 15 times to obtain the different coalitions' TAC values.

$$\phi_a(\nu) = \sum_{c \epsilon C} \frac{1}{C} \left(\nu(\{a\} \cup z_{c(a)}) - \nu(z_{c(a)}) \right) \cdot CL_c \quad (5.2)$$

5.2.2 Results

The solution to the model was exported to a spreadsheet and analysed. Table 5.3 presents the TAC and total cost savings, CS ($/y×$10^5$) for each possible coalition. The cost savings are determined by the difference between the sum of the individual players' TACs and the TAC when the players form a coalition. To solve the model, the TAC for each coalition is calculated independently, as shown in Table 5.3, and these values are used as the objective function in Equation (5.1). Table 5.4 outlines the contributions of each player across all possible permutations in the case of a grand coalition. Notably, every row in table 5.4 has the same total of 1,047.73 ($/y ×$10^5$) which matches the grand coalition value shown in the last row of Table 5.3. This is because ultimately, the TAC of the grand coalition remains the same. What changes is the cost allocated to each player based on their position in the coalition.

Table 5.3: Cost savings for each coalition

Coalition	TAC ($/y ×$10^5$)	CS ($/y ×$10^5$)
1 (SCN-CHP)	817.926	0.000
2 (MEE)	4.424	0.000
3 (HEN)	464.023	0.000
4 (ARS)	0.875	0.000
1.2 (SCN-CHP, MEE)	820.865	-1.485
1.3 (SCN-CHP, HEN)	1,047.648	-234.301
2.3 (MEE, HEN)	238.684	-229.763
1.4 (SCN-CHP, ARS)	817.974	-0.827
2.4 (MEE, ARS)	5.276	-0.023
3.4 (HEN, ARS)	464.857	-0.041
1.2.3 (SCN-CHP, MEE, and HEN)	820.848	-465.525
1.2.4 (SCN-CHP, MEE, ARS)	820.892	-2.333
1.3.4 (SCN-CHP, HEN, ARS)	1,047.678	-235.146
2.3.4 (MEE, HEN, ARS)	239.557	-229.765
1.2.3.4 (SCN-CHP, MEE, HEN, ARS)	1,047.725	-239.523

In Table 5.4, the marginal contribution of Player 1 remains consistent across the first six coalitions because Player 1 is always the first to join these coalitions. A similar trend is observed for other players when they are the first to enter their respective coalitions. The marginal contribution of a player reflects the value they add to a specific coalition, which varies

based on the coalition's existing members and the sequence in which players join, as it represents an incremental value. The Shapley value is then applied to fairly allocate cost savings across all possible coalition permutations (Ahmad Fadzil et al., 2022), (Chalkiadakis, Elkind & Wooldridge, 2012). Table 5.3 highlights that this cooperative game exhibits sub-additivity, as the grand coalition does not achieve the highest cost savings. This indicates that forming a larger coalition does not always guarantee greater savings (Passacantando et al., 2021). In the model's solution, coalition 1.2.3 is identified as the optimal coalition, delivering the highest cost savings without replacing any players. The ARS (Player 4) is excluded from the optimal coalition because it does not contribute enough to justify its inclusion. Table 5.3 shows that all coalitions involving the ARS, such as 1.4, 2.4, and 3.4, yield minimal cost savings. This is due to the ARS's low individual TAC ($0.875\ \$/y \times 10^5$), which fails to significantly enhance cost savings in any coalition. The ARS's low TAC can be attributed to the small amount of LPS required and its low investment cost.

Table 5.4: Player contributions for each coalition permutation in grand coalition ($/y ×10^5)

Coalition	1st Entry	2nd Entry	3rd Entry	4th Entry
1.2.3.4	817.926	2.939	-0.017	226.877
1.2.4.3	817.926	2.939	0.027	226.833
1.3.2.4	817.926	229.722	-226.800	226.877
1.3.4.2	817.926	229.722	0.031	0.047
1.4.2.3	817.926	0.048	2.918	226.833
1.4.3.2	817.926	0.048	229.704	0.047
2.1.3.4	4.424	816.441	-0.017	226.877
2.1.4.3	4.424	816.441	0.027	226.833
2.3.1.4	4.424	234.260	582.164	226.877
2.3.4.1	4.424	234.260	0.873	808.168
2.4.1.3	4.424	0.852	815.616	226.833
2.4.3.1	4.424	0.852	234.281	808.168
3.1.2.4	464.023	583.625	-226.800	226.877
3.1.4.2	464.023	583.625	0.031	0.047
3.2.1.4	464.023	-225.339	582.164	226.877
3.2.4.1	464.023	-225.339	0.873	808.168
3.4.1.2	464.023	0.834	582.821	0.047
3.4.2.1	464.023	0.834	-225.300	808.168
4.1.2.3	0.875	817.099	2.918	226.833
4.1.3.2	0.875	817.099	229.704	0.047
4.2.1.3	0.875	4.401	815.616	226.833
4.2.3.1	0.875	4.401	234.281	808.168
4.3.1.2	0.875	463.981	582.821	0.047
4.3.2.1	0.875	463.981	-225.300	808.168

Key

Player 1	
Player 2	
Player 3	
Player 4	

Table 5.5 presents the marginal contributions within the optimal coalition, with Shapley values for players 1, 2, and 3 calculated using Equation (2.2) as 700.0 ($/y×$10^5$), −111.2 ($/y×10^5), and 232.0 ($/y×$10^5$) respectively. The entry sequence, from 1st to 3rd, indicates the order in which players join the coalition. Player 2 has a negative Shapley value because the MEE contributes significantly less to reducing the TAC compared to the SCN-CHP. Consequently, this negative value suggests that Player 2 would require compensation to participate in the coalition.

Table 5.5: Marginal contributions for a coalition between players 1, 2 and 3 ($/y ×105)

Permutation	1st Entry	2nd Entry	3rd Entry
1.2.3	817.926	2.939	-0.017
1.3.2	817.926	229.722	-226.800
2.1.3	4.424	816.441	-0.017
2.3.1	4.424	234.260	582.164
3.1.2	464.023	583.625	-226.800
3.2.1	464.023	-225.339	582.164

In the optimal coalition 1.2.3, the SCN-CHP integrates with the MEE and HEN, achieving a TAC of 820.8 ($/y×$10^5$) and cost savings of 465.5 ($/y×$10^5$). These savings result from reduced condensation costs for the CHP, the elimination of operating costs for the MEE, and decreased operating expenses for the HEN. In this setup, the CHP generates 8,546.5 kW of power and procures 16,000 kW from the grid. The MEE consists of 13 effects, achieving a gained output ratio of 10.0 with a distillate flow rate of 28 kg/s. The HEN includes 38 heat exchanger matches, facilitating a total heat exchange of 90,156 kW. In the SCN-CHP subnetwork, the solar thermal network is excluded from the optimal solution due to its high costs, as economic considerations drive the selection process. However, if environmental impact were considered as an additional objective, the substantial installation cost of the solar thermal network might be justified. The optimal SCN configuration, detailed in Table 5.6, reveals that rail is the most utilised transport mode. This preference stems from its low transport cost per kilogram per kilometre and minimal tortuosity factor, making it cost-effective for moving large quantities despite its high investment cost per kilometre. In seasons 1 and 3, road transport is chosen for coal due to its relatively smaller quantities, which do not warrant the high investment cost of rail.

Additionally, coal's higher price justifies the selection of a lower-cost transport mode. Pipeline is not selected in the model, despite having a negligible return trip factor of 1, because it carries the highest investment cost.

Table 5.6: Optimal SCN configuration

Fuel Type	**Transport mode**	**Fuel transported per season (1000 × t)**		
		S1	S2	S3
Sewage sludge	rail	38.0	162.3	20.0
Forestry residue	rail	78.0		50.0
Biogas	rail	78.0	50.0	50.0
Coal	road	4.6		18.6

Figure 5.1 presents the optimal solution, highlighting a coalition between the SCN-CHP, MEE, and HEN, which emerges as the most favourable configuration for the case study discussed in this chapter. The figure also indicates that the ARS receives an external LPS supply of 4.9 kg/s. As in the first case study, it is important to analyse how changes in certain parameters may affect the optimal solution. A sensitivity analysis is therefore necessary.

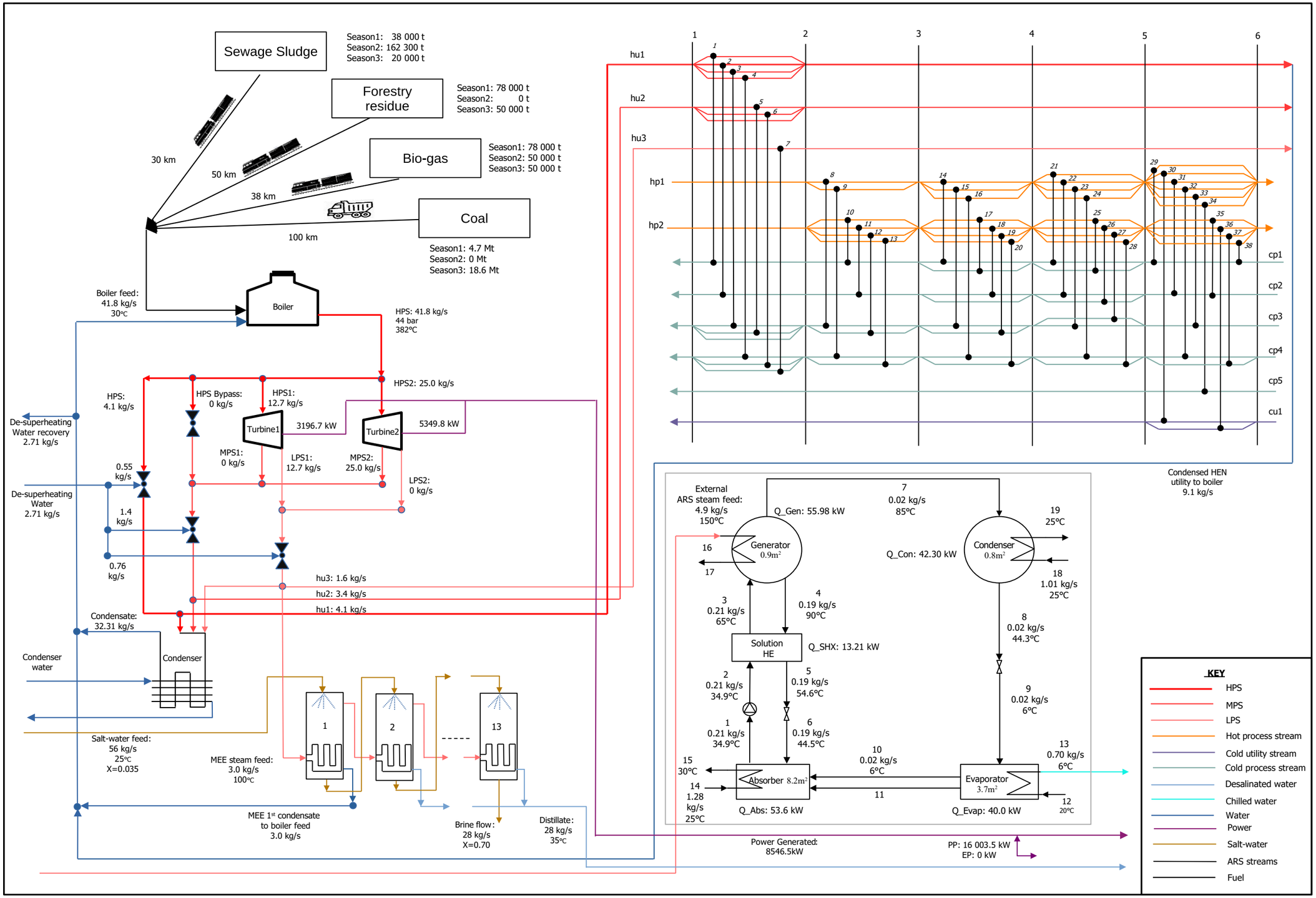

Figure 5.1: Superstructure solution – Case 2

5.2.3 Sensitivity Analysis

Biomass availability is a crucial factor that can vary seasonally, impacting its feasibility as a renewable energy source. To assess this, a sensitivity analysis was performed by adjusting the capacity of sewage sludge in season 1, priced second lowest in the case study, in increments of 4 %. The model demonstrated a preference for the least expensive fuels, prioritising forestry residue, sewage sludge, and biogas in sequence before transitioning to coal. This order corresponds to the ascending fuel prices listed in Table 1. Figure 5.2 illustrates how increasing the availability of sewage sludge influences the utilisation of other fuels, SCN fixed and variable costs, and the overall SCN-CHP annual cost. The TAC declines steadily as sewage sludge availability rises, with fixed and variable costs showing a similar trend. Variations in fixed and variable cost patterns are linked to the choice of transport mode. At 16 % and 24 % increased sewage sludge capacity, road transport is used for forestry residue, which raises fixed and variable costs but has a negligible impact on the overall TAC. Overall, the observed changes in SCN-CHP TAC did not result in any changes in the optimal coalition.

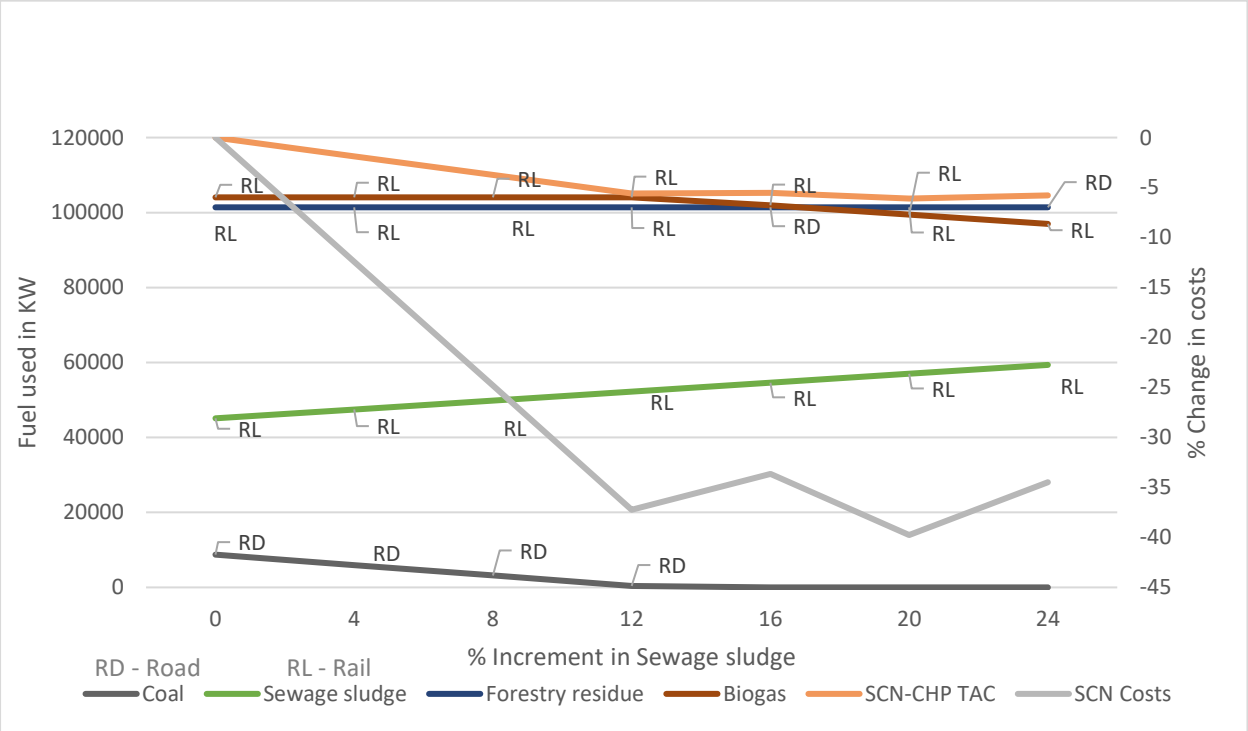

Figure 5.2: SCN sensitivity analysis

Chapter 6

Conclusion and Recommendations

6.0 Conclusion and Recommendations

This dissertation presented a polygeneration network designed to supply power, fresh water and hot and cold utility. Existing technologies such as multi-effect evaporation, combined heat and power generation, absorption refrigeration cycle and the stage-wise HENs model were integrated with a renewable and non-renewable energy supply chain network to satisfy the utility demand. In addition, solar thermal energy was included as an option for boiler feed preheating.

In the first case study, a multi-objective function with an equal weighting of CO_2 emissions and TAC was used, and this highlighted important trade-offs that industries need to make in order to achieve profits in a sustainable manner. The case study emphasises how to maximise total energy usage and minimise environmental effect by using surplus steam to power the ARS, MEE and supply hot utility to the HEN. The integrated network is shown as a superstructure, with the installation and operating costs of energy generation, saltwater desalination, cooling and transportation-related emissions carefully considered. Furthermore, the seasonal availability of feedstocks and the corresponding seasonally dependent pricing are taken into consideration by the superstructure.

In the second case study, game theory was used on the TAC values of the SCN-CHP, MEE, ARS, and HEN, which were considered as independent players with the ability to form coalitions. It was determined that a coalition between the SCN-CHP, MEE and HEN is the most profitable as it presented the highest cost savings. This case study shows how collaboration across resource utilising industries may result in advantages for all parties involved. By applying equal weighting factors to the Shapley values, each player's contribution was given equal consideration, ensuring the fairness of the game theory principle remained intact.

Figures 4.6 and 5.1 show the superstructures for the two cases considered. These figures differ in that Figure 4.6 shows an integration of all the technologies with steam supplied from the SCN-CHP feeding to the MEE, ARS and HEN, whereas Figure 5.1 shows the optimal coalition between the SCN-CHP, MEE, and HEN, with the ARS receiving steam from an external source.

The case studies revealed that the combined capital expenses for power generation and transport network infrastructure were the most significant, resulting in a TAC approaching a billion dollars. To speed up the shift to renewable energy, it might be essential to make adjustments to the existing infrastructure, wherever feasible, to reduce capital expenditure.

Additionally, government intervention, such as offering rebates for the installation and adoption of renewable energy technologies, could further support this transition.

It is important to note that the optimal solutions obtained in this work are based on the parameters used, and whilst a sensitivity analysis was carried out for both cases, a more robust sensitivity analysis on additional parameters can be conducted in future work. Due to the nature of the solvers used in this study, global optimality is not guaranteed. This is key in highlighting how changes in parameters affect the optimal solution. The technologies considered in this work were not exhaustive, several other technologies can be considered for future work, for example adding a heat recovery steam generator to the CHP to recover heat from the flue gas. Alternatively, a gas-driven turbine system can be integrated to make use of the kinetic energy from the flue gas and add to the power generation capacity. A more sophisticated supply chain network may also be setup to include intermediate storage to make the model more realistic. The use of arbitrary data in this work was done for simplicity, but to generate more robust models, case studies with realistic data may need to be considered.

For a game theoretical analysis, it may be beneficial to additionally analyse minimum TAC and cost saving values from an individual player's perspective, than as a whole, as each player would to maximise individual benefits. The future consideration of other game theory methods such as the nucleolus and bargaining solution methods is recommended to ensure accuracy and best fit for specific cases.

In addition, to enhance the optimisation of such a network, future studies may need to include an exergy balance to fully account for irreversibilities in processes for example heat transfer across finite temperature differences, and to accurately determine the actual energy in the system after losses.

Furthermore, whilst GAMS is powerful mathematical optimisation tool, there are newer modelling tools such as Julia, that possess superior performance. Julia also has a mathematical programming package, JuMP, that offers a high-level interface allowing the concise and efficient defining of complex models. The use of such of such a tool in any future work would be more ideal.

Nomenclature

Abbreviations

ARS	Absorption Refrigeration System
BSCN	Bioenergy Supply Chain Network
CHP	Combined Heat and Power
GDP	Gross Domestic Product
GHG	Greenhouse Gas Emissions
HEN	Heat Exchanger Network
HTFFE	Horizontal-Tube Falling Film Evaporator
MED	Multiple Effect Desalination
MEE	Multi-Effect Evaporation
MINLP	Mixed Integer Non-Linear Program
ORC	Organic Rankine Cycle
SCN	Supply Chain Network
TAC	Total Annual Cost
TVC	Thermal Vapor Compression

Sets

sp	Set of renewable energy sources
f	Set of transport modes
s	Set of annual seasons of renewable fuel availability
i	Set of hot streams
i(hu)	Hot utility stream in set *i*
j	Set of cold streams
k	Set of heat exchange stages in the heat exchanger network
C	Set of all possible coalitions

Parameters

$C^{F}_{sp,s}$	Cost of purchasing feedstock from supply point *sp* in season *s* ($/kg).
C^{V}_{f}	Cost of transporting each feedstock by the freight mode *f* ($/kg.km).
D_{sp}	Straight-line distance from supply points *sp* to the utility hub (km).
τ_f	Tortuosity factor for each freight mode *f*.
r_f	Return trip factor for each freight mode *f*.
NCV_{sp}	Net calorific value of each fuel from supply point *sp* (kWh/kg).
η^{bl}	Boiler efficiency
DS_s	Duration of each season *s*.
n	Number of annual operating hours (h/y).
AF_{SCN}	Annualization factor for the supply chain network.
C^{I}_{f}	Capital cost associated with each freight mode *f* ($/km).
$Cap_{sp,s}$	Maximum available fuel at supply point *sp* in season *s* (kg).
P^{Demand}	Power demand (kW).
η_0	Solar collector efficiency.
a_1	Solar collector thermal loss coefficient (kW/m^{2}K).

a_2	Solar collector thermal loss coefficient (kW/m^{2}K).
T_c	Average of temperatures of the boiler feed water before and after pre-heating (℃).
T_a	Ambient temperature (℃).
GHI	Global horizontal irradiation (kW/m^2).
C_p	Capture fluid heat capacity (kJ/kg. ℃),.
ρ	Capture fluid density (kg/m^3).
T^s	Capture fluid supply temperature (℃).
T^t	Capture fluid target temperature (℃).
$LMTD_{SA}$	Logarithmic mean temperature difference between the solar capture fluid and the boiler feedwater
U_{SA}	Heat transfer coefficient between the solar capture fluid and boiler feedwater (kW/(m^2. ℃)).
T_{1SA}	Initial temperature of boiler feed water (℃).
T_{2SA}	Final temperature of boiler feed water (℃).
C_{pf}	Heat capacity of boiler feed water (kJ/kg. ℃).
AF_{SA}	Annualization factor for the solar thermal unit.
C_{TS}	Installation cost of thermal storage tank per unit volume ($/m^3).
C_{SC}	Installation cost of solar collector per unit area ($/m^2).
H^{LPS}	Enthalpy of superheated LPS (kJ/kg).
H^{LPSd}	Enthalpy of desuperheated LPS (kJ/kg).
H^{MPS}	Enthalpy of superheated MPS (kJ/kg).
H^{MPSd}	Enthalpy of desuperheated MPS (kJ/kg).
H^W	Enthalpy of desuperheating water (kJ/kg).
H_{vap}	Enthalpy of vaporisation of LPS (kJ/kg).
CP_{wt}	Heat capacity of cooling water (kJ/kg. ℃).
ΔT_{wt}	Change in temperature of cooling water (℃).
U_{Cnd}	heat transfer coefficient of the condenser (kW/(m^2. ℃)).
ΔT_{lm}	logarithmic mean temperature difference in the condenser
FI_{cnd}	Fixed investment cost per condenser ($).
$Ecnd$	Area cost index for condenser.
VI_{cnd}	Variable investment cost of condenser ($/m^2).
a_{Bl}	Boiler costing constant.
b_{Bl}	Boiler costing constant.
a_T	Turbine costing constant.
b_T	Turbine costing constant.
$e1$	Boiler costing exponent.
$e2$	Turbine costing exponent.
AF_{CHP}	Annualization factor for CHP.
λ_{ave}	Average latent heat of condensation for MEE distillate (kJ/kg).
U^{HTFFE}	MEE overall heat transfer coefficient (kW/m^{2}K).
ΔT_{VAC}	Average distillate temperature over all MEE effects (K).
TV_{ave}	Average MEE distillate temperature (K).
TV_1	Temperature of the first MEE distillate (K).
TV_{fd}	Condensation temperature of final distillate (K).
C^{Stm}	Cost of MEE steam feed ($/kg).
x_F	Mass fraction of brine in MEE saltwater feed stream.
x_B	Mass fraction of brine in MEE brine stream.
Q_{evap}	ARS evaporator capacity (kW).

T_{10}, T_3, T_7, T_{12} to T_{19}	ARS stream temperatures (℃).
x_1, x_4	ARS Li-Br stream mass fraction.
H_{12} to H_{19}	ARS stream enthalpies (kJ/kg).
CI	ARS heat exchanger cost index
C_H	ARS heat exchanger installation cost per unit area ($/m^2).
C_{HI}	ARS heat exchanger fixed installation cost ($).
AF_{ars}	ARS annualization factor
T_i^{in}	HEN hot stream inlet temperature (℃).
T_i^{out}	HEN hot stream outlet temperature (℃).
T_j^{in}	HEN cold stream inlet temperature (℃).
T_j^{out}	HEN cold stream outlet temperature (℃).
F_i	Heat capacity flowrate of HEN hot stream (kW/°℃).
F_j	Heat capacity flowrate of HEN hot stream (kW/℃).
$t_{i,k}$	Temperature of hot stream *i*, in stage *k* (℃).
$t_{j,k}$	Temperature of cold stream *j*, in stage *k* (℃).
Ω	Minimum available heat in matched streams.
γ	Upper bound for approach temperature
Emat	Minimum approach temperature
AF_{HEN}	HEN annualization factor
C_j	Cost of cold utility ($/kW).
C_i	Cost of hot utility ($/kW).
R1, R2, R3, R4	Objective function weighting factors.

Variables

$x_{sp,f,s}$	Quantity of feedstock transported from supply point *sp*, by freight mode *f*, in season *s* (kW)
$C_{SCN}^{F,V,I}$	Total annual cost for the Supply Chain Network ($/y).
$z_{sp,f}$	Binary variable denoting choice of freight mode.
$bd_{sp,s}$	Boiler fuel demand (kW).
HPS_{Tot}	Flowrate of high-pressure steam generated by the boiler (kg/s).
ΔH_{sp}	Energy required by the boiler to generate high pressure steam (kW).
MPS	Flowrate of medium-pressure steam exiting the turbines (kg/s).
LPS	Flowrate of low-pressure steam exiting the turbines (kg/s).
HEN_{Fin}^1	High-pressure steam split to the heat exchanger network (kg/s).
P^{T1}	Power generated from turbine 1 (Kw).
P^{T2}	Power generated from turbine 2 (kW).
$P^{Purchased}$	Power sourced from the external grid (kW).
F_{SA}	Flowrate of boiler feed water to solar-thermal preheating.
A_{sc}	Area of solar collector (m^2).
Q_{SA}	Heat transferred from solar collector to capture fluid (kW).
z_{SA}	Binary variable that denoting solar inclusion.
V_{TS}	Volume of thermal storage tank (m^3).
A_{SA}	Area of solar capture fluid heat exchanger (m^2).
CI_{SA}	Annualized installation cost of solar thermal unit (m^2).
W^F	Mass flowrate of desuperheating spray water (kg/s).
FCL_{LPS}	Flow rate of cooling water for condensing LPS (kg/s).

F_{LPS}	Flow rate of LPS to condenser (kg/s).
A_{LPS}	Area of condenser for condensing LPS (m^2).
A_{MPS}	Area of condenser for condensing MPS (m^2).
A_{HPS}	Area of condenser for condensing HPS (m^2).
CI_{cnd}	Capital cost for condenser ($).
CI_{CHP}	Capital cost for CHP ($/y).
TAC_{CHP}	Total annual cost for CHP ($/y).
WTC	Total water used in CHP (kg/s).
EP	Excess power (kW).
Q_{MEE}	Total heat load of the MEE (kW).
F^{dist}	MEE distillate flowrate (kg/s).
N^{EFF}	Number of effects in MEE.
A_{HTFFE}	Heat exchange area in MEE (m^2).
AFC	Annualized investment cost for MEE evaporator ($/y).
AOC	Annual operating cost for MEE ($).
F^{Stm}	Flowrate of MEE steam feed (kg/s).
GOR	MEE gained output ratio
F^{Dst}	Flowrate of MEE distillate (kg/s).
F^{SwF}	Flowrate of MEE saltwater feed (kg/s).
F^{Brine}	Flowrate of MEE brine (kg/s).
D_{in}	Internal pipe diameter (m).
D_{ext}	External pipe diameter (m).
W	Pipe weight per unit length (kg/m).
P_{cst}	Pipe cost per unit length ($/m).
TAC_{MEE}	MEE Total annual cost ($/y).
P_{MEE}	MEE Piping cost ($/y).
m_1 to m_{19}	ARS stream mass flowrates (kg/s).
H_1 to H_{11}	ARS stream enthalpies (kJ/kg).
Q_{abs}	ARS absorber heat duty (kW).
Q_{gen}	ARS generator heat duty (kW).
Q_{con}	ARS condenser heat duty (kW).
Q_{SHX}	ARS solution heat exchanger heat duty (kW).
C_{ARS}	ARS total annual cost ($/y).
A_{ARS}	ARS heat exchanger area (m^2).
P_{ars}	ARS piping cost ($/y)
$q_{i,j,k}$	Heat exchanged between hot stream *i*, and cold stream *j*, at stage *k* (kW).
$y_{i,j,k}$	Binary variable denoting a match between a hot stream *i* and cold stream *j* in stage *k*.
TAC_{HEN}	Total annual cost for HEN ($/y).
P_{HEN}	HEN piping costs ($/y).
m_{HEN}	Flowrate of steam to HEN (kg/s).
HEN^{Huin}	Energy supplied by hot utility to HEN
$MC_a(z)$	Marginal contribution of player a to coalition *z* ($/y).
$\nu(z \cup \{a\})$	Coalition value including player *a* ($/y).
$\nu(z)$	Coalition value excluding player *a* ($/y).
$\phi_a(\nu)$	Shapely value for player a ($/y).
CL_c	Binary variable denoting formation of a coalition

References

Abikoye, B., Čuček, L., Isafiade, A.J. & Kravanja, Z. 2019. Synthesis of solar thermal network for domestic heat utilization. *Chemical Engineering Transactions*. 76:1015–1020. DOI: 10.3303/CET1976170.

Aguilar-Jiménez, J.A., Velázquez, N., López-Zavala, R., Beltrán, R., Hernández-Callejo, L., González-Uribe, L.A. & Alonso-Gómez, V. 2020. Low-temperature multiple-effect desalination/organic Rankine cycle system with a novel integration for fresh water and electrical energy production. *Desalination*. 477. DOI: 10.1016/j.desal.2019.114269.

Ahmad Fadzil, F., Andiappan, V., Ng, D.K.S., Ng, L.Y. & Hamid, A. 2022. Sharing carbon permits in industrial symbiosis: A game theory-based optimisation model. *Journal of Cleaner Production*. 357. DOI: 10.1016/j.jclepro.2022.131820.

Ali, F., Dawood, A., Hussain, A., Alnasir, M.H., Khan, M.A., Butt, T.M., Janjua, N.K. & Hamid, A. 2024a. Fueling the future: biomass applications for green and sustainable energy. *Discover Sustainability*. 5(1):156. DOI: 10.1007/s43621-024-00309-z.

Ali, F., Dawood, A., Hussain, A., Alnasir, M.H., Khan, M.A., Butt, T.M., Janjua, N.K. & Hamid, A. 2024b. Fueling the future: biomass applications for green and sustainable energy. *Discover Sustainability*. 5(1):156. DOI: 10.1007/s43621-024-00309-z.

Allouhi, A., Rehman, S., Buker, M.S. & Said, Z. 2022. DOI: 10.1016/j.jclepro.2022.132339.

Amjed, M.A., Sobic, F., Romano, M.C., Faravelli, T. & Binotti, M. 2024. Techno-economic analysis of a solar-driven biomass pyrolysis plant for bio-oil and biochar production. *Sustainable Energy & Fuels*. 8(18):4243–4262. DOI: 10.1039/D4SE00450G.

Atashbar, N.Z., Labadie, N. & Prins, C. 2016. Modeling and optimization of biomass supply chains: A review and a critical look. In *IFAC-PapersOnLine*. V. 49. Elsevier B.V. 604–615. DOI: 10.1016/j.ifacol.2016.07.742.

Baljit, S.S.S., Chan, H.Y. & Sopian, K. 2016. DOI: 10.1016/j.jclepro.2016.07.150.

BP. 2021. *Full report – Statistical Review of World Energy 2021*.

Calise, F., Cipollina, A., Dentice d'Accadia, M. & Piacentino, A. 2014. A novel renewable polygeneration system for a small Mediterranean volcanic island for the combined production of energy and water: Dynamic simulation and economic assessment. *Applied Energy*. 135:675–693. DOI: 10.1016/j.apenergy.2014.03.064.

Chalkiadakis, G., Elkind, E. & Wooldridge, M.J. 2012. *Computational aspects of cooperative game theory*. R.J. Brachman, W.W. Cohen, & T. Dietterich, Eds.

Chang, C., Wang, Y., Ma, J., Chen, X. & Feng, X. 2018. An energy hub approach for direct interplant heat integration. *Energy*. 159:878–890. DOI: 10.1016/j.energy.2018.06.164.

Chen, J.J.J. 1987. Comments on improvements on a replacement for the logarithmic mean. *Chemical Engineering Science*. 42(10):2488–2489. DOI: 10.1016/0009-2509(87)80128-8.

Chew, I.M.L., Tan, R.R., Foo, D.C.Y. & Chiu, A.S.F. 2009. Game theory approach to the analysis of inter-plant water integration in an eco-industrial park. *Journal of Cleaner Production*. 17(18):1611–1619. DOI: 10.1016/J.JCLEPRO.2009.08.005.

Chitsiga, T.B. & Isafiade, A.J. 2023. Integrated Renewable Energy and Polygeneration Hub Design for Industrial Heat and Power Utilisation. *Chemical Engineering Transactions*. 103:529–534. DOI: 10.3303/CET23103089.

Chowdhury, P., Mahi, N.A., Yeassin, R., Chowdhury, N.-U.-R. & Farrok, O. 2025. Biomass to biofuel: Impacts and mitigation of environmental, health, and socioeconomic challenges. *Energy Conversion and Management: X*. 25:100889. DOI: 10.1016/j.ecmx.2025.100889.

Cowen, N., Vogel, A., Isafiade, A.J., Čuček, L. & Kravanja, Z. 2019. Synthesis of combined heat exchange network and utility supply chain. *Chemical Engineering Transactions*. 76:391–396. DOI: 10.3303/CET1976066.

DiPippo, R. 2008. Geothermal Power Generating Systems. In *Geothermal Power Plants*. Elsevier. DOI: 10.1016/B978-075068620-4.50009-5.

Donohue, K. 2001. Desuperheater Selection and Optimization. *Chemical Engineering*. 108(8).

Edenhofer, O., Steckel, J.C., Jakob, M. & Bertram, C. 2018. Reports of coal's terminal decline may be exaggerated. *Environmental Research Letters*. 13(2). DOI: 10.1088/1748-9326/aaa3a2.

Edgar, T.F., Himmelblau, D.M. (David M. & Lasdon, L.S. 2001. *Optimization of chemical processes*. McGraw-Hill.

El-Halwagi, M.M. 2017. *Sustainable Design Through Process Integration: Fundamentals and Applications to Industrial Pollution Prevention, Resource Conservation, and Profitability Enhancement*. Elsevier. DOI: 10.1016/B978-0-12-809823-3.00022-9.

Emmons, S., Oesterheld, C., Critch, A., Conitzer, V. & Russell, S. 2022. For Learning in Symmetric Teams, Local Optima are Global Nash Equilibria. In *Proceedings of the 39th International Conference on Machine Learning*. Baltimore: PMLR. 5924–5943. Available: https://proceedings.mlr.press/v162/emmons22a.html [2025, March 23].

Evangelisti, L., De Lieto Vollaro, R. & Asdrubali, F. 2019. DOI: 10.1016/j.rser.2019.109318.

Fatihah Salleh, S., Halim Shamsuddin, A., Ab Rashid bin Tuan Abdullah, T., fikri Zulkornain, M., Fadzil Gunawan, M., Fikri Bin Zulkarnain, M., Halim Shamsuddin, A. & Ab Rashid Tuan Abdullah, T. 2019. Modelling and Optimization of Biomass Supply Chain for Bioenergy Production. *Journal of Environmental Treatment Techniques*. 7(4):689–695. Available: http://www.jett.dormaj.com.

Ferrer, I., Garfí, M., Uggetti, E., Ferrer-Martí, L., Calderon, A. & Velo, E. 2011. Biogas production in low-cost household digesters at the Peruvian Andes. *Biomass and Bioenergy*. 35(5):1668–1674. DOI: 10.1016/j.biombioe.2010.12.036.

Fleischman, N.D., Botha, M.F. & Germanis, J.P. 2014. *Sewage sludge and biomass incineration in South Africa using a fluidized-bed reactor*.

Florides, G.A., Kalogirou, S.A., Tassou, S.A. & Wrobel, L.C. 2003. Design and construction of a LiBr-water absorption machine. *Energy Conversion and Management*. 44(15):2483–2508. DOI: 10.1016/S0196-8904(03)00006-2.

Gavrilescu, D. 2008. Energy from Biomass in Pulp and Paper Mills. *Environmental Engineering and Management Journal*. 7(5):537–546. Available: http://omicron.ch.tuiasi.ro/EEMJ/ [2022, April 03].

Gonzalez, H.M., Karelin, O. & Tarasenko, A. 2014. Mathematical Modelling Using Semantic Networks for Teaching. *European Journal of Educational Sciences*. 1(3).

Grammelis, P., Margaritis, N. & Karampinis, E. 2016. Solid fuel types for energy generation. In *Fuel Flexible Energy Generation*. Elsevier. 29–58. DOI: 10.1016/B978-1-78242-378-2.00002-X.

Gxavu, S. & Smail, P. 2012. Design of Heat Exchanger Networks to Minimize Cost and Environmental Impact. University of Cape Town.

Hald-Mortensen, C. 2025. Net Zero through Circular Economy: Insights From the Billund Biorefinery and the Kalundborg Industrial Symbiosis. *Journal of Current Trends in Agriculture, Environment and Sustainability*. 5(3):1–8. Available: https://www.katalystpublishers.com/.

Halkos, G. & Gkampoura, E.C. 2023. Assessing Fossil Fuels and Renewables' Impact on Energy Poverty Conditions in Europe. *Energies*. 16(1). DOI: 10.3390/en16010560.

Hendricks, K. 2010. Activity-Based GHG Accounting. A detailed approach for greenhouse gas accounting.

Herold Keith, Radermacher Reinhard & Klein A. Sanford. 2016. *Absorption Chillers and Heat Pumps*. 2nd ed. CRC Press.

Hossein Davood Abadi Farahani, M., Vatanpour, V. & Hooshang Taheri, A. Eds. 2020. *Desalination - Challenges and Opportunities*. IntechOpen. DOI: 10.5772/intechopen.77449.

Hu, E., Yang, Y. & Nishimur, A. 2012. Solar Aided Power Generation: Generating "Green" Power from Conventional Fossil Fuelled Power Stations. In *Thermal Power Plants*. InTech. DOI: 10.5772/28483.

Hussain, J. & Zhou, K. 2022. Globalization, industrialization, and urbanization in Belt and Road Initiative countries: implications for environmental sustainability and energy demand. *Environmental Science and Pollution Research 2022 29:53*. 29(53):80549–80567. DOI: 10.1007/S11356-022-21520-3.

IEA. 2022. *Buildings*. Paris. Available: https://www.iea.org/reports/buildings [2023, July 06].

IEA Bioenergy. 2018. *Is energy from woody biomass positive for the climate?* Available: https://www.ieabioenergy.com/wp-content/uploads/2018/01/FAQ_WoodyBiomass-Climate_final-1.pdf [2022, April 02].

Isafiade, A.J. & Short, M. 2022a. Multi-Objective Optimisation of Integrated Renewable Energy Feedstock Supply Chain and Work-Heat Exchanger Network Synthesis Considering

Economics and Environmental Impact. *Chemical Engineering Transactions*. 94. DOI: 10.3303/CET2294187.

Isafiade, A.J. & Short, M. 2022b. Multi-Objective Optimisation of Integrated Renewable Energy Feedstock Supply Chain and Work-Heat Exchanger Network Synthesis Considering Economics and Environmental Impact. DOI: 10.3303/CET2294187.

Isafiade, A., Bogataj, M. & Fraser, D. 2015. Optimal synthesis of heat exchanger networks for multi-period operations involving single and multiple utilities. *Chemical Engineering Science*. 127:175–188. DOI: 10.1016/j.ces.2014.12.037.

Isafiade, A., Cowen, N., Vogel, A., Čuček, L. & Kravanja, Z. 2022. Synthesis of utility supply chain network and industrial symbioses for heat integration. *Journal of Cleaner Production*. 380. DOI: 10.1016/j.jclepro.2022.134921.

Isafiade, A.J., Kravanja, Z. & Bogataj, M. 2016. Design of integrated solar thermal energy system for multi-period process heat demand. *Chemical Engineering Transactions*. 52:1303–1308. DOI: 10.3303/CET1652218.

Kalogirou, S.A. 2004. DOI: 10.1016/j.pecs.2004.02.001.

Karakurt, I., Avci, B.D. & Aydin, G. 2024. Leveraging the trend analysis for modeling of the greenhouse gas emissions associated with coal combustion. *Environmental Science and Pollution Research*. 31(39):52448–52472. DOI: 10.1007/s11356-024-34654-3.

Kijewska, K., Konicki, W. & Iwan, S. 2016. Freight Transport Pollution Propagation at Urban Areas Based on Szczecin Example. In *Transportation Research Procedia*. V. 14. Elsevier B.V. 1543–1552. DOI: 10.1016/j.trpro.2016.05.119.

Klein, J., Molnár-in 't Veld, H., Geilenkirchen, G., Hulskotte, J., Ligterink, N. & Dellaert, S. 2018. *Methods for calculating the emissions of transport in the Netherlands*.

Kumar, N.M., Chopra, S.S. & Rajput, P. 2020. Life cycle assessment and environmental impacts of solar PV systems. In *Photovoltaic Solar Energy Conversion*. Elsevier. 391–411. DOI: 10.1016/B978-0-12-819610-6.00012-0.

Kuparinen, K. & Vakkilainen, E. 2017. Green Pulp Mill: Renewable Alternatives to Fossil Fuels in Lime Kiln Operations. *BioResources*. 12(2):4031–4048.

Kurniawan, T., Hakiki, R. & Sidjabat, F.M. 2018. Wastewater Sludge as an Alternative Energy Resource: A Review. *Journal of Env. Engineering & Waste Management*. 3(1):1–12.

Lamb, W.F., Wiedmann, T., Pongratz, J., Andrew, R., Crippa, M., Olivier, J.G.J., Wiedenhofer, D., Mattioli, G., et al. 2021. DOI: 10.1088/1748-9326/abee4e.

Leão, R.R. de C.C., Hamacher, S. & Oliveira, F. 2011. Optimization of biodiesel supply chains based on small farmers: A case study in Brazil. *Bioresource Technology*. 102(19):8958–8963. DOI: 10.1016/j.biortech.2011.07.002.

Li, Y., Alaimo, C.P., Kim, M., Kado, N.Y., Peppers, J., Xue, J., Wan, C., Green, P.G., et al. 2019. Composition and Toxicity of Biogas Produced from Different Feedstocks in California. *Environmental Science & Technology*. 53(19):11569–11579. DOI: 10.1021/acs.est.9b03003.

Lotfi, R., Khanbaba, A., Ali, S.S., Afshar, M., Mehrjardi, M.S. & Omidi, S. 2024. Net-zero, resilience, and agile closed-loop supply chain network design considering robustness and renewable energy. *Environmental Science and Pollution Research*. (March, 13). DOI: 10.1007/s11356-024-32661-y.

Lozano, M.A., Serra, L.M. & Pina, E.A. 2022. Optimal design of trigeneration systems for buildings considering cooperative game theory for allocating production cost to energy services. *Energy*. 261:125299. DOI: 10.1016/j.energy.2022.125299.

Lozano, S., Moreno, P., Adenso-Díaz, B. & Algaba, E. 2013. Cooperative game theory approach to allocating benefits of horizontal cooperation. *European Journal of Operational Research*. 229(2):444–452. DOI: 10.1016/J.EJOR.2013.02.034.

Lu, M. & Lai, J. 2020. Review on carbon emissions of commercial buildings. *Renewable and Sustainable Energy Reviews*. 119:109545. DOI: 10.1016/j.rser.2019.109545.

Madu, K.E., Uyaelumuo, A.E., Ani, E.A. & Udeani, F.O. 2020. Thermodynamic Modelling and Comparison of the Properties of Refrigerant/Absorbent Pairs of a Vapour Absorption Refrigeration System (VARS). *Iconic Research and Engineering*. 3(10).

Maradin, D. 2021. Advantages and disadvantages of renewable energy sources utilization. *International Journal of Energy Economics and Policy*. 11(3):176–183. DOI: 10.32479/ijeep.11027.

Marinelli, S., Butturi, M.A., Rimini, B., Gamberini, R. & Marinello, S. 2020. Evaluating the environmental benefit of energy symbiosis networks in eco-industrial parks. *IFAC-PapersOnLine*. 53(2):13082–13087. DOI: 10.1016/j.ifacol.2020.12.2260.

Maximov, S.A., Mehmood, S. & Friedrich, D. 2021. Multi-objective optimisation of a solar district heating network with seasonal storage for conditions in cities of southern Chile. *Sustainable Cities and Society*. 73:103087. DOI: 10.1016/J.SCS.2021.103087.

McKinnon, A. 2008. *The Potential of Economic Incentives to Reduce CO 2 Emissions from Goods Transport*. Available: http://www.sml.hw.ac.uk/logistics.

McKinnon, A.C., Cullinane, S., Browne, M. & Whiteing, A. 2010. *Green logistics : improving the environmental sustainability of logistics*. Kogan Page.

Meana-Fernández, A., González-Caballín, J.M., Martínez-Pérez, R., Rubio-Serrano, F.J. & Gutiérrez-Trashorras, A.J. 2022. DOI: 10.3390/en15238982.

Mendiburu, A.Z., Roberts, J.J., Rodrigues, L.J. & Verma, S.K. 2023. Thermodynamic modelling for absorption refrigeration cycles powered by solar energy and a case study for Porto Alegre, Brazil. *Energy*. 266:126457. DOI: 10.1016/j.energy.2022.126457.

Muggy, L. & L. Heier Stamm, J. 2014. Game theory applications in humanitarian operations: a review. *Journal of Humanitarian Logistics and Supply Chain Management*. 4(1):4–23. DOI: 10.1108/JHLSCM-07-2013-0026.

Murugan, S. & Horák, B. 2016. Tri and polygeneration systems - A review. *Renewable and Sustainable Energy Reviews*. 60:1032–1051. DOI: 10.1016/j.rser.2016.01.127.

Naseem, I. & Khan, J. 2015. *Impact of Energy Crisis on Economic Growth of Pakistan*. Available: www.iiste.org.

Niu, Y., Lv, Y., Lei, Y., Liu, S., Liang, Y., Wang, D. & Hui, S. 2019. DOI: 10.1016/j.rser.2019.109395.

Nunes, L.J.R., Matias, J.C.O., Loureiro, L.M.E.F., Sá, L.C.R., Silva, H.F.C., Rodrigues, A.M., Causer, T.P., Devallance, D.B., et al. 2020. Evaluation of the Potential of Agricultural Waste Recovery: Energy Densification as a Factor for Residual Biomass Logistics Optimization. DOI: 10.3390/app11010020.

Onishi, V.C., Quirante, N., Ravagnani, M.A.S.S. & Caballero, J.A. 2018. Optimal synthesis of work and heat exchangers networks considering unclassified process streams at sub and above-ambient conditions. *Applied Energy*. 224:567–581. DOI: 10.1016/j.apenergy.2018.05.006.

Osborne, M.J. 2004. *An introduction to game theory*. 3rd ed. V. 3. New York: Oxford University Press.

Pang, K.Y., Liew, P.Y., Woon, K.S., Ho, W.S., Wan Alwi, S.R. & Klemeš, J.J. 2023. Multi-period multi-objective optimisation model for multi-energy urban-industrial symbiosis with heat, cooling, power and hydrogen demands. *Energy*. 262:125201. DOI: 10.1016/j.energy.2022.125201.

Párraga, M., Fajardo, A., Rodríguez-Urrego, L. & Vuelvas, J. 2024. A non-cooperative game approach on isolated water-energy microgrids. *Sustainable Energy, Grids and Networks*. 38:101392. DOI: 10.1016/j.segan.2024.101392.

Partnership for Policy Integrity. 2011. *Carbon emissions from burning biomass for energy*. Available: https://www.pfpi.net/wp-content/uploads/2011/04/PFPI-biomass-carbon-accounting-overview_April.pdf [2022, April 02].

Passacantando, M., Gnecco, G., Hadas, Y. & Sanguineti, M. 2021. Braess' paradox: A cooperative game-theoretic point of view. *Networks*. 78(3):264–283. DOI: 10.1002/net.22018.

Piluso, C. & Huang, Y. 2009. Collaborative profitable pollution prevention: an approach for the sustainable development of complex industrial zones under uncertain information. *Clean Technologies and Environmental Policy*. 11(3):307–322. DOI: 10.1007/s10098-008-0187-y.

Qin, J., Hu, E. & Li, X. 2020. Solar aided power generation: A review. *Energy and Built Environment*. 1(1):11–26. DOI: 10.1016/j.enbenv.2019.09.003.

Qiu, K. & Entchev, E. 2024. Modeling, design and optimization of integrated renewable energy systems for electrification in remote communities. *Sustainable Energy Research*. 11(1):10. DOI: 10.1186/s40807-024-00103-5.

Ranta, T. 2005. Logging residues from regeneration fellings for biofuel production-a GIS-based availability analysis in Finland. *Biomass and Bioenergy*. 28(2):171–182. DOI: 10.1016/J.BIOMBIOE.2004.08.010.

Ravagnani, M.A.S.S., Silva, A.P., Arroyo, P.A. & Constantino, A.A. 2005. Heat exchanger network synthesis and optimisation using genetic algorithm. *Applied Thermal Engineering*. 25(7):1003–1017. DOI: 10.1016/J.APPLTHERMALENG.2004.06.024.

Ren, J., Qian, Z., Yao, Z., Gan, N. & Zhang, Y. 2019. Thermodynamic evaluation of LiCl-H2O and LiBr-H2O absorption refrigeration systems based on a novel model and algorithm. *Energies*. 14(15). DOI: 10.3390/en12153037.

Rommel, M., Kovács, P. & Kramer, K. 2010. Solar thermal technology update. *Renewable Energy Focus*. 11(5):36–38. DOI: 10.1016/S1755-0084(10)70114-9.

Rong, A. & Lahdelma, R. 2016. Role of polygeneration in sustainable energy system development challenges and opportunities from optimization viewpoints. *Renewable and Sustainable Energy Reviews*. 53:363–372. DOI: 10.1016/J.RSER.2015.08.060.

Rulkens, W. 2008. Sewage sludge as a biomass resource for the production of energy: Overview and assessment of the various options. *Energy and Fuels*. 22(1):9–15. DOI: 10.1021/ef700267m.

Sahoo, U., Kumar, R., Pant, P.C. & Chaudhury, R. 2015. Scope and sustainability of hybrid solar-biomass power plant with cooling, desalination in polygeneration process in India. *Renewable and Sustainable Energy Reviews*. 51:304–316. DOI: 10.1016/J.RSER.2015.06.004.

Schwerhoff, G. & Sy, M. 2015. *Renewable energy sources, especially solar, are ideal for meeting Africa's electrical power needs*.

Shapley, L. 1953. A Value for n-Person Games. In *Contributions to the Theory of Games II*. H.W. Kuhn, Ed. Princeton: Princeton University Press. 307–317.

Sheng, C. & Azevedo, J.L.T. 2005. Estimating the higher heating value of biomass fuels from basic analysis data. *Biomass and Bioenergy*. 28(5):499–507. DOI: 10.1016/j.biombioe.2004.11.008.

Shenoy, U. V. 1995. *Heat exchanger network synthesis: process optimization by energy and resource analysis*. Gulf Professional Publishing.

Smith, R. 2005. *Chemical process: Design and Integration*. John Wiley & Sons.

Smith, C.C. & Weiss, T.A. 1977. Design application of the Hottel-Whillier-Bliss equation. *Solar Energy*. 19(2):109–113.

Smołka-Danielowska, D. & Jabłońska, M. 2022. Chemical and mineral composition of ashes from wood biomass combustion in domestic wood-fired furnaces. *International Journal of Environmental Science and Technology*. 19(6):5359–5372. DOI: 10.1007/s13762-021-03506-9.

Sørensen, C.G., Sambra, A., Sørensen, C.G. & Kristensen, E.F. 2008. *Optimized harvest and logistics for biomass supply chain.* Available: https://www.researchgate.net/publication/237652559.

Stolarski, M., Krzyżaniak, M., Stolarski, M., Rybczyńska, B., Peni, D., Bordiean, A., Lajszner, W. & Graban, Ł. 2019. Thermophysical properties and elemental composition of agricultural and forest solid biofuels versus fossil fuels. *Journal of Elementology*. (4/2019). DOI: 10.5601/jelem.2019.24.1.1819.

Sultana, A. & Kumar, A. 2014. Development of tortuosity factor for assessment of lignocellulosic biomass delivery cost to a biorefinery. *Applied Energy*. 119:288–295. DOI: 10.1016/J.APENERGY.2013.12.036.

Sun, J., Fu, L. & Zhang, S. 2012. A review of working fluids of absorption cycles. *Renewable and Sustainable Energy Reviews*. 16(4):1899–1906. DOI: 10.1016/j.rser.2012.01.011.

Tan, R.R., Andiappan, V., Wan, Y.K., Ng, R.T.L. & Ng, D.K.S. 2016. An optimization-based cooperative game approach for systematic allocation of costs and benefits in interplant process integration. *Chemical Engineering Research and Design*. 106:43–58. DOI: 10.1016/j.cherd.2015.11.009.

Tanuma, T. 2017. *Advances in Steam Turbines for Modern Power Plants*. Elsevier Science.

Towler, G. & Sinnott, R. 2021. *Chemical Engineering Design: Principles, Practice and Economics of Plant and Process Design*. Elsevier Science.

Towler, G. & Sinnott, R.K. 2013. Chemical Engineering Design Principles, Practice and Economics of Plant and Process Design. 2nd ed. Elsevier. Available: "https://app.knovel.com/hotlink/khtml/id:kt00ANU161/chemical-engineering/annualized-capital-cost" [2023, July 03].

Wang, C.-N., Cao, T.-B.-O., Duy Nguyen, D. & Dang, T.-T. 2024. Bi-objective optimization modeling for biomass supply chain planning. *Measurement and Control*. 57(8):1087–1098. DOI: 10.1177/00202940241226603.

West, T.O., Marland, G., Singh, N., Bhaduri, B.L. & Roddy, A.B. 2009. The human carbon budget: an estimate of the spatial distribution of metabolic carbon consumption and release in the United States. *Biogeochemistry*. 94(1):29–41. DOI: 10.1007/s10533-009-9306-z.

Yang, Y., Yan, Q., Zhai, R., Kouzani, A. & Hu, E. 2011. An efficient way to use medium-or-low temperature solar heat for power generation - Integration into conventional power plant. *Applied Thermal Engineering*. 31(2–3):157–162. DOI: 10.1016/j.applthermaleng.2010.08.024.

Yee, T.F. & Grossmann, I.E. 1990. Simultaneous optimization models for heat integration—II. Heat exchanger network synthesis. *Computers & Chemical Engineering*. 14(10):1165–1184. DOI: 10.1016/0098-1354(90)85010-8.

Zakaria, M.S., Hassan, S. & Nor, F. 2015. *Calorific value of the sewage sludge in the thermal dryer*. Available: https://www.researchgate.net/publication/288208299_Calorific_value_of_the_sewage_sludge_in_the_thermal_dryer [2022, April 03].

Zhou, S., Gong, L., Liu, X. & Shen, S. 2019. Mathematical modeling and performance analysis for multi-effect evaporation/multi-effect evaporation with thermal vapor compression desalination system. *Applied Thermal Engineering*. 159. DOI: 10.1016/j.applthermaleng.2019.113759.

Appendix A

A1

H = vapour enthalpy (kJ/kg)

T = temperature (°C)

H_{cnd} = latent heat of condensation (kJ/kg)

$$H = -0.00125397T^2 + 1.8806037T + 2500.559 \quad \text{(A1.1)}$$

$$H_{cnd} = -0.00132635T^2 - 2.29983657T + 2500.43063 \quad \text{(A1.2)}$$

A2. LiBr solution and refrigerant temperature and pressure (45% < x < 70%)

T_{ref} = refrigerant saturation temperature (-15°C < T_{ref} < 110°C)

T_{sol} = solution temperature (5°C < T_{sol} < 175°C)

P = saturation pressure (kPa)

A_0 = -2.00755, A_1 = 0.16976, A_2 = -0.003133362, A_3 = 0.0000197668

B_0 = 124.937, B_1 = -7.71649, B_2 = 0.152286, B_3 = -0.0007959

$$\sum A = A_0x^0 + A_1x^1 + A_2x^2 + A_3x^3$$

$$\sum B = B_0x^0 + B_1x^1 + B_2x^2 + B_3x^3$$

C = 7.05, D = -1596.49, E = -104095.5

$$LogP = C + \frac{D}{T_{ref} + 273} + \frac{E}{(T_{ref} + 273)^2} \quad \text{(A2.1)}$$

$$T_{ref} = \frac{T_{sol} - \sum B}{\sum A} \quad \text{(A2.2)}$$

$$T_{ref} = \frac{-2E}{D + [D^2 - 4E(C - logP)]^{0.5}} - 273 \quad \text{(A2.3)}$$

A3. LiBr solution enthalpy (40% < x < 70%)

T = solution temperature (°C)

h = enthalpy (kJ/kg)

A_0 = -2024.33, A_1 = 163.309, A_2 = -4.88161, A_3 = 0.06302948, A_4 = -0.0002913704

B_0 = 18.2829, B_1 = -1.1691757, B_2 = 0.03248041, B_3 = -0.0004034184,

B_4 = 0.0000018520569

C_0 = -0.037008214, C_1 = 0.0028877666, C_2 = -0.000081313015, C_3 = 0.00000099116628,

C_4 = -0.0000000044441207

$$\sum A = A_0x^0 + A_1x^1 + A_2x^2 + A_3x^3 + A_4x^4$$

$$\sum B = B_0x^0 + B_1x^1 + B_2x^2 + B_3x^3 + B_4x^4$$

$$\sum C = C_0x^0 + C_1x^1 + C_2x^2 + C_3x^3 + C_4x^4$$

$$h = \sum A + T \cdot \sum B + T^2 \cdot \sum C \qquad \text{(A3.1)}$$

A4. LiBr solution density (20% < x < 60%)

T = solution temperature (0°C < T < 200°C)

ρ_x = solution density (kg/m^3)

x_0 = x/100

$$\rho_x = 1145.36 + 470.84x_0 + 1374.79x_0^2 - [(0.333393 + 0.571749x_0)(273 + T)] \qquad \text{(A4.1)}$$

Appendix B

Table B1: Feedstock Carbon compositions (weight fraction)

Feedstock	**Distance from supplier (km)***	**Carbon composition**
Sewage sludge	30	0.101 (West et al., 2009)
Forestry residue	50	0.458 (Smołka-Danielowska & Jabłońska, 2022)
Biogas	38	0.563 (Li et al., 2019)
Coal	100	0.775 (Grammelis, Margaritis & Karampinis, 2016)

Table B2: CHP stream parameters

Parameter	**T_s (℃)**	**T_t (℃)**	**H_1 (kJ/kg)**
Boiler feed water	30	-	125.7
Pre-heated boiler feed water	30	60	271.9
Solar capture fluid	120	85	-
De-superheating spray water	30	-	125.7

Table B3: Solar-aided Power Generation input parameters

Nomenclature	**Parameter**	**Value**
η^{bl}	Boiler efficiency	0.75 (Edgar, Himmelblau & Lasdon, 2001)
$MaxG_1$	Maximum turbine generative capacity T1 (kW)	6 250 (Edgar, Himmelblau & Lasdon, 2001)
$MinG_1$	Minimum turbine generative capacity T1 (kW)	2 500 (Edgar, Himmelblau & Lasdon, 2001)
$MaxG_2$	Maximum turbine generative capacity T1 (kW)	9 000 (Edgar, Himmelblau & Lasdon, 2001)
$MinG_2$	Minimum turbine generative capacity T1 (kW)	3 000 (Edgar, Himmelblau & Lasdon, 2001)
BSSP	Base power purchased (kW)	12 000
P^{Demand}	Electric power demand (kW)	24 550
T_a	Ambient temperature (°C)	30
GHI	Global horizontal irradiation (kW/m^2)	0.8 (Isafiade et al., 2016)
a_1	thermal loss coefficient (kW/m^2)	0.00153 (Isafiade et al., 2016)
a_2	thermal loss coefficient (kW/m^2)	0.0000003 (Isafiade et al., 2016)
η_{sl}	Solar panel efficiency	0.764 (Isafiade et al., 2016)
n	Annual Operating hours (hrs)	8160

Appendix C

```
*Sample Code: Case 1
set
 sp                  supply points             /HW, WP, BG,
                     CL/
 f                   freight mode              /road, rail,
                     pipe/
 FreightCosts        Freight costs             /FFC, VFC, AF,
                     FIC, tau, RF/
 S                   supply chain season       /s1, s2, s3/;

Parameters

DS(s) Duration of season as a fraction of the year
/  s1          0.35
   s2          0.35
   s3          0.3/

NC (sp)           'net calorific value in kWh per kg'
BE                'boiler efficiency'
OH                'plant operating hours per year'
d (sp)            'distance between supply points and power generation
point in km'
Ccomp (sp)        'Carbon composition of fuel type'
RO                'ratio of CO2 to carbon upon oxidation i.e. 44/12'
CpF (f)           'Capacity factor- mass of feed stock per load in kg'
Emf  (f)          'Emission factor in gCO2 per ton-km';

 NC ('HW')      = 4.52;
 NC ('WP')      = 4.95;
 NC ('BG')      = 5.08;
 NC ('CL')      = 7.20;
 BE             = 0.75;
 OH             = 8160;
 d ('HW')       = 30;
 d ('WP')       = 50;
 d ('BG')       = 38;
 d ('CL')       = 100;
 Ccomp ('HW')   = 0.101;
 Ccomp ('WP')   = 0.458;
 Ccomp ('BG')   = 0.563;
 Ccomp ('CL')   = 0.775;
 RO             = 3.67;
 Emf ('road')   = 72;
```

```
 Emf ('rail')  = 35;
 CpF ('road')  = 35000;
 CpF ('rail')  = 1000000;
 CpF ('pipe')  = 1;


Table capacity(sp,S) capacity of the supply points per season in kg per
year

                s1              S2              S3
       HW       30000000        45000000        20000000
       WP       250000000       210000000       300000000
       BG       450000000       500000000       20000000
       CL       50000000        50000000        50000000;


* Feedstock Cost Table
Table FeedCost(sp, S) Cost of feedstock from each supply point in each
season in $ per kg
                    s1        s2        s3
    HW            0.024     0.022     0.027
    WP            0.040     0.045     0.025
    BG            0.050     0.030     0.070
    CL            0.900     0.900     0.900;

* Freight Cost Data
Table FreightCost (f, FreightCosts)
          FFC      VFC          AF       FIC       tau    RF
road     0.002    0.00009     0.2       5000      1.27    2
rail     0.005    0.000007    0.25      50000     1.1     2
pipe     0.000    0.0000001   0.50      150000    1.27    1;

* FFC  = Fixed Freight Costs ($/kg)
* VFC  = Variable Freight Costs ($/kg.km)
* AF   = Annualization factor (years)
* FIC  = Freight investment cost ($/km)
* tau  = Tortuosity factor
* RF   = Return trip factor

Positive Variables
   FSCN       'Supply chain fixed and variable cost'
   ISCN       'Supply chain investment cost'
   x          'Fuel quantity in kW'
   x_kg       'Fuel quantity in kg'
   bb(sp,s)   'Boiler demand in kW'
   EmT(f)     'Transport emissions (tonnes/year)'
   EmB(sp)    'Boiler emissions (tonnes/year)'
```

```
   trips(s,f) 'Number of trips per transport mode per season';

Binary Variable
 z(sp,f  'Denotes link between supply point and freight mode';

* Logical Constraints for Transport Links
Equations
    con1         'Wood pulp may not be transported through pipe'
    con2         'Coal may not be transported through pipe'
    con3         'Human waste may not be transported through pipe'
    con4(sp,s,f) 'Total fuel transported by each transport mode ≤ supply
                 capacity';

con1.. z('WP', 'pipe') =e= 0;
con2.. z('CL', 'pipe') =e= 0;
con3.. z('HW', 'pipe') =e= 0;

con4(sp,s,f)..
    (x(sp,f,s)/(BE*NC(sp)/(OH*DS(s))))/CpF(f) =l= capacity(sp,s)/CpF(f);

* Other Constraints
Equation
    Supply(sp,s)       'Supply constraint for SP capacity'
    demand(sp,s)       'Demand constraint'
    FreightCap(sp,f,s) 'Freight capacity'
    EISCN(sp,f)        'SCN investment costs'
    EFSCN(sp,f,s)      'SCN fixed and variable costs'
    EmissionsT(f)      'Transport CO2 emissions (tonnes/year)'
    EmissionsB(sp)     'Biomass combustion CO2 emissions (tonnes/year)'
    Etrips(s,f)        'Number of trips per transport mode per season'
    Ex_kg(sp,f,s)      'Quantity of feedstock supplied (kg)';

Supply(sp,s)..
    sum((f), x(sp,f,s)) =l= capacity(sp,s)*BE*NC(sp)/(OH*DS(s));

demand(sp,s)..
    sum((f), x(sp,f,s)) =g= bb(sp,s);

FreightCap(sp,f,s)..
    x(sp,f,s) =l= capacity(sp,s)*z(sp,f)*BE*NC(sp)/(OH*DS(s));

Ex_kg(sp,f,s)..
    x_kg(sp,f,s) =e= x(sp,f,s)/(BE*NC(sp)/(OH*DS(s)));

EFSCN(sp,f,s)..
    FSCN(sp,f,s) =e=
        ((FreightCost(f,'FFC') +
```

```
(FreightCost(f,'VFC')*FreightCost(f,'tau')*d(sp)*FreightCost(f,'RF')))
        *x(sp,f,s)/(BE*NC(sp)/(OH*DS(s)))*z(sp,f))
        + (FeedCost(sp,s) * x(sp,f,s)/(BE*NC(sp)/(OH*DS(s))));

EISCN(sp,f)..
    ISCN(sp,f) =e=
        FreightCost(f,'AF')*FreightCost(f,'FIC')*
        FreightCost(f,'tau')*d(sp)*z(sp,f);

Etrips(s,f)..
    trips(s,f) =e= sum(sp, (x(sp,f,s)/(BE*NC(sp)/OH))/CpF(f));

EmissionsT(f)..
    EmT(f) =e=
        sum((sp,s), ((x(sp,f,s)/(BE*NC(sp)/OH))*d(sp)*Emf(f)/1e9) *
                    (x(sp,f,s)/(BE*NC(sp)/OH)/CpF(f)));

EmissionsB(sp)..
    EmB(sp) =e=
        sum((f,s), ((x(sp,f,s)/BE*NC(sp))*Ccomp(sp)*RO*OH)/1000);


*Emissions divided by 1000 to convert to tonnes per year and  stay
within GAMS range of values

*FSCN.lo(sp,f,s)    = 0.000001;
*FSCN.up(sp,f,s)    = 999999999;
*ISCN.lo(sp,f,s)    = 0.0001;
*ISCN.up(sp,f,s)    = 999999999;

*=====================================================================*

Set
T   Turbines              /Tb1,Tb2/
Ws  Water Stream          /ws1,ws2,ws3,ws4, ws5, ws6/
Stp Stream Properties     /sTmp1, sTmp2, sE2, sRC, sCst/;

Table Streamproperties (Ws, Stp)

           sTmp1    sTmp2       sE2           sRC        sCst

ws1        30        30        125.7      9900000000     0
ws2        30        60        271.9      9900000000     0
ws3        120       85          0        9999999999     0
ws4        30        0         125.7      9999999999     0
ws5        25        80          0            0          0
```

```
ws6        25       100       2675.57          0          0.016;

*ws1 = boiler feed, ws2 = boiler feed 2, ws3 = solar capture fluid, ws4
= desuperheating water,
*ws5 = salt water feed, ws6 = condenser water

*sTmp = stream temperature [degrees Celcius]
*sE2  = stream final enthalpy (from steam tables) [kJ per kg]
*sRC  = annual stream reservoir capacity [kg]
*sCst = stream cost in $/kg [Turton et al 2018 Analysis Synthesis &
        Design f Chemical Processes]

Parameter
Mingencap(t)      Minimum generative capacity of turbine in kW
Maxgencap(t)      Maximum generative capacity of turbine in kW
Maxexitflow(t)    Maximum exit flowrate from turbine i in kg per sec
Maxcondflow(t)    Maximum condensate flow from turbine 1 in kg per sec
Maxintflow(t)     Maximum internal flow in turbine in kg per sec
MaxLPSout(t)      Maximum LPS exhaust from turbine in kg per sec
Basepowerpur      Base power purchased in kw
MPSconstraint     Demand on system i.e. minimumof MPS that must
                  be produced in kg per sec
LPSconstraint     Demand on system i.e. minimumof LPS that must be
                  produced in kg per sec
EP_d              Electric power demand in kW
Best              Best objective function values (dollars per year for
                  cost and tonnes per year for emissions)
Ta                Ambient temperature [Degrees Celcius]
GHI               Global horizontal irradiation [kW per square meter]
aa1               thermal loss coefficient 1 (kW per meter squared)
aa2               thermal loss coefficient 2 (kW per meter squared)
n                 Solar panel efficiency
Cp                Heat capacity of water
SPc               solar panel cost [$ per square meter]
exp               exponent in area equation;

*Parameter specifications
Ta               = 30;
GHI              = 0.8;
aa1              = 0.00153;
aa2              = 0.0000003;
n                = 0.764;
Cp               = 4.2;
SPc              = 100;
exp              = 2;
```

```
Best('COST')          = 38.045562;
Best('E')             = 69580205.410751;

Mingencap('tb1')      = 2500;
Maxgencap('tb1')      = 6250;

Mingencap('tb2')      = 3000;
Maxgencap('tb2')      = 9000;

Maxexitflow('tb1')    = 87089.75/3600;
Maxexitflow('tb2')    = 156035.8/3600;

Maxintflow('tb1')     = 59874.2/3600;
Maxintflow('tb2')     = 110676.55/3600;

Maxcondflow('tb1')    = 28122.727/3600;
Maxcondflow('tb2')    = 0;


MaxLPSout('tb1')      = 453.59/3600;
MaxLPSout('tb2')      = 64410.12/3600;

Basepowerpur          = 12000;

MPSconstraint         = 123166.67/3600;
LPSconstraint         = 45641.83/3600;
EP_d                  = 24550;


Positive Variables
Power(t)               Power generated by turbines
Turbineoutflow(t)      Total flowrate out of turbines
Condensateoutflow(t)   Condensate flowing out of turbines
DeltaH(sp)             Boiler load
Inletflowturb(t)       HPS flowing into Turbines [kg per s]
InletflowHEN           HPS flowing directly into HEN [kg per s]
C                      condensate flow rate from turbine 1 [kg per s]
LPSoutflow(t)          LPS flowing from turbines [kg per s]
HPST                   Total HPS [kg per s]
MPS                    Total MPS [kg per s]
LPS                    Total LPS [kg per s]
BF1                    Bypass flow rate from 635 psi to 195 psi header
                       [kg per s]
BF2                    Bypass flow rate from 195 psi to 62 psi header
                       [kg per s]
EP                     Excess power [kW]
PP                     Purchased power [kW];
```

```
Positive Variables
Fws (ws) stream flow rate in kg per s;

variables
wD    Water required for power generation [kg per s]
wTC   Total Cost of water in $ per year
Q_fw  Energy present in feed water [kw]
T_c   Average collector temperature [Degrees Celcius];

Parameter
wc     price of water in $ per kg [Turton et al 2018 Analysis Synthesis
       & Design f Chemical Processes] /w  0.15/
CP_s   Heat capacity of thermal storage stream [kJ per kg C] /4.2/
r      density of thermal storage stream [kg per m3]         /1000/
U_st   Heat transfer coefficient of thermal storage stream   /0.25/
CST    cost per unit volume of thermal storage tank [$ per cubic meter]
       /50/
CHE    cost per unit area of HE [$ per square meter]        /641.7/
CI     cost index for heat exchanger                        /0.83/
HEI    heat exchanger installation cost [$]                 /8333.3/;

equation

WaterB   'water balance in boiler'
WaterC   'Total cost of water in $ per year'
FeedQ    'Energy present in feed water[kw]'
ws1Cap   'stream 1 source capacity constraint'
ws2Cap   'stream 2 source capacity constraint'
SpTc     'Average panel temperature'
AreaSP   'area of solar panel'
AreaHE1  'area of heat exchanger'
VolumeST 'volume of thermal storage tank'
EfwsB
;

Binary Variable
S_A Denotes use of solar to aid power generation;

waterB..   wD-C   =e= HPST;

WaterC..   wTC    =e= wD *wc('w');
FeedQ..    Q_fw   =e= fws('ws2')*CP_s*(streamproperties('ws2', 'sTmp2')-
                     streamproperties('ws2', 'sTmp1'))*S_A;
```

```
ws1Cap..  fws('ws1')*3600*8160 =l= streamproperties('ws1', 'sRC');
ws2Cap..  fws('ws2')*3600*8160 =l= streamproperties('ws2', 'sRC');

EfwsB..   fws('ws1')*(1-s_a) + fws('ws2')*s_a =e= HPST;

*EfwsB2.. fws('ws1')* s_a                     =E= 0;

*EfwsB2.. fws('ws2')* s_a                     =E= 0;

Q_fw.lo = 0;
Q_fw.up = 9999999999;

Variable
cost              'TAC objective function value'
E                 'Emission objective function value'
Multiobjective    'Dual objective function value';

Positive variable
ASP    'area of solar panel [Square meters]'
VST    'volume of thermal storage tank [cubic meters]'
AHE1   'area of heat exchanger1 [Square meters]'
AHE2   'Area of heat exchanger2 [Square meters]';

SpTc..      T_c  =e= (((streamproperties('ws2',
            'sTmp1'))+(streamproperties('ws2','sTmp2')))/2);

AreaSP..    ASP  =e= ((fws('ws2')*((streamproperties('ws2','sTmp2'))-
           (streamproperties('ws2', 'sTmp1')))*cp_s) +(fws('ws5')
           *((streamproperties('ws5','sTmp2'))-(streamproperties('ws5',
           'sTmp1')))*cp_s))/((n*GHI)-(aa1*(T_c-Ta))-(aa2*(T_c-Ta)*(T_c-
           Ta)))*S_A;

*AreaHE1.. AHE1 =g= (((fws('ws2')*((streamproperties('ws2','sTmp2'))-
           (streamproperties('ws2','sTmp1')))*cp_s)*/(((streamproperties
           ('ws3','sTmp1') -(streamproperties('ws2','sTmp1')))
           *(streamproperties('ws3','sTmp2') -
           (streamproperties('ws2','sTmp2')))
           **((((streamproperties('ws3','sTmp1')-
           (streamproperties('ws2','sTmp1')))+
           (streamproperties('ws3','sTmp2')-
           (streamproperties('ws2','sTmp2'))))/2)**0.3333))*U_st)))*S_A;

AreaHE1..   AHE1 =g= S_A * (((fws('ws2') *
           (streamproperties('ws2','sTmp2') -
           streamproperties('ws2','sTmp1')) * cp_s)
           / (((streamproperties('ws3','sTmp1') -
           streamproperties('ws2','sTmp1')) *
```

```
            (streamproperties('ws3','sTmp2') -
            streamproperties('ws2','sTmp2')))
            * ((((streamproperties('ws3','sTmp1') -
            streamproperties('ws2','sTmp1')) +
            (streamproperties('ws3','sTmp2') -
            streamproperties('ws2','sTmp2'))) / 2)**0.3333) * U_st)));

VolumeST..  VST  =g= ((fws('ws2')*((streamproperties('ws2','sTmp2'))-
            (streamproperties('ws2', 'sTmp1')))*cp_s)/2)
            /(CP_s*r*(streamproperties('ws3', 'sTmp1')-
            streamproperties('ws3', 'sTmp2')))*S_A;

*AHE1.LO = 0;

*AHE1.UP = 99;
*=====================================================================*

Equation

Mingencaptub(t)       Minimum generative capacity of turbine in kW
Maxgencaptub(t)       Maximum generative capacity of turbine in kW
Turbineexitflow(t)    Maximum exit flow from turbine i lb per h
Mxcondensateflow(t)   Maximum condensate flow from turbine 1
Balanceturb1(t)       Mass flow balance over turbine i
Balanceturb2(t)
Maximumlowpressout(t)
Massbal3              Mass balance of HPS flowing from boiler to BF1 +
turbines + HEN
Massbal4
Massbal5
Massbal6
Massbal7
Massbal8
Limitpowerpurchased
Mediumpress
Lowpress
Totpowerdemand
Energybal1
Energybal2
BoilerB(sp)
Cost_obj               SCN objective function
Em_obj                 Emissions objective function
Multi_obj              Dual objective function
DeltaHdist1(sp)        Delta H distribution over season 1 and 2
DeltaHdist2(sp)        Delta H distribution over season 2 and 3
WaterB                 Water mass balance in boiler
HPSb                   HPS energy balance;
```

```
*Minimum and maximum generative capacity from turbines 1 and 2
Mingencaptub(t)..Power(t)=g=Mingencap(t);
Maxgencaptub(t)..Power(t)=l=Maxgencap(t);


*Maximum exit flow from turbines 1 and 2 to the MPS header
Turbineexitflow(t)..    Turbineoutflow(t)=l= Maxexitflow(t);

*Maximum condensate flow out of turbine 1
Mxcondensateflow(t)..   Condensateoutflow('tb1')=l= Maxcondflow('tb1');

Balanceturb1(t) ..      Inletflowturb('tb1')- Turbineoutflow('tb1')
                        =l= Maxintflow('tb1');

Balanceturb2(t) ..      Inletflowturb('tb2')=l= Maxintflow('tb2') ;

Maximumlowpressout(t).. LPSoutflow('tb2')=l= MaxLPSout('tb2');


*Massbal2..             HPSTOT=E= Sum((sp),DeltaH(sp)/(NC(sp)*3600));

*Material balance over HPS splitting point
Massbal3..              HPST - Inletflowturb('tb1')-
                        Inletflowturb('tb2') - BF1 - InletflowHEN =E=0;

Massbal4..     Inletflowturb('tb1')+Inletflowturb('tb2') + BF1 -
               Condensateoutflow('tb1') -MPS - LPS =E=0;

Massbal5..     Inletflowturb('tb1') - Turbineoutflow('tb1') -
               LPSoutflow('tb1') - Condensateoutflow('tb1') =E=0;

Massbal6..     Inletflowturb('tb2') - Turbineoutflow('tb2') -
               LPSoutflow('tb2') =E=0;

Massbal7..     Turbineoutflow('tb1') + Turbineoutflow('tb2') + BF1 - BF2
               -MPS  =E=0;

Massbal8..     LPSoutflow('tb1') +LPSoutflow('tb2') + BF2 -LPS  =E=0;

*Power purchased
Limitpowerpurchased..  EP + PP =G= Basepowerpur;

*Demands
Mediumpress..          MPS =G= MPSconstraint;

Lowpress..             LPS =G= LPSconstraint;
```

```
Totpowerdemand..       Power('tb1')+Power('tb2') + PP =G= EP_d;

*Energy balances
Energybal1..   3160.78*Inletflowturb('tb1')-
               2789.9*Turbineoutflow('tb1')- 2750.6*LPSoutflow('tb1') -
               446.29* Condensateoutflow('tb1')-Power('tb1') =E=0;

Energybal2..   3160.78*Inletflowturb('tb2')-2789.9*Inletflowturb('tb2')-
               2750.6*LPSoutflow('tb2') -Power('tb2') =E=0;

*Boiler Balance

BoilerB (sp)..     DeltaH(sp)- (Q_fw/2)*s_a =e= sum(s, bb(sp,s));
HPSb..             HPST =e= sum((sp), DeltaH(sp)/(NC(sp)*3600));
DeltaHdist1(sp).. (bb('HW', 's1')+bb('WP', 's1')+
                   bb('BG','s1')+bb('CL','s1'))=e= bb('HW',
                  's2')+bb('WP','s2')+bb('BG','s2')+bb('CL','s2');
DeltaHdist2(sp).. (bb('HW', 's3')+bb('WP', 's3')+
                   bb('BG','s3')+bb('CL','s3'))=e= (0.3/0.35)*(bb('HW',
                  's2')+bb('WP','s2')+bb('BG','s2')+bb('CL','s2'));


*=====================================================================*
*CONDENSATION CALCULATIONS
*Assuming MPS and LPS are not used for heating, they will be condensed
to restart the rankine cycle.
*HPS @43 bar, mps @13.44 bar, LPS @4.27 bar (ALL SATURATED)
*desuperheating
Parameter
h_LPS  enthalpy of superheated LPS   [kJ per kg]       /2910.76/
h_LPSd enthalpy of desuperheated LPS [kJ per kg]       /2752.78/
h_MPS  enthalpy of superheated MPS   [kJ per kg]       /2948.90/
h_MPSd enthalpy of desuperheated MPS [kJ per kg]       /2798.21/
h_HPS  enthalpy of superheated HPS  [kJ per kg]         /3162.89/
h_HPSd enthalpy of desuperheated HPS [kJ per kg]        /2798.90/
hw_ds  enthalpy of cooling water @25 dgrees [kJ per kg] /104.93/;


Positive variable
mw_ds1     mass flow rate of cooling water required for LPS [kg per s]
mw_ds2     mass flow rate of cooling water required for MPS [kg per s]
mw_ds3     mass flow rate of cooling water required for HPS [kg per s]

MPSd, HPSd, LPSd mass flow rates of desuperheated steam [kg per s]

FlowHEN1   Excess HPS to be used for HEN or condensed for recycle
```

```
           [kg per s]
FlowHEN2   Excess MPS
FlowHEN3   Excess LPS;


Equation
Emw_ds1,emw_ds2, Emw_ds3, EMPSd, ELPSd, EHPSd, FlowtoHEN1;

Emw_ds1..    mw_ds1       =e= (LPS*(h_LPS-h_LPSd))/(h_LPSd-hw_ds);
Emw_ds2..    mw_ds2       =e= (MPS*(h_MPS-h_MPSd))/(h_MPSd-hw_ds);
Emw_ds3..    mw_ds3       =e= (FlowHen1*(h_HPS-h_HPSd))/(h_HPSd-hw_ds);
FlowtoHEN1.. InletflowHEN =e=  FlowHEN1;


EMPSd.. MPSd =e= MPS      + mw_ds2;
ELPSd.. LPSd =e= LPS      + mw_ds1;
EHPSd.. HPSd =e= FlowHEN1 + mw_ds3;

*=====================================================================*
*BOILER COSTING; The constatnts used below are derived from the text
book, Chemical engineering design

Parameter
*constants for costing equation
BCcnst1 /130000/

BCcnst2 /53/

BXpnt   /0.9/;

Positive Variable

Bcst 'capital cost of boiler in dollars';

Equation

BCstE  'boiler cost eqaution' ;

BCstE.. Bcst =e= (BCcnst1 + (BCcnst2 * ((HPST*3600)**BXpnt)));

*Bcst.lo = 0.000000001;
 Bcst.up = 999999999;


*TURBINE COSTING

Parameter
```

```
*constants for turbine cost equation'
TbCcnst1 /-14000/

TbCcnst2 / 1900/

TbXpnt   /0.75/;

Positive variable

 TbCst 'capital cost of turbine in dollars';

Equation

TbCstE;

TbCstE.. TbCst =e= sum(T, TbCcnst1 + (TbCcnst2 * (Power(t)**TbXpnt)));

*Cable costing
Parameter
*according to https://www.power-sonic.com/blog/single-phase-and-three-
phase-voltage-by-country/
LV Three phase Line voltage [volts]            /400/
D_Demand   distance from Demand [m]            /13000/

*Daniel DeSantis, Brian D. James, Cassidy Houchins, Genevieve Saur,
Maxim Lyubovsky,
*Cost of long-distance energy transmission by different carriers,
*iScience, Volume 24, Issue 12, 2021,

CbP Cable price [Electricity (500 kV HVDC)][dollars per mile - MWh]
/41.5/;

Equation
ECb_cst;

variable
Cb_cst;

ECb_cst.. Cb_cst =e= (CbP/1.6)*(EP_d/1000)*(D_Demand/1000);

*Cb_cst.lo = 0.000001;
*Cb_cst.up = 999999;


*HEN PIPING COST
Parameter
LPS_CP     heat capacity of LPS [kJ per kg . K]          /2.39/
```

```
MPS_CP     heat capacity of MPS [kJ per kg . K]          /2.9/
HPS_CP     heat capacity of HPS [kJ per kg . K]          /4.13/
LPS_Rh     desnity of desuperheated LPS [kg per m3]      /491/
MPS_Rh     desnity of desuperheated MPS [kg per m3]      /367/
HPS_Rh     desnity of desuperheated HPS [kg per m3]      /314/
AF_HEN     Annualization factor for HEN                  /0.322/;

Parameter
A_1 /0.82/
A_2 /185/
A_3 /6.8/
A_4 /295/;

Positive Variable
DL_in  Internal diameter for LPS hot stream [m]
DM_in  Internal diameter for MPS hot stream [m]
DH_in  Internal diameter for HPS hot stream [m]

DL_ex  External diameter for LPS hot stream  [m]
DM_ex  External diameter for MPS hot stream  [m]
DH_ex  External diameter for HPS hot stream  [m]

WL_p   Weight of LPS hot pipe [kg per m]
WM_p   Weight of MPS hot pipe [kg per m]
WH_p   Weight of HPS hot pipe [kg per m]

PL_cst Cost of LPS hot pipe [$ per m]
PM_cst Cost of MPS hot pipe [$ per m]
PH_cst Cost of HPS hot pipe [$ per m]

HEN_Pcst Anualized cost of HEN steam supply piping;

Equation

EDL_in  Internal diameter for LPS hot stream [m]
EDM_in  Internal diameter for MPS hot stream [m]
EDH_in  Internal diameter for HPS hot stream [m]

EDL_ex  External diameter for LPS hot stream  [m]
EDM_ex  External diameter for MPS hot stream  [m]
EDH_ex  External diameter for HPS hot stream  [m]

EWL_p   Weight of LPS hot pipe [kg per m]
EWM_p   Weight of MPS hot pipe [kg per m]
EWH_p   Weight of HPS hot pipe [kg per m]

EPL_cst Cost of LPS hot pipe [$ per m]
```

```
EPM_cst Cost of MPS hot pipe [$ per m]
EPH_cst Cost of HPS hot pipe [$ per m]

EHEN_Pcst  Anualized cost of HEN steam supply piping;

EDL_in..  DL_in  =E= 0.363*(FlowHEN3**0.45) * (LPS_CP**(-0.45))*
                 (LPS_Rh**(-0.32));
EDM_in..  DM_in  =E= 0.363*(FlowHEN2**0.45) * (MPS_CP**(-0.45))*
                 (MPS_Rh**(-0.32));
EDH_in..  DH_in  =E= 0.363*(FlowHEN1**0.45) * (HPS_CP**(-0.45))*
                 (HPS_Rh**(-0.32));

*FlowHEN3.lo  = 0.00000000000001;
*FlowHEN3.up  = 1999;
*FlowHEN2.lo  = 0.00000000000001;
*FlowHEN2.up  = 3000;
*FlowHEN1.lo  = 0.00000000000001;
*FlowHEN1.up  = 999;

EDL_ex.. DL_ex =E= 1.101 * DL_in + 0.006349;
EDM_ex.. DM_ex =E= 1.101 * DM_in + 0.006349;
EDH_ex.. DH_ex =E= 1.101 * DH_in + 0.006349;

EWL_p.. WL_p =e= 1330 * (DL_in**2) + (75.18*DL_in) + 0.9268;
EWM_p.. WM_p =e= 1330 * (DM_in**2) + (75.18*DM_in) + 0.9268;
EWH_p.. WH_p =e= 1330 * (DH_in**2) + (75.18*DH_in) + 0.9268;

EPL_cst..  PL_cst     =e= (A_1*WL_p) + (A_2 * (DL_ex**0.48)) + A_3 +
                          (A_4*DL_ex);
EPM_cst..  PM_cst     =e= (A_1*WM_p) + (A_2 * (DM_ex**0.48)) + A_3 +
                          (A_4*DM_ex);
EPH_cst..  PH_cst     =e= (A_1*WH_p) + (A_2 * (DH_ex**0.48)) + A_3 +
                          (A_4*DH_ex);


EHEN_Pcst..HEN_Pcst   =e= AF_HEN * ((PL_cst + PM_cst + PH_cst)
*D_Demand);

HEN_Pcst.UP = 9999999999;
HEN_Pcst.LO = 0;

WH_p.lo = 1;
WH_p.up = 10;

WL_p.lo = 0.01;
WL_p.up = 11;
```

```
WM_p.lo = 0.1;
WM_p.up = 10;

Equation
ESCN_CHP_TAC;

Variable
SCN_CHP_TAC;

*=====================================================================*
Parameters
xF              mole fraction of salt in feed sea water
xB              mole fraction of salt in brine solution
TSteam          Inlet temperature of steam in first effect [K]
TVfinal         Condesnation temperature of final distilate [K]
TV1             Temperature of first distillate [K]
Watercost       Cost of water in $ per kg
St_cst          Cost of steam in $ per tonne;

xF = 0.035;   xB = 0.07; TSteam = 373;   TVfinal = 308; TV1 = 373;
St_cst = 1.8;


Variables
MEE_TAC;

Positive variable
SF              Salt water feed flowarate [kg per s]
Brineflow       Brine flowrate [kg per s]
TVavg           Average distillate temperature [K]
DeltaTVac       Average distillate temperature difference over all the
                effects [K]
UHTFFEAC        Overall heat transfer coefficient of heating tubes [kW
                per meter squared]
LambdaAvg       Average Latent heat of condensation for the distillate
                [kJ per kg]
Qtotal
GOR             Gained Output Ratio
MS              Flow rate of steam [kg per second]
A               Area of heat exchange [square meters]
AFC             Annualized fixed cost of evaporator [$ per year]
AOC2            Annual operating cost of evaporator [$ per year] with
                no coalition
Distflow        distillate flow rate in kg per second ;

Integer variable NEFF number of effects;
```

```
Equations
Massbalance
Compbalance
EqTVavg
EqDeltaTVac1
EqUHTFFEAC
EqLambdaAvg
EqQtotal
EqQTotal1
EqGOR
EqMS
EqAFC
EqAOC
E_MB1
EMEE_TAC;

Massbalance..  Distflow  =E= SF - Brineflow;

Compbalance .. SF*xF     =E= Brineflow*xB;

EqTVavg..      TVavg     =E= (Tsteam + TVfinal)/2;

EqDeltaTVac1.. DeltaTVac =E= (TV1 - TVfinal)/NEFF;

EqUHTFFEAC..   UHTFFEAC  =E= 0.8552 + 0.0047*TVavg;

EqLambdaAvg..  LambdaAvg =E= -2.7532*TVavg + 3278.8;

EqQtotal..     Qtotal    =E= Distflow*LambdaAvg;

EqQtotal1..    Qtotal    =E= NEFF*UHTFFEAC*A*DeltaTVac;

EqGOR..        GOR       =E= NEFF*(0.98**NEFF);

EqMS..         MS        =E= Distflow/(GOR+.0000001);

EqAOC..        AOC2      =E= St_cst*MS*3600*OH/1000;

EqAFC..        AFC       =E= NEFF*600*(A**0.6);

E_MB1.. Brineflow + Distflow =e= SF;

NEFF.LO = 2;
NEFF.UP = 15;
AFC.up  = 9999999;
AFC.lo  = 10;
```

```
GOR.L         = 3;
GOR.LO        = 1;
GOR.UP        = 15;
Distflow.lo   = 30;
Distflow.up   = 50;
*SF.LO        = 50;
*SF.UP        = 70;
*Brineflow.LO = 30;
*Brineflow.UP = 30;

*MEE Piping calculations
Positive Variable
Dsf_in    Internal diameter for saltwater feed stream [m]
Dsf_ex    External diameter for saltwater feed stream  [m]
Dd_ex     External diameter for distillate stream [m]
Dd_in     Internal diameter for distillate stream [m]
Wsf_p     Weight of saltwater pipe [kg per m]
Wd_p      Weight of distillate pipe [kg per m]
Psf_cst   Cost of saltwater pipe [$ per m]
Pd_cst    Cost of distillate pipe [$ per m]
MEE_Pcst  Annualized capital cost of piping for the MEE;


Equation
EDsf_in    Internal diameter for saltwater feed stream [m]
EDsf_ex    External diameter for saltwater feed stream  [m]
EDd_ex     External diameter for distillate stream [m]
EDd_in     Internal diameter for distillate stream [m]
EWsf_p     Weight of saltwater pipe [kg per m]
EWd_p      Weight of distillate pipe [kg per m]
EPsf_cst   Cost of saltwater pipe [$ per m]
EPd_cst    Cost of distillate pipe [$ per m]
EMEE_Pcst  Annualized capital cost of piping for the MEE;

*Steam Density values obtained from Isafiade et al 2022

Parameter
SF_Rh   density of slatwater feed [kg per m3]          /880/
SF_Cp   heat capacity of saltwater feed                /3.1/
D_Cp    heat capacity of distillate                    /4.2/
D_Rh    density of distillate                         /1000/
D_SF    distance from saltwater feed source [m]       /100/
AF_MEE  annualization factor for MEE                  /0.2/;


EDsf_in..    Dsf_in   =e=  0.363*(SF**0.45) * (SF_Cp**(-0.45))*
                           (SF_Rh**(-0.32));
```

```
EDd_in..      Dd_in     =e=  0.363*(Distflow**0.45) * (D_CP**(-0.45))*
                             (D_Rh**(-0.32));

EDsf_ex..     Dsf_ex    =e=  1.101 * Dsf_in + 0.006349;
EDd_ex..      Dd_ex     =e=  1.101 * Dd_in  + 0.006349;

EWsf_p..      Wsf_p     =e=  1330 * (Dsf_in**2) + (75.18*Dsf_in) + 0.9268;
EWd_p..       Wd_p      =e=  1330 * (Dd_in**2)  + (75.18*Dd_in)  + 0.9268;

EPsf_cst..    Psf_cst   =e= (A_1*Wsf_p) + (A_2 * (Dsf_ex**0.48)) + A_3 +
                            (A_4*Dsf_ex);
EPd_cst..     Pd_cst    =e= (A_1*Wd_p)  + (A_2 * (Dd_ex**0.48))  + A_3 +
                            (A_4*Dd_ex);

EMEE_Pcst.. MEE_Pcst  =e= AF_MEE* ((Psf_cst*D_sf) +
                            (Pd_cst*D_Demand));


EMEE_TAC..    MEE_TAC   =E=  AFC + MEE_Pcst ;


MEE_Pcst.lo = 1;
MEE_Pcst.up = 999999999;
Dsf_in.up   = 0.5;
Dd_in.up    = 2;

*HEAT EXCHANGER NETWORK
*=====================================================================*
Scalar
     nhut number of hot utilities /3/
     ncut number of cold utilities /3/

 Sets i hot streams /1*5/
      j cold streams /1*5/
      k temperature locations  nok + 1 /1*6/
      data  data /tin,tout,h,f,cost/



 hut(i)             hot utilities
 hps(i)             hot process streams
 cps(j)             cold process streams
 cut(j)             cold utilities
 st(k)              stages
 first(k)           first temperature location
 last(k)            last temperature location
 hx_st(k)           heat recovery stages
```

```
 hut_st(k)          hot utility stages
 cut_st(k)          cold utility stages
 fhps(k)            first temperature location of hps(i)
 fcps(k)            first temperature location of cps(j)
 first_tlhot(k)     intervals where hps(i) exist
 last_tlhot(k)      last temperature location of hps(i)
 first_tlcold(k)    intervals where cps(j) exist
 last_tlcold(k)     last temperature location of cps(j);


 st(k)             = yes$(ord(k) < card(k))  ;
 first(k)          = yes$(ord(k) eq 1)        ;
 last(k)           = yes$(ord(k) eq card(k))  ;
 hut(i)            = yes$(ord(i) <= nhut);
 cut(j)            = yes$(ord(j) >= ncut);
 hps(i)            = yes$(ord(i) >nhut);
 cps(j)            = yes$(ord(j) < ncut);
* hut_st(k)        = yes$(ord(k) <=card(k)-1);
 hut_st(k)         = yes$(ord(k) = 1);
 cut_st(k)         = yes$(ord(k) = card(k) -1);
 hx_st(k)          = yes$(ord(k)>=2 and ord(k)<=card(k)-2);
 fhps(k)           = yes$(ord(k)=1);
 fcps(k)           = yes$(ord(k)=card(k));
 first_tlhot(k)    = yes$(ord(k)>=2 and ord(k) <card(k));
 last_tlhot(k)     = yes$(ord(k)=card(k));
 first_tlcold(k)   = yes$(ord(k)<=card(k)-2);
 last_tlcold(k)    = yes$(ord(k)=1);



TABLE HOTS(I,DATA) Hot streams data
          TIN           TOUT          H           F           COST
1         257           256          0.5          0.0          0
2         196.60       195.60        0.5          0.0          0
3         154           153          0.5          0.0          0
4         155.00        85.00        0.5        150.0          0
5         230.00        40.00        0.5        285.0          0;

TABLE COLDS(J,DATA) Cold streams data
          TIN          TOUT         H            F            COST
1        25.00         240.00       0.5          140.0         0
2        20.00         250.00       0.5          150.0         0
3        50            180          0.5          70            0
4        70            100          0.5          120           0
5        6.5           10.00        0.5          0.0           0 ;

PARAMETER
```

```
*Capital cost parameters
AF           Annualisation factor
CF           Investment cost
AC           Area cost
AE           Area cost index
gamma(i,j)
EMAT         Exchanger minimum approach temperature;


AF= 0.322;    CF=13000;     AC =1000;       AE = 0.83;

gamma(i,j) =6210.3;

ALIAS (j jj);
ALIAS (k kk);

*Flags
Parameter
a_hps(i,k)        intervals in which hps(i) are present
a_cps(j,k)        intervals in which cps(i) are present
a_hut(i,k)        intervals in which hot utilities are present
a_cut(j,k)        intervals in whc cold utilities are present
match(i,j,k)      define possible macthes between streams i and j in
                  interval k
temp_in_hot(i,k)
temp_in_cold(j,k);

*Initialise flags
a_hps(i,k)$(hps(i) and first_tlhot(k)) = 1;
a_cps(j,k)$(cps(j) and first_tlcold(k))= 1;

a_hut(i,k)       = 0;
a_cut(j,k)       = 0;
match(i,j,k)     = 0;
temp_in_hot(i,k) = 0;
temp_in_cold(j,k)= 0;

a_hut(i,k)$(hut(i) and hut_st(k)) = 1;
a_cut(j,k)$(cut(j) and cut_st(k) )= 1;

match(i,j,k)$(st(k) and ((a_hps(i,k) and a_cps(j,k)$(hps(i) and cps(j)))
or (a_cut(j,k)$((hps(i) and cut(j)))) or (a_hut(i,k)$((hut(i) and
cps(j))))))=1;

temp_in_hot(i,k)$hps(i)  = fhps(k);
temp_in_cold(j,k)$cps(j) = fcps(k);
```

```
Display
hut, hps, cps, cut, k, st, hut_st, cut_st, first, last, hx_st, fhps,
fcps,first_tlhot, last_tlhot,
first_tlcold,  last_tlcold, a_hps, a_cps, a_hut, a_cut,
match,temp_in_hot, temp_in_cold ;

VARIABLES
HEN_TAC
dt(i,j,k)  approach between i and j at location k  ;

Binary Variables
y(i,j,k);

Positive Variables
th(i,k)    temperature of  hot stream i as it enters stage k
tc(j,k)    temperature of cold stream j as it leaves stage k
q(i,j,k)   energy exchanged between i and j in stage k
FlowHEN11
FlowHEN22
FlowHEN33
FlowHEN44
FlowHEN4
FlowrateHPS;

Equations
thot_in(i,k)          asignment of hot process stream inlet temperatures
tcold_in(j,k)         asignment of cold process stream inlet
temperatures
total_heat_hot(i)     total heat balance of hot process stream hps(i)
total_heat_cold(j)    total heat balance of cold process stream cps(i)
stage_heat_hot(i,k)   stage heat balance of hot process stream hps(i)
stage_heat_cold(j,k)  stage heat balance of cold process stream cps(i)
monot_hot(i,k)        monotonicity on temperatures - constraint
monot_cold(j,k)       monotonicity on temperatures - constraint

log_q_hps_cps(i,j,k) logical constraint on heat exchanged between hps(i)
and cps(j)
log_q_hps_cut(i,j,k) logical constraint on heat exchanged between hps(i)
and cut(j)
log_q_hut_cps(i,j,k) logical constraint on heat exchanged between hut(i)
and cps(j)

log_dt_hps_cps_hs(i,j,k)  logical constraint on hot side tmeperature
difference between hps(i) and cps(j)
log_dt_hps_cps_cs(i,j,k)  logical constraint on cold side tmeperature
difference between hps(i) and cps(j)
```

```
log_dt_hps_cut_hs(i,j,k)  logical constraint on hot side tmeperature
difference between hps(i) and cut(j)
log_dt_hps_cut_cs(i,j,k)  logical constraint on cold side tmeperature
difference between hps(i) and cut(j)

log_dt_hut_cps_hs(i,j,k)  logical constraint on hot side tmeperature
difference between hut(i) and cps(j)
log_dt_hut_cps_cs(i,j,k)  logical constraint on cold side tmeperature
difference between hut(i) and cps(j)

TurbHENconnect1(i)
TurbHENconnect2(i)
TurbHENconnect3(i)
*TurbARSconnect1(j)
FlowtoHEN1b
FlowtoHEN2
FlowtoHEN3
*FlowtoHEN4

FlowtoHEN111
FlowtoHEN222
FlowtoHEN333
*FlowtoHEN444

TAC_OBJ HEN TAC OBJECTIVE FUNCTION;
*=====================================================================*
*assignment of stream inlet temperatures

thot_in(i,k)$(hps(i) and temp_in_hot(i,k)).. th(i,k) =e= hots(i,'tin');

tcold_in(j,k)$(cps(j) and temp_in_cold(j,k))..
  tc(j,k) =e= colds(j,'tin');
*=====================================================================*
*stream overall enthalpy balance

total_heat_hot(i)$(hps(i)).. hots(i,'f')*(hots(i,'tin')-hots(i,'tout'))
=e= sum((j,k)$(match(i,j,k)), q(i,j,k));

total_heat_cold(j)$(cps(j)).. colds(j,'f')*(colds(j,'tout')-
colds(j,'tin'))  =e=     sum((i,k)$(match(i,j,k)), q(i,j,k));
*=====================================================================*
*stream stage heat exchange

stage_heat_hot(i,k)$(hps(i) and sum(j,match(i,j,k))).
hots(i,'f')*(th(i,k)-th(i,k+1))  =e= sum(j$match(i,j,k), q(i,j,k));

stage_heat_cold(j,k)$(cps(j) and sum(i,match(i,j,k))).
```

```
colds(j,'f')*(tc(j,k)-tc(j,k+1)) =e= sum(i$match(i,j,k), q(i,j,k));

*=============================================================*
*logic equations

*monotocity of temperature
monot_hot(i,k)$(hps(i) and st(k) )..   th(i,k) =g= th(i,k+1);
monot_cold(j,k)$(cps(j) and st(k) )..  tc(j,k) =g= tc(j,k+1);

log_q_hps_cps(i,j,k)$(hps(i) and cps(j) and match(i,j,k))..
q(i,j,k) =l= min(hots(i,'f')*(hots(i,'tin')-
hots(i,'tout')),colds(j,'f')*(colds(j,'tout')-colds(j,'tin')))*y(i,j,k);

log_q_hps_cut(i,j,k)$(hps(i) and cut(j) and match(i,j,k))..
q(i,j,k) =l= hots(i,'f')*(hots(i,'tin')-hots(i,'tout'))*y(i,j,k);

log_q_hut_cps(i,j,k)$(hut(i) and cps(j) and match(i,j,k))..
q(i,j,k) =l= colds(j,'f')*(colds(j,'tout')-colds(j,'tin'))*y(i,j,k);

log_dt_hps_cps_hs(i,j,k)$(hps(i) and cps(j) and match(i,j,k))..dt(i,j,k
) =l= th(i,k) - tc(j,k) + gamma(i,j)*(1-y(i,j,k));

log_dt_hps_cps_cs(i,j,k)$(hps(i) and cps(j) and
match(i,j,k))..dt(i,j,k+1) =l= th(i,k+1) - tc(j,k+1) + gamma(i,j)*(1-
y(i,j,k));

log_dt_hps_cut_hs(i,j,k)$(hps(i) and cut(j) and match(i,j,k))..dt(i,j,k
)$(hps(i) and cut(j) and match(i,j,k)) =l= (th(i,k) - colds(j,'tout')) +
gamma(i,j)*(1-y(i,j,k));

log_dt_hps_cut_cs(i,j,k)$(hps(i) and cut(j) and
match(i,j,k))..dt(i,j,k+1)$(hps(i) and cut(j) and match(i,j,k)) =l=
(th(i,k+1) - colds(j,'tin')) + gamma(i,j)*(1-y(i,j,k));

log_dt_hut_cps_hs(i,j,k)$(hut(i) and cps(j) and match(i,j,k))..dt(i,j,k
)$(hut(i) and cps(j) and match(i,j,k)) =l= (hots(i,'tin') - tc(j,k)) +
gamma(i,j)*(1-y(i,j,k));

log_dt_hut_cps_cs(i,j,k)$(hut(i) and cps(j) and
match(i,j,k))..dt(i,j,k+1)$(hut(i) and cps(j) and match(i,j,k))
=l=(hots(i,'tout') - tc(j,k+1)) + gamma(i,j)*(1-y(i,j,k));

*=============================================================
====================================

*Flowrate of HPS to HEN
FlowtoHEN1b.. HPSd  =g= FlowHEN1;
```

```
FlowtoHEN2..  MPSd  =g= FlowHEN2;
FlowtoHEN3..  LPSd  =g= FlowHEN3;

FlowtoHEN111.. FlowHEN11  =E= FlowHEN1*2798.13;
FlowtoHEN222.. FlowHEN22  =E= FlowHEN2*2789.9;
FlowtoHEN333.. FlowHEN33  =E= FlowHEN3*2750.6;
*FlowtoHEN444..FlowHEN44  =E= FlowHEN4*25.31;

TurbHENconnect1('1').. FlowHEN11 =E=sum((j,K),Q('1',J,K)$(HUT('1') AND
                       HUT_ST(K)));
TurbHENconnect2('2').. FlowHEN22 =E=sum((j,K),Q('2',J,K)$(HUT('2') AND
                       HUT_ST(K)));
TurbHENconnect3('3').. FlowHEN33 =E=sum((j,K),Q('3',J,K)$(HUT('3') AND
                       HUT_ST(K)));
*TurbARSconnect1('5')..FlowHEN44 =E=sum((i,K),Q(I,'5',K)$(CUT('1') AND
                       CUT_ST(K)));

*=====================================================================
==================================
*OBJECTIVE
TAC_OBJ..HEN_TAC=E=

         AF_HEN*(CF*SUM((I,J,K)$(MATCH(I,J,K)),Y(I,J,K)) +

         ac*sum((i,j,k)$(match(i,j,k) and hps(i) and
         cps(j)),(q(i,j,k)*(1/hots(i,'h')+1/colds(j,'h'))/
         ((((1e-6)**3+(dt(i,j,k)*dt(i,j,k+1))*
         ((dt(i,j,k)+dt(i,j,k+1))*0.5))**0.3333)+1e-6)+1e-6)**ae) +
         ac*sum((i,j,k)$(match(i,j,k) and hps(i) and
         cut(j)),(q(i,j,k)*(1/hots(i,'h')+1/colds(j,'h'))/
         ((((1e-6)**3+(dt(i,j,k)*dt(i,j,k+1))*
         ((dt(i,j,k)+dt(i,j,k+1))*0.5))**0.3333)+1e-6)+1e-6)**ae) +
         ac*sum((i,j,k)$(match(i,j,k) and hut(i) and
         cps(j)),(q(i,j,k)*(1/hots(i,'h')+1/colds(j,'h'))/
         ((((1e-6)**3+(dt(i,j,k)*dt(i,j,k+1))*
         ((dt(i,j,k)+dt(i,j,k+1))*0.5))**0.3333)+1e-6)+1e-6)**ae)) +
         sum((i,j,k)$(hps(i) and cut(j) and
         match(i,j,k)),colds(j,'cost')*q(i,j,k))
         +sum((i,j,k)$(hut(i) and cps(j) and
         match(i,j,k)),hots(i,'cost')*q(i,j,k)));

*initialisation for exchanger approach temperatures between hps(i) and
cps(j)
emat=1;
dt.l(i,j,k)$(hps(i)    and cps(j) and match(i,j,k))=hots(i,'tin')-
colds(j,'tin') ;
```

```
dt.l(i,j,k+1)$(hps(i)  and cps(j) and match(i,j,k))=hots(i,'tin')-
colds(j,'tin');
dt.lo(i,j,k)$(hps(i)   and cps(j) and match(i,j,k))=emat;
dt.lo(i,j,k+1)$(hps(i) and cps(j) and match(i,j,k))=emat;
dt.up(i,j,k)$(hps(i)   and cps(j) and match(i,j,k))=400;
dt.up(i,j,k+1)$(hps(i) and cps(j) and match(i,j,k))=400;

*initialisation for exchanger approach temperatures between hps(i) and
cut(j)
dt.l(i,j,k)$(hps(i)    and cut(j) and match(i,j,k))=hots(i,'tin')-
colds(j,'tin');
dt.l(i,j,k+1)$(hps(i)  and cut(j) and match(i,j,k))=hots(i,'tin')-
colds(j,'tin');
dt.lo(i,j,k)$(hps(i)   and cut(j) and match(i,j,k))=emat;
dt.lo(i,j,k+1)$(hps(i) and cut(j) and match(i,j,k))=emat;
dt.up(i,j,k)$(hps(i)   and cut(j) and match(i,j,k))=400;
dt.up(i,j,k+1)$(hps(i) and cut(j) and match(i,j,k))=400;

*initialisation for exchanger approach temperatures between hut(i) and
cps(j)
dt.l(i,j,k)$(hut(i)    and cps(j) and match(i,j,k))=hots(i,'tin')-
colds(j,'tin');
dt.l(i,j,k+1)$(hut(i)  and cps(j) and match(i,j,k))=hots(i,'tin')-
colds(j,'tin');
dt.lo(i,j,k)$(hut(i)   and cps(j) and match(i,j,k))=emat;
dt.lo(i,j,k+1)$(hut(i) and cps(j) and match(i,j,k))=emat;
dt.up(i,j,k)$(hut(i)   and cps(j) and match(i,j,k))=400;
dt.up(i,j,k+1)$(hut(i) and cps(j) and match(i,j,k))=400;



*initialisations for q(i,j,k) between hps(i) and cps(j)
q.l(i,j,k)$(hps(i) and cps(j) and
match(i,j,k))=min(hots(i,'f')*(hots(i,'tin')-
hots(i,'tout')),colds(j,'f')*(colds(j,'tout')-colds(j,'tin')));

q.l(i,j,k)$(hps(i) and cut(j) and match(i,j,k)) =
hots(i,'f')*(hots(i,'tin')-hots(i,'tout'));

q.l(i,j,k)$(hut(i) and cps(j) and match(i,j,k))=
colds(j,'f')*(colds(j,'tout')-colds(j,'tin'));

q.up(i,j,k)$(hps(i) and cps(j) and
match(i,j,k))=min(hots(i,'f')*(hots(i,'tin')-
hots(i,'tout')),colds(j,'f')*(colds(j,'tout')-colds(j,'tin')));
```

```
q.up(i,j,k)$(hps(i) and cut(j) and match(i,j,k)) =
hots(i,'f')*(hots(i,'tin')-hots(i,'tout'));

q.up(i,j,k)$(hut(i) and cps(j) and match(i,j,k))=
colds(j,'f')*(colds(j,'tout')-colds(j,'tin'));
*$offtext

*Q.UP(I,J,K)$(HUT(I) AND Cut(J))= 10000;

*Intialisations and bounds for intermediate temperatures
TH.L(I,K)$(first(k))=HOTS(I,'TIN');
TC.L(J,K)$(last(k))=COLDS(J,'TIN');

TH.LO(I,K)$(last(k))=HOTS(I,'TOUT');
TH.UP(I,K)$(first(k))=HOTS(I,'TIN');

TC.LO(J,K)$(last(k))=COLDS(J,'TIN');
TC.UP(J,K)$(first(k) and cps(j))=COLDS(J,'TOUT');

*=================================================================*

*HEAT PUMP
Set
ARS /Evap, Abs, SHX, Gen, Con/;

Parameter
T10   /6/
T4    /90/
X1    /55/
X3    /55/
X4    /60/
T3    /65/
T7    /85/
ma_11 /0.025/;

Parameter

P10, hlt10,P4;

Variable
h10, h11, h4, Qr(ars);

Equation
EH4, EH10, EH11, EQEvap;

EQEvap(ars).. Qr('Evap')=e= 10;
```

```
*Sauration pressure of water

P10 = (0.000000000002*(T10**6))- (0.000000003*(T10**5))+
      (0.0000002*(T10**4))+(0.00003*(T10**3))+(0.0014*(T10**2))
      +(0.0444*T10)+ 0.6108;

display p10;

EH10..  h10 =e= (-0.00125397*(T10**2))+(1.88060937*T10)+2500.559;

hlt10 = (-0.00132635*(T10**2))-(2.29983657*T10)+2500.43063;

EH11..  h11 =e= h10- hlt10;

display  hlt10;

*=================================================================*
*CALCULATION OF P4
Parameter

A0 /-2.00755/
A1 /0.16976/
A2 /-0.003133362/
A3 /0.0000197668/
B0 /124.937/
B1 /-7.71649/
B2 /0.152286/
B3 /-0.0007959/
C1 /7.05/
D1 /-1596.49/
E1 /-104095.5/
SA
SB
tREF;

VARIABLE
LP4;

SA    = (A0*(X4**0))+(A1*(X4**1))+(A2*(X4**2))+ (A3*(X4**3));
SB    = (B0*(X4**0))+(B1*(X4**1))+(B2*(X4**2))+ (B3*(X4**3));
TREF  = (t4-sb)/SA;

LP4.L = C1+ (D1/(TREF+273))+ (E1/((TREF+273)**2));

TREF  = (t4-sb)/SA;

P4    = 10**LP4.L;
```

```
DISPLAY P4, LP4.L, TREF, SA, SB;

*Calculation of h4
Parameter
A00 /-2024.33/
A11 /163.309/
A22 /-4.88161/
A33 /0.06302948/
A44 /-0.0002913704/

B00 /18.2829/
B11 /-1.1691757/
B22 /0.03248041/
B33 /-0.0004034184/
B44 /0.0000018520569/
C00 /-0.037008214/
C11 /0.0028877666/
C22 /-0.000081313015/
C33 /0.00000099116628/
C44 /-0.0000000044441207/

SA2, SB2, SC2, tREF;

SA2 = (A00*(X4**0))+(A11*(X4**1))+(A22*(X4**2))+ (A33*(X4**3))+
      (A44*(X4**4));
SB2 = (B00*(X4**0))+(B11*(X4**1))+(B22*(X4**2))+ (B33*(X4**3)) +
      (B44*(X4**4));
SC2 = (C00*(X4**0))+(C11*(X4**1))+(C22*(X4**2))+ (C33*(X4**3)) +
      (C44*(X4**4));

EH4..h4 =e= SA2 + (T4*SB2)+ (SC2*(T4**2));

DISPLAY sa2, sb2, sc2;

*=============================================================*
Parameter
p8, hf7;

variable
h8, h9, h7;

Equation
EH8, EH9, EH7;

*Calculation of h8
EH7..h7 =e= (-0.00125397*(Tref**2))+ (1.88060937*Tref)+2500.559;
```

```
*Enthalpy of condensation for 7

hf7 = (-0.00132635*(Tref**2))-(2.29983657*Tref)+2500.43063;

EH8..h8 =e= h7-hf7;

EH9..h9 =e= h8;

*=============================================================*

*Mass balance on the evaporator
Positive variables
ma9, ma10, ma11;

Equation
EQ_Evap, Ema11, Ema9;

Ema11.. ma11 =e= 0.025*ma10;
Ema9..  ma9  =e= (0.975*ma10) + ma11;

EQ_Evap(ars).. Qr('Evap') =e= (ma10*h10)+(ma11*h11)-(ma9*h9);

*Absorber

Positive Variables
ma6;

Variable
h1, ma1;

parameter
X6, X5, Tref2, SA3, SB3, T1, T2;

X6 = X4;
X5 = X4;

*ma10.l = 1;

*ma11.l = 1;
*MA6.L  = 1;
*MA1.L  = 1;

*ma9.l  = 1;

Equation
Abs1, ABS2, EH1;
```

```
ABS2..    ma1 =E= ma10 + ma11 + ma6;

Abs1.. x1*ma1 =e= X6*ma6;

Tref2 = ((-2*E1)/(D1+((abs(D1)**2)-(4*E1*(C1-LOG10(P10))))**0.5))-273;

SA3   = (A0*(X1**0))+(A1*(X1**1))+(A2*(X1**2))+ (A3*(X1**3));
SB3   = (B0*(X1**0))+(B1*(X1**1))+(B2*(X1**2))+ (B3*(X1**3));

T1    = SB3 + (SA3*tREF2);

T2    = T1;

Parameter
SA4, SB4, SC4;

SA4 = (A00*(X1**0))+(A11*(X1**1))+(A22*(X1**2))+ (A33*(X1**3))+
      (A44*(X1**4));
SB4 = (B00*(X1**0))+(B11*(X1**1))+(B22*(X1**2))+ (B33*(X1**3)) +
      (B44*(X1**4));
SC4 = (C00*(X1**0))+(C11*(X1**1))+(C22*(X1**2))+ (C33*(X1**3)) +
      (C44*(X1**4));

EH1..h1 =e= SA4 + (T1*SB4)+ (SC4*(T1**2));

*Solution Heat Exchanger
Positive Variable
ma2, ma3,ma5, ma4;

variable
h3
h2
h5
h6;

Equation
EH3;

Parameter
SA5
SB5
SC5;

SA5 = (A00*(X3**0))+(A11*(X3**1))+(A22*(X3**2))+ (A33*(X3**3))+
      (A44*(X3**4));
SB5 = (B00*(X3**0))+(B11*(X3**1))+(B22*(X3**2))+ (B33*(X3**3)) +
      (B44*(X3**4));
```

```
SC5 = (C00*(X3**0))+(C11*(X3**1))+(C22*(X3**2))+ (C33*(X3**3)) +
      (C44*(X3**4));

EH3.. h3 =e= SA5 + (T3*SB5)+ (SC5*(T3**2));

Positive VARIABLE
w pump work input in kW
ma7 ;

Equation
Ew Pump minimum work input
EH2;

Parameter
v1, P2, P1, r1;

P1 = P10;
P2 = P4;

r1 = 1145.36 + (470.84*(X1/100))+ (1374.79*((X1/100)**2))-
((0.333393+(0.571749*(X1/100)))*(273+T1));

v1 = 1/r1;

Ew..   W =E= ma1*v1*(P2-P1);

Eh2.. h2 =e= h1;

Scalar
cfshx1 "correction factor for shx1" /0.067246/ ;

Equation

SHX1, EMa2, EMa3,  EMa5,ema4,  EH6, EMA7;

EMA2.. ma2 =e= ma1;
EMA3.. ma3 =e= ma2;
EMa4.. ma4 =e= ma3 - ma7;
EMa5.. ma5 =e= ma6;
EH6..   H6 =E= H5;
EMA7.. ma7 =e= ma9;

SHX1.. (ma2*h2)+(ma4*h4) =e= (ma3*h3) +(ma5*h5)+ cfshx1;

*Calculation of T5, T6 AND T8 from the correlations from Appendix A.3,
A.2 and A.10 respectively
*for T6, tref2 applies as it is the same pressure as P10
```

```
*for T8, use h7 as vapour enthalpy

variable
T5, T6, T8;

Parameter
SA6, SB6, SC6, SA7, SB7 ;

Equation

ET5, ET6, ET8;


SA6 = (A00*(X5**0))+(A11*(X5**1))+(A22*(X5**2))+ (A33*(X5**3))+
(A44*(X5**4));
SB6 = (B00*(X5**0))+(B11*(X5**1))+(B22*(X5**2))+ (B33*(X5**3)) +
(B44*(X5**4));
SC6 = (C00*(X5**0))+(C11*(X5**1))+(C22*(X5**2))+ (C33*(X5**3)) +
(C44*(X5**4));

SA7 = (A0*(X6**0))+(A1*(X6**1))+(A2*(X6**2))+ (A3*(X6**3));
SB7  = (B0*(X6**0))+(B1*(X6**1))+(B2*(X6**2))+ (B3*(X6**3));

ET5.. h5 =e= SA6 + (SB6*T5) + (SC6*(T5**2));
ET6.. T6 =e= SB7 + (SA7*tREF2);

ET8.. h7 =e= (-0.00125397*(abs(T8)**2)) + (1.88060937*T8) +2500.559;

Equations
EQG, EQC, EQA, EQS;

EQA(ars).. Qr('Abs') =e= (ma10*h10)+(ma11*h11)+(ma6*h6) - (ma1*h1);

EQG(ars).. Qr('Gen') =e= (ma4*h4) + (ma7*h7) - (ma3*h3);

EQC(ars).. Qr('Con') =e= ma7*(h7-h8);

EQS(ars).. Qr('SHX') =e= ma3*(h3-h2);

Parameter

T14 /25/, T15 /30/, T16 /150/, T17/145/, T18 /25/, T19 /30/, t9,

h12/83.91/, h13/27.12/,h14 /104.93/, h15/146.73/, h16 /2752.78/, h17
/2741.26/, h18/104.93/, h19/146.73/;

t9= t10;
```

```
VARIABLE
T12, T13, LMTDr(ars), Tabs_in, te1, te2, te3, te4;

Equations
ET12(J), ET13(J), ELMTDE, ETabs,ELMTDS, ELMTDG, ELMTDC, ete1, ete2,
ete3, ete4,  ELMTDA;


ET12(J)..T12 =e= colds('5', 'Tout');
ET13(J)..T13 =e= colds('5', 'Tin');

ELMTDE(ars).. LMTDr('Evap') =e= ((T12-T10)-(T13-T9))/(Log((T12-
T10)/(T13-T9))+0.000000001);

*Solution temperature entering the absorber i.e 10+11+6

ETabs.. Tabs_in =e= SB3+ SA3*T10;

ete1..  te1     =e= (T1-T14)-(Tabs_in-T15);

ete2..  te2     =e= (T1-T14)/(Tabs_in-T15);


ELMTDA(ars).. LMTDr('Abs')=e= te1/log(te2+0.00000000000001);


ete3.. te3 =e= (T4-T3)-(T5-T2);
ete4.. te4 =e= (T4-T3)/(T5-T2);

ELMTDS(ars).. LMTDr('shx') =E= te3/Log(ABS(te4)+0.0000000000001);

*Assume generator exit temperature to be equal to T4

ELMTDG(ars).. LMTDr('Gen') =e= ((T16- T4)-(T17-T3))/LOG((T16- T4)/(T17-
T3));

ELMTDC(ars).. LMTDr('Con') =e= ((T7-T19)-(T8-T18))/(Log(abs((T7-
T19)/(T8-T18))));


Positive variable

ma12, ma14, ma16, ma18;

Equation
```

```
Ema12, EMa14, EMa16, EMa18;

Ema12(ars).. ma12 =e= Qr('Evap')/(h12-h13);
EMa16(ars).. ma16 =e= Qr('Gen')/(h16-h17);
EMa14(ars).. ma14 =e= Qr('Abs')/(h15-h14);
EMa18(ars).. ma18=e= Qr('Con')/(h19-h18);

*ma12.lo = 0.0001;
*ma12.up = 5;

*ma16.lo = 0.0001;
*ma16.up = 30;

*ma14.lo = 0.0001;
*ma14.up = 20;

*ma18.lo = 0.0001;
*ma18.up = 30;

*FlowtoHEN4.. Ma16 =g= flowHEN4;

set
U /Ur/;

Positive Variable

UA (ars), Ar(ars);

*Heat transfer coefficients from

TABLE coefficients (ARS, U)

          Ur
Abs     0.85
Evap    1.50
Shx     1.10
Gen     0.85
Con     1.40;

Equation

EA1, ETACR;

EA1(ars,u).. Qr(ars) =e= Ar(ars)* coefficients(ars, 'Ur')*LMTDr(ars);
```

```
*The costing of heat exchangers was done using the method and values
from Isafiade et al 2016

Parameter
Cr     cost heat esxchanger cost per unit area [$ per m2] /641/
CrIn   cost of heat exchanger installation /8333.3/
CrI    cost index for HE area /0.83/
AF_ARS Annualization factor for ARS /0.32/;

Equation
E_LPSB;

E_LPSB.. LPSd =g= ma16 + FlowHEN3 + MS;

*ARS PIPING CALCULATIONS
Parameter
cw_CP    Heat capacity of chill water [kJ per kg.K]    /4.2/
cw_Rh    Density of chilled water [kg per cubic meter] /1000/;

Positive Variable
Dcw_in   Internal diameter for chilled water stream [m]
Dcw_ex   External diameter for chilled water stream [m]
Wcw_p    Weight of chilled water pipe [kg per m]
Pcw_cst  Price of chilled water pipe [$ per m]
ARS_Pcst Annualized cost of ARS demand supply piping [$ per yr];

Equation
EDcw_in   Internal diameter for chilled water stream [m]
EDcw_ex   External diameter for chilled water stream [m]
EWcw_p    Weight of chilled water pipe [kg per m]
EPcw_cst  Price of chilled water pipe [$ per m]
EARS_Pcst Annualized cost of ARS demand supply piping [$ per yr];



EDcw_in..    Dcw_in    =e= 0.363*(ma12**0.45) * (cw_CP**(-0.45))*
             (cw_Rh**(-0.32));
EDcw_ex..    Dcw_ex    =e= 1.101 * Dcw_in + 0.006349;
EWcw_p..     Wcw_p     =e= 1330 * (Dcw_in**2) + (75.18*Dcw_in) + 0.9268;
EPcw_cst..   Pcw_cst   =e= (A_1*Wcw_p) + (A_2 * (Dcw_ex**0.48)) + A_3 +
             (A_4*Dcw_ex);
EARS_Pcst..  ARS_Pcst  =e= (Pcw_cst  *D_Demand );


ARS_Pcst.lo = 0.001;
ARS_Pcst.up = 999999999;
```

```
Dcw_in.lo = 0.00001;
Dcw_in.up = 1.2;

Variable
ARS_TAC;

ETACR.. ARS_TAC =e= (CrIn + sum((ars,u), (Ar(ars)**CrI)*Cr) + ARS_Pcst)
* AF_ARS;

ARS_TAC.LO = 0.00001;
ARS_TAC.UP = 999999999;


*=============================================================*
*Condensation
set
Cndr condensers for LPS MPS & HPS /cndL, cndM, cndH/
Stm  steam streams                /LPSs, MPSs, HPSs/
SStp Steam Properties             /sTemp1, sTemp2,sH1, sH2, sCp1/;


table  St_Pr (stm, sstp)
          sTemp1       sTemp2       sH1          sH2          sCp1
LPSs      154.44       143.61      2752.78      2738.06      2.27
MPSs      193.6        180         2948.90      2787
HPSs      382.22       253         3162.89      2799         2.40

Parameter
H_VapL  enthalpy of vaporization of LPS [kJ per kg]/2122.72/
H_VapM  enthalpy of vaporization of MPS [kJ per kg] /1965.18/
H_VapH  enthalpy of vaporization of HPS [kJ per kg] /1690.7/
Tw_in  inlet temperature of cooling water           /25/
Tw_out outlet temperature of cooling water          /100/
Cp_wt  specific heat capacity of cooling water      /4.18/  ;

PARAMETER
*Capital cost parameters for condenser
AF_cnd          Annualisation factor
CF_cnd          Fixed Investment cost  [$]
AC_cnd          Variable Area cost [$ per square meter]
AE_cnd          Area cost index;


AF_cnd= 0.322;    CF_cnd=13000;     AC_cnd =1000;       AE_cnd = 0.83;

Positive Variable
Cl_Wt    cooling water flowrates for LPS MPS HPS and total
```

```
Wt_Total total cooling water
Wt_cost  cost of cooling water for LPS MPS HPS and total
A_CndL   LPS condenser heat exchanger area in square meters
A_CndM   MPS condenser heat exchanger area in square meters
A_CndH   HPS condenser heat exchanger area in square meters
Cnd_Cst  condenser capital cost;

Equations
EWt_L, EWt_M, EWt_H, EWt_Total, EWt_Cst, ECnd_cst, EA_CndL, EA_CndM,
EA_CndH ;

EWt_L.. Cl_Wt('cndL') =e= ((LPSd-FlowHEN3-MS-
ma16)*H_VaPL)/(Cp_wt*(Tw_out-Tw_in));
EWt_M.. Cl_Wt('cndM') =e= ((MPSd-FlowHen2)*H_VaPM)/(Cp_wt*(Tw_out-
Tw_in));
EWt_H.. Cl_Wt('cndH') =e= ((HPSd-FlowHeN1)*H_VaPM)/(Cp_wt*(Tw_out-
Tw_in));

EWt_Total.. Wt_Total  =e=  SUM((Cndr), Cl_wt(cndr));
EWt_cst..   Wt_cost   =e=  Wt_Total * (streamproperties('ws6', 'sCst'));

EA_CndL.. A_CndL   =e=
(cl_wt('cndL')*((streamproperties('ws6','sTmp2'))-
(streamproperties('ws6', 'sTmp1')))*cp_s)/
                        (((st_Pr('LPSs','sTemp1')-
(streamproperties('ws6','sTmp2')))*(st_Pr('LPSs','sTemp2')-
(streamproperties('ws6','sTmp1')))
                        *((((st_Pr('LPSs','sTemp1')-
(streamproperties('ws6','sTmp2')))+(st_Pr('LPSs','sTemp2')-
(streamproperties('ws6','sTmp1'))))/2)**0.3333))*U_st);

EA_CndM.. A_CndM   =e=
(cl_wt('cndM')*((streamproperties('ws6','sTmp2'))-
(streamproperties('ws6', 'sTmp1')))*cp_s)/
                        (((st_Pr('MPSs','sTemp1')-
(streamproperties('ws6','sTmp2')))*(st_Pr('MPSs','sTemp2')-
(streamproperties('ws6','sTmp1')))
                        *((((st_Pr('MPSs','sTemp1')-
(streamproperties('ws6','sTmp2')))+(st_Pr('MPSs','sTemp2')-
(streamproperties('ws6','sTmp1'))))/2)**0.3333))*U_st);


EA_CndH.. A_CndH   =e=
(cl_wt('cndH')*((streamproperties('ws6','sTmp2'))-
(streamproperties('ws6', 'sTmp1')))*cp_s)/
```

```
                        (((st_Pr('HPSs','sTemp1')-
(streamproperties('ws6','sTmp2')))*(st_Pr('HPSs','sTemp2')-
(streamproperties('ws6','sTmp1')))
                        *((((st_Pr('HPSs','sTemp1')-
(streamproperties('ws6','sTmp2')))+(st_Pr('HPSs','sTemp2')-
(streamproperties('ws6','sTmp1'))))/2)**0.3333))*U_st);


ECnd_cst.. Cnd_cst =e=   AF_cnd*(CF_cnd + (((A_cndL + A_cndM +
A_cndH)**AE_cnd)*AC_cnd));


a_cndm.lo    = 0.00001;
a_cndm.up    = 1000000;
*mps.lo      = 0.000001;
*FlowHEN1.lo = 0.000001;

ESCN_CHP_TAC.. SCN_CHP_TAC =E= (sum((sp,f,s), FSCN(sp,f,s) +
ISCN(sp,f))+ ((0.0239*PP*OH) + (0.00983*EP*OH)) +
sum((ws('ws2')),(ASP*SPc) + (VST*CST) +(((AHE1+ AHE2)**CI)*CHE)+
HEI)*S_A + HEN_Pcst + Cb_cst + wtc + Bcst + TbCst)/1000000;

SCN_CHP_TAC.lo = 0.0001;
SCN_CHP_TAC.up = 999999999;

*HEN_TAC.LO = 0.009;
*HEN_TAC.L  =  99;
*HEN_TAC.UP = 9999999;

*=====================================================================*
Cost_obj.. cost =e= SCN_CHP_TAC + ((HEN_TAC + ARS_TAC +
MEE_TAC)/1000000);
Em_obj..  E =e= (sum(sp,EmB(sp))) + sum(f, EmT(f));

Multi_obj.. 0.1*multiobjective =e=
((0.5)*(cost/best('cost')))+((0.5)*(E/best('E')));

*cost.lo = 0.001;
*cost.up = 999;

e.lo = 0.001;
e.up = 9999999999;

*multiobjective.LO = 0.0001;
*multiobjective.UP = 9999;
```

```
*=========================================================================*

model powergen /all/;

solve powergen using minlp minimizing cost;
solve powergen using minlp minimizing E;
solve powergen using minlp minimizing multiobjective;
```